

AD 744526

NUMERICAL TECHNIQUES AND SOLUTIONS FOR AXISYMMETRICAL VISCOUS COMPRESSIBLE FLOWS

KENNETH W. SMITH

Office of the Assistant for Study Support
Kirtland Air Force Base, New Mexico

VICTOR J. SKOGLUND

Department of Mechanical Engineering
The University of New Mexico

May 1972

Approved for public release;
distribution unlimited

Reproduced by
NATIONAL TECHNICAL
INFORMATION SERVICE
U.S. Department of Commerce
Springfield, VA 22151

OFFICE OF THE ASSISTANT FOR STUDY SUPPORT
DCS/Development Plans, Air Force Systems Command
Kirtland Air Force Base, New Mexico 87117

175

Unclassified
Security Classification

DOCUMENT CONTROL DATA - R & D

(Security classification of title, body of abstract and indexing annotation must be entered when the overall report is classified)

1. ORIGINATING ACTIVITY (Corporate author) Office of the Assistant for Study Support (AFSWC), DCS/Development Plans, AFSC, Kirtland AFB NM 87117		2a. REPORT SECURITY CLASSIFICATION Unclassified	
		2b. GROUP NA	
3. REPORT TITLE NUMERICAL TECHNIQUES AND SOLUTIONS FOR AXISYMMETRICAL VISCOUS COMPRESSIBLE FLOWS			
4. DESCRIPTIVE NOT. (Type of report and inclusive dates) Dissertation Reprint (Final Rpt) Jan 69-Dec 71			
5. AUTHOR(S) (First name, middle initial, last name) Kenneth W. Smith Victor J. Skoglund			
6. REPORT DATE May 1972		7a. TOTAL NO. OF PAGES 171	7b. NO. OF REFS 75
8a. CONTRACT OR GRANT NO. None		8b. ORIGINATOR'S REPORT NUMBER(S) OAS-TR-72-4	
b. PROJECT NO.		9b. OTHER REPORT NO(S) (Any other numbers that may be assigned this report) None	
c.			
d.			
10. DISTRIBUTION STATEMENT Approved for public release; distribution unlimited.			
11. SUPPLEMENTARY NOTES None		12. SPONSORING MILITARY ACTIVITY Office of the Assistant for Study Support (AFSWC) Kirtland AFB NM 87117	
13. ABSTRACT The purpose of this investigation was to develop numerical techniques for solving axisymmetrical, viscous, compressible flow around blunt bodies. Solutions were limited to systems of ideal gases with laminar unseparated boundary layers. The bow wave was represented by a moving discontinuity. The remainder of the system was represented by second order accuracy, time dependent difference equations. In this investigation the difference equations were derived from basic time dependent, viscous compressible flow equations that were transformed into body related coordinates. The addition of stabilizing terms to basic difference equations was used to achieve numerical stability. Numerical experiments were performed to minimize the effect of the stabilizing terms on the results. Solutions for a hemisphere forebody were obtained at Mach 2 and 4 for inviscid flow and for several Reynolds numbers. At Mach 4, solutions were obtained for a hemisphere-cylinder for inviscid flow and for a Reynolds number of 4000. Where possible, calculated and experimental results were compared. Their agreement was satisfactory. Prior solutions of viscous compressible flow in the afterbody region of blunt bodies were not found in any publication. It was concluded that accurate solutions for axisymmetrical, viscous, compressible flows can be obtained in the forebody and afterbody regions of blunt bodies using the time dependent numerical techniques of this investigation. In the forebody region of a hemisphere-cylinder, approximate solutions may be obtained by solving the forebody system alone. Stabilization of the modified Lax-Wendroff technique seemed necessary, but improvements in wave fitting, boundary and digitizing techniques might eliminate that need.			

DD FORM 1 NOV 65 1473

ia

Unclassified
Security Classification

Unclassified

Security Classification

14. KEY WORDS	LINK A		LINK B		LINK C	
	ROLE	WT	ROLE	WT	ROLE	WT
Laminar Boundary Layers Blunt Body Solutions Afterbody Viscous Flows Viscous Compressible Flows Body Related Coordinates Hemisphere-Cylinder Bodies Numerical Solutions Time Dependent Methods Finite Difference Equations Bow Shock Fitting Boundary Conditions Initial Values Numerical Techniques Numerical Stability						
<i>ib</i>						

Unclassified

Security Classification

NOTICE

Reprinted by permission of Kenneth Wayne Smith. All rights reserved.
Reproduction in whole or in part is permitted for any purpose of the
United States Government. Do not return this report to the originator.
Retain or destroy as appropriate.

ic

**NUMERICAL TECHNIQUES AND SOLUTIONS
FOR AXISYMMETRICAL VISCOUS COMPRESSIBLE FLOWS**

**Kenneth W. Smith
Office of the Assistant for Study Support
Kirtland Air Force Base, New Mexico**

**Victor J. Skoglund
Department of Mechanical Engineering
The University of New Mexico**

**Approved for public release;
distribution unlimited**

id

FOREWORD

This research project of numerical techniques and solutions for axisymmetrical viscous compressible flows was initiated in January 1969 as a part of a doctoral program in Mechanical Engineering at the University of New Mexico with support by the Air Force. The original manuscript was submitted to the University of New Mexico by Dr. Kenneth W. Smith as his doctoral dissertation. Professor Victor J. Skoglund, Department of Mechanical Engineering, served as the faculty advisor and collaborated in this research.

Viscous compressible flows around blunt bodies are of primary interest in a number of relevant aerospace applications including, for example, missile design and reentry of missile warheads. Functional solutions for these flows are inaccurate because of necessary mathematical simplifications and detailed measurements of flow characteristics are difficult and costly. In this investigation, a complete set of numerical techniques for axisymmetrical, viscous, compressible flows around blunt bodies is presented and accurate solutions are obtained.

Publication of this report does not constitute Air Force approval of the reported findings or conclusions. It is published only for the exchange and stimulation of ideas.

ABSTRACT

The purpose of this investigation was to develop numerical techniques for solving axisymmetrical, viscous, compressible flow around blunt bodies. Solutions were limited to systems of ideal gases with laminar unseparated boundary layers. The bow wave was represented by a moving discontinuity. The remainder of the system was represented by second order accuracy, time dependent difference equations. In this investigation the difference equations were derived from basic time dependent, viscous compressible flow equations that were transformed into body related coordinates. In a development phase, many numerical techniques were tested on digital computers before adopting the ones that were used in obtaining the results that are presented. The addition of stabilizing terms to basic difference equations was used to achieve numerical stability. Numerical experiments were performed to minimize the effect of the stabilizing terms on the results.

Solutions for a hemisphere forebody were obtained at Mach 2 and 4 for inviscid flow and for several Reynolds numbers. At Mach 4, solutions were obtained for a hemisphere-cylinder for inviscid flow and for a Reynolds number of 4000. Where possible, calculated and experimental results were compared. Their agreement was satisfactory. Prior solutions of viscous compressible flow in the afterbody region of blunt bodies were not found in any publication.

It was concluded that accurate solutions for axisymmetrical, viscous, compressible flows can be obtained in the forebody and afterbody regions of blunt bodies using the time dependent numerical techniques of this investigation. In the forebody region of a hemisphere-cylinder, approximate solutions may be obtained by solving the forebody system alone. Stabilization of the modified Lax-Wendroff technique seemed necessary, but improvements in wave fitting, boundary and digitizing techniques might eliminate that need.

TABLE OF CONTENTS

	<u>Page</u>
1. INTRODUCTION	1
1.1 Motivation	1
1.2 Purpose	1
1.3 Scope	2
2. REVIEW	4
2.1 Introduction	4
2.2 Initial Values	7
2.2.1 Initial Bow Wave	7
2.2.2 Boundary Layer	7
2.3 Differencing Techniques	8
2.3.1 Introduction	8
2.3.2 Lax-Wendroff Differencing Technique.	9
2.3.3 Aungier Differencing Technique	10
2.4 Wave Fitting	11
2.5 Numerical Solutions of Blunt Body Systems	11
2.6 Experimental Results	19
2.7 Summary.	20
3. THEORY	22
3.1 Introduction	22
3.1.1 System	22
3.2 Basic Differential Equations	23
3.3 Coordinate Transformations	25
3.3.1 Introduction	25

TABLE OF CONTENTS (cont)

	<u>Page</u>
3.3.2 Body Related Coordinates.	25
3.3.3 Nonlinear Coordinate Transformations.	27
3.4 Transformation of Differential Equations	28
3.4.1 Introduction.	28
3.4.2 Inviscid Equations	28
3.4.3 Viscous Equations	31
3.4.4 Equations Along the Stagnation Streamline	35
3.5 Method of Characteristics.	37
4. NUMERICAL TECHNIQUES.	41
4.1 Introduction	41
4.2 Initial Values	42
4.2.1 Initial Bow Wave Coordinates	42
4.2.2 Coordinates of Nodes.	44
4.2.3 Boundary Layer	46
4.2.4 Initial Field Values	48
4.3 Field Equations	48
4.3.1 Introduction.	48
4.3.2 Lax-Wendroff Technique	49
4.3.3 Aungier Technique.	53
4.3.4 Approximations of Derivatives	53
4.4 Equations Along the Stagnation Streamline.	55

TABLE OF CONTENTS (cont)

	<u>Page</u>
4.5 Stabilizing Terms	57
4.5.1 Introduction	57
4.5.2 Lapidus Stabilizing Term.	58
4.5.3 Aungier Stabilizing Term.	59
4.6 Bow Wave Technique	61
4.6.1 Bow Wave Equations	61
4.6.2 Iteration Techniques	65
4.7 Boundary Equations.	66
4.7.1 At the Downstream Boundary	66
4.7.2 At the Body Surface with Viscous Flow . . .	68
4.7.3 At the Body Surface with Inviscid Flow . . .	69
5. COMPUTATIONS AND RESULTS	72
5.1 Introduction	72
5.2 Computer Codes	74
5.2.1 INITIAL	74
5.2.2 MAIN.	81
5.2.3 Computational Times.	84
5.3 Stabilization of Computations	85
5.3.1 Introduction.	85
5.3.2 Unstabilized Computations	85
5.3.3 Development of Stabilizing Terms	91

TABLE OF CONTENTS (cont)

	<u>Page</u>
5.4 Accuracy.	106
5.4.1 Comparisons with Measurements.	106
5.4.2 Comparison with Calculated Results of Others	113
5.5 Results	114
5.5.1 Introduction	114
5.5.2 Results for a Hemisphere	114
5.5.3 Results for a Hemisphere-Cylinder	123
5.6 Summary of Results	143
6. CONCLUSIONS.	145
REFERENCES.	146

LIST OF FIGURES

<u>Figure</u>		<u>Page</u>
1	Specifications of the Blunt Body System. . .	22
2	Body Related Coordinate System.	26
3	$\hat{\eta}$ and $\hat{\xi}$ Coordinate Frame.	38
4	Blunt Body System	43
5	Digitized System.	43
6	Curvature κ of a Hemisphere-Cylinder . . .	55
7	Characteristic at the Bow Wave	63
8	Location of $\omega_w (\lambda_{\ell+1})$	67
9	Characteristic at Body Surface	70
10	INITIAL Code	76
11	Computed and Experimental Bow Wave Coordinates at $M_o = 4$	77
12	Initial Values of Body Pressure for $M_o = 4$.	79
13	Initial Values of Velocity Thickness ω_e of Boundary Layer for $M_o = 4$ and $Re_o = 4000$.	80
14	MAIN Code	82
15	Percentage of Computer Time for Wave Fitting	84
16	Instabilities in Forebody Region at $I = 3$. Run 1. Viscous Flow around a Hemisphere with $\psi_i = 0$	87
17	Instabilities in Afterbody Region at $I = 19$. Run 2. Viscous Flow around a Hemisphere- Cylinder with $\psi_i = 0$	88

LIST OF FIGURES (cont.)

<u>Figure</u>		<u>Page</u>
18	Instability in Forebody Region at $I = 3$. Run 3. Inviscid Flow around a Hemisphere with $\psi_i = 0$	89
19	Instability in Afterbody Region at $I = 19$. Run 4. Inviscid Flow around a Hemisphere- Cylinder with $\psi_i = 0$	90
20	Computed and Experimental Body Surface Pressures around Hemisphere-Cylinder. $M_o = 4$	91
21	Computed and Experimental Bow Wave Coordinates around Hemisphere-Cylinder. $M_o = 4$	97
22	Body Surface Pressures Near Junction of Hemisphere-Cylinder. $M_o = 4$	98
23	Computed v-velocities. Near Junction at $I = 16$. Inviscid Flow around Hemisphere- Cylinder. $M_o = 4$	99
24	Viscous Term ϕ_2 and Stabilizing Term ψ_2 at $I = 8$ and $K = 2000$. Run 11. Hemisphere at $M_o = 4$ and $Re_o = 10^4$. Computed by Section 4.3.2 with Equation 116	100
25	Viscous Term ϕ_3 and Stabilizing Term ψ_3 at $I = 8$ and $K = 2000$. Run 11. Hemisphere at $M_o = 4$ and $Re_o = 10^4$. Computed by Section 4.3.2 with Equation 116	101
26	Viscous Term ϕ_4 and Stabilizing Term ψ_4 at $I = 8$ and $K = 2000$. Run 11. Hemisphere at $M_o = 4$ and $Re_o = 10^4$. Computed by Section 4.3.2 with Equation 116	102
27	Pressure Oscillations at $I = 19$. Hemisphere- Cylinder at $M_o = 4$ and $Re_o = 10^4$. Computed by Section 4.3.2	103

LIST OF FIGURES (cont)

<u>Figure</u>		<u>Page</u>
28	Viscous Term ϕ_2 and Stabilizing Term ψ_2 at $I = 19$ and $K = 1400$. Run 13. Hemisphere- Cylinder at $M_0 = 4$ and $Re_0 = 10^4$. Computed by Section 4.3.2 with Equation 110	104
29	Viscous Term ϕ_2 and Stabilizing Term ψ_2 at $I = 24$ and $K = 800$. Run 15. Hemisphere- Cylinder at $M_0 = 4$ and $Re_0 = 4000$. Computed by Section 4.3.2 with Equation 116	105
30	Computed and Experimental Bow Wave Coordinates around Hemisphere. $M_0 = 2$. . .	108
31	Computed and Experimental Body Surface Pressures around Hemisphere. $M_0 = 2$. . .	109
32	Boundary Layer Velocity Ratios around Hemisphere at $M_0 = 2$ and $Re_0 = 10^4$	110
33	Boundary Layer Velocity Ratios around Hemisphere at $M_0 = 2$ and $Re_0 = 10^4$	111
34	Boundary Layer Velocity Ratios around Hemisphere at $M_0 = 2$ and $Re_0 = 10^4$	112
35	Standoff Distance for Flow around a Hemi- sphere at $M_0 = 4$. Computed by Section 4.3.2	117
36	Body Surface Pressures of Hemisphere at $M_0 = 4$	118
37	Boundary Layer Displacement Thicknesses for Hemisphere at $M_0 = 4$. Computed by Section 4.3.2 and Equation 116	119
38	u-velocities for Hemisphere at $M_0 = 4$ and $\theta_c = 32.8$. Computed by Section 4.3.2 and Equation 116	120

LIST OF FIGURES (cont)

<u>Figure</u>		<u>Page</u>
39	Pressures for Hemisphere at $M_o = 4$ and $\theta_c = 32.8^\circ$. Computed by Section 4.3.2 and Equation 116	121
40	Temperatures for Hemisphere at $M_o = 4$ and $\theta_c = 32.8^\circ$. Computed by Section 4.3.2 and Equation 116	122
41	Mach Number Contours for Hemisphere-Cylinder at $M_o = 4$ and $Re_o = 4000$. Run 15. Computed by Section 4.3.2 and Equation 116	127
42	Temperature Contours for Hemisphere-Cylinder at $M_o = 4$ and $Re_o = 4000$. Run 15. Computed by Section 4.3.2 and Equation 116	128
43	Pressure Contours for Hemisphere-Cylinder at $M_o = 4$ and $Re_o = 4000$. Run 15. Computed by Section 4.3.2 and Equation 116.	129
44	Entropy Contours for Hemisphere-Cylinder at $M_o = 4$ and $Re_o = 4000$. Run 15. Computed by Section 4.3.2 and Equation 116.	130
45	Boundary Layer Displacement and Momentum Thickness for Hemisphere-Cylinder at $M_o = 4$ and $Re_o = 4000$. Run 15. Computed by Section 4.3.2 and Equation 116.	131
46	u-velocities for Hemisphere-Cylinder at $M_o = 4$ and $Re_o = 4000$. Run 15. Computed by Section 4.3.2 and Equation 116	132
47	v-velocities in Forebody Region of Hemisphere-Cylinder at $M_o = 4$ and $Re_o = 4000$. Run 15. Computed by Section 4.3.2 and Equation 116	133

LIST OF FIGURES (cont)

<u>Figure</u>		<u>Page</u>
48	v-velocities in Afterbody Region of Hemisphere-Cylinder at $M_0 = 4$ and $Re_0 = 4000$. Run 15. Computed by Section 4.3.2 and Equation 116	134
49	Temperature for Hemisphere-Cylinder at $M_0 = 4$ and $Re_0 = 4000$. Run 15. Computed by Section 4.3.2 and Equation 116	135
50	u-velocities in Forebody Region of Hemisphere-Cylinder at $I = 8$ with and without Stabilizing Terms. Computed by Section 4.3.2. $M_0 = 4$ and $Re_0 = 4000$	136
51	v-velocities in Forebody Region of Hemisphere-Cylinder at $I = 8$ with and without Stabilizing Terms. Computed by Section 4.3.2. $M_0 = 4$ and $Re_0 = 4000$	137
52	Pressures in Forebody Region of Hemisphere-Cylinder at $I = 8$ with and without Stabilizing Terms. Computed by Section 4.3.2. $M_0 = 4$ and $Re_0 = 4000$	138
53	Pressure versus K Index at $I = 19$, $J = 26$. Computed by Section 4.3.2. $M_0 = 4$ and $Re_0 = 4000$	139
54	u-velocities in Afterbody Region of Hemisphere-Cylinder at $I = 19$ with and without Stabilizing Terms. Computed by Section 4.3.2. $M_0 = 4$ and $Re_0 = 4000$	140
55	v-velocities in Afterbody Region of Hemisphere-Cylinder at $I = 19$ with and without Stabilizing Terms. Computed by Section 4.3.2. $M_0 = 4$ and $Re_0 = 4000$	141
56	Pressures in Afterbody Region of Hemisphere-Cylinder at $I = 19$ with and without Stabilizing Terms. Computed by Section 4.3.2. $M_0 = 4$ and $Re_0 = 4000$	142

LIST OF TABLES

<u>Table</u>		<u>Page</u>
1	Systems	73
2	Specifications of Computer Runs	75
3	Percentage Differences of Computations and Measurements	107
4	Percentage Differences of Computed Results of this Investigation and Others. . .	114
5	Percentage Differences of Computed Results of Hemisphere and Hemisphere- Cylinder. Runs 15 and 19, $M_o = 4$, $Re_o = 4000$	125

LIST OF SYMBOLS

a	acoustic speed
a_{ij}	$= \partial G_i / \partial f_j$ jacobian with respect to conservative variables
b_{ij}	$= \partial H_i / \partial f_j$ jacobian with respect to conservative variables
\underline{B}	specific body force per unit volume
B_i	nonconservative term of flow equation
c_1, c_2	constants in method of characteristics
c_{ij}	$= \partial B_i / \partial f_j$ jacobian with respect to conservative variables
C_i	constants in stabilizing terms
C_ℓ	coefficient relating μ and T
C_λ, C_ω	coefficient of interpolation with respect to λ and ω
d_w	standoff distance of bow wave
e	number of increments
$e_{\lambda\lambda}, e_{\lambda\omega}$ $e_{\omega\omega}, e_{\varphi\varphi}$	elements of the rate of strain tensor
f	Cohen and Reshotko function of a boundary layer
f_i	$= \rho, m, n$ or S
g	Cohen and Reshotko function of a boundary layer
G_i	conservative term of flow equations
h	coordinate scale factor

LIST OF SYMBOLS (cont)

H_i	conservative term of flow equations
I	index of node
I	idemfactor
\approx	
IF	index of node in forebody
J	index of node
k	thermal conductivity
k_i	transformation coefficients
K	index of time
L_{ij}	parameter of stabilizing term
m	= $\rho u \lambda$ momentum per unit volume
M	Mach number
n	= $\rho v \omega$ momentum per unit volume
p	pressure
Pr	Prandtl number
\dot{Q}	heat flux
r	radius
r_o	maximum body radius
Re_a	= $\rho_o a_o r_o / \mu_o$ a Reynolds number
Re_o	= $\rho_o v_o r_o / \mu_o$ a Reynolds number
s	entropy per unit mass
S	= ρs entropy per unit volume
t	time

LIST OF SYMBOLS (cont)

T	temperature
u	λ component of velocity
v	ω component of velocity
v^η, v^ξ	η and ξ components of velocity
w	bow wave speed normal to the wave
x	coordinate parallel to centerline of body
X	variable of a combination of Mangler and Stewartson transformations
α	parameter of λ coordinate transformation in equation 13 or an angle
α_c	compressibility factor in equation 73
α_i	parameter in equations 111 and 125
β	parameter of ω coordinate transformation in equation 14, an angle, or a characteristic variable
β_c	Cohen and Reshotko compressibility factor of equation 73
γ	ratio of specific heats
δ^*	boundary layer displacement thickness
$\delta_{ij}, \delta_{\alpha\beta}$	kroncker delta
Δ	increment
ζ	transformed λ coordinate of equation 13
η	coordinate normal to bow wave, Cohen and Reshotko similarity variable or bulk viscosity

LIST OF SYMBOLS (cont)

θ	angle between $\hat{\lambda}$ and \hat{x}
κ	$= -d\theta/d\lambda$ body curvature
K_{su}	Sutherland constant
λ	coordinate tangent to body
Λ	tabulated Cohen and Reshotko function
μ	shearing viscosity
ν	transformed ω coordinate of equation 14
ξ	coordinate tangent to bow wave
$\dot{\mathbb{H}}$	rate of strain dyad
ρ	density
$\sigma_{\eta}, \sigma_{\omega}$	parameters of characteristic equations 60 and 62
τ	$= t$ time
ϕ	angle from y to r coordinate axes
ϕ_i	diffusion term of flow equations
Φ	viscous stress dyad
χ	orthogonal curvilinear coordinate
ψ_i	stabilizing term
ω	coordinate normal to body
∇	vector operator del
Subscripts	
a	average, Aungier or referred to acoustic speed

LIST OF SYMBOLS (cont)

b	body surface
e	edge of boundary layer
i	index
j	junction of hemisphere-cylinder or index
l	downstream boundary
o	reference value
s	stagnation point
t	time
w	bow wave
α, β	indices
ζ	perturbation
η	η direction or coordinate
λ	λ direction or coordinate
ν	ν direction or coordinate
ξ	ξ direction or coordinate
τ	time
ω	ω direction or coordinate
1	upstream of bow wave
2	downstream side of bow wave
,	partial derivative with respect to variables which follow
Superscripts	
-	forward difference

LIST OF SYMBOLS (cont)

- backward difference
- average
- ' intersection of characteristic β with axis or derivative with respect to η
- substantial derivative $f_{i,t} + v_j f_{i,j}$

1. INTRODUCTION

1.1 Motivation

Analysis of the performance of supersonic vehicles is required in their design. Their flow fields are complicated by detached bow waves and by complex flow fields behind the waves which interact with viscous boundary layers. Functional solutions for viscous, compressible flow about blunt bodies are inaccurate because of necessary mathematical simplifications. Accurate measurements are costly and difficult, particularly detailed measurements of flow characteristics. In addition, most measurements are limited to special systems and may not apply to a new design. Recently, numerical analysis has become a valuable supplement to other types of analyses and experiments. When better numerical techniques are developed and larger and faster computers become available, they may become the main analytical tools of designers of supersonic vehicles. Numerical techniques have been developed and solutions reported for viscous, compressible, supersonic flow in the forebody region of a two dimensional body. In this investigation, a complete set of numerical techniques was developed for axisymmetrical, viscous, compressible flow around blunt bodies.

1.2 Purpose

The purpose was to develop numerical techniques for axisymmetrical viscous, compressible flows in both the forebody and afterbody region of blunt bodies.

1.3 Scope

The investigation included development of numerical techniques and solutions of axisymmetrical, viscous, compressible flows around hemispheres and hemisphere-cylinders. The solutions were restricted to systems of ideal gases with laminar unseparated boundary layers.

In the development phase, the time dependent differencing technique of Lax and Wendroff [45, 1960]¹ was used to represent the basic flow equations which were expressed in terms of body related coordinates. The detached bow wave was represented by a moving discontinuity. It was coupled to the digitized field by a wave fitting technique. The addition of stabilizing terms to the difference equations was used to achieve numerical stability. Numerical experiments were used to minimize the effect of stabilizing terms on results.

Solutions were obtained for hemispheres at Mach 2 and 4 for inviscid flows and Reynolds numbers from 10^3 to 10^5 . Inviscid flow results agreed with measurements of Baer [4, 1961]. Computed velocities in the boundary layer agreed with measurements of Wells and Blumer [75, 1968]. Solutions were also obtained for a hemisphere-cylinder for Mach 4 for inviscid flow and a Reynolds number of 4000. A steady solution for a hemisphere-cylinder was used as the initial condition for a subsequent solution in which the stabilizing terms were zero.

¹ Numbers in brackets [] designate references listed at the end of this report.

The "Review" section describes previous research that was pertinent to this investigation. The "Theory" section presents the basis of the adopted numerical techniques. The section on "Numerical Techniques" presents the equations that were the basis of computer programs. The "Computations and Results" section describes computer programs and the data and results of this investigation.

2. REVIEW

2.1 Introduction

The procedure used in the "Review" was to first survey titles and secure abstracts of literature pertinent to solutions of blunt body systems. From these titles and abstracts, literature was selected for further study. Using the literature that was collected, different methods of solving for the flow about blunt body systems were studied. From this study, the explicit time dependent method was selected as the method to be used in this investigation. The purpose of this "Review" section is to summarize information that was useful in this investigation. Topics that are covered are methods for obtaining initial values, explicit time dependent differencing techniques, wave fitting, prior solutions and experimental results for blunt body systems.

Studies of the literature collected were focused on the advantages and disadvantages of available methods for solving axisymmetrical, viscous, compressible flows. Without high speed computers, the extent of early computations was limited. One of the common methods used to solve for viscous flow around a blunt body system is to divide the shock layer into an inviscid and viscous region. Basic textbooks on boundary layer theory by Schlichting [63, 1966] and Rosenhead [42, 1963] deal with the Prandtl boundary layer theory in which the inviscid solution is matched with the viscous flow next to solid surfaces. In solving axisymmetrical, viscous, compressible flows early methods required many assumptions and results were only approximate. Recent availability

of high speed digital computers has permitted more accurate solutions in which functional and numerical methods are combined. The literature on these methods is extensive. A few examples are given in [32, 1955; 41, 1959; 23, 1964; 28, 1968; 22, 1968; and 25, 1969] in which an inviscid flow solution provides boundary conditions for the boundary layers. Functional methods involve assumptions and provide only approximate solutions of the inviscid flow. Hayes and Probstein [38, 1966] deal with methods of solving inviscid flow systems.

More accurate solutions of viscous compressible flows are obtained by using finite differences to approximate the governing partial differential equations of a system. In addition to the solution accuracy gained by using numerical methods, flexibility is improved in representing boundary conditions. Numerical techniques were selected for use in this investigation because of their accuracy and flexibility. Numerical techniques and solutions are described in sections 2.3 and 2.5.

In the study of numerical techniques, attention was focused on their advantages and disadvantages for blunt body systems including differencing and initial and boundary conditions. After studying the literature, a class of explicit, time dependent, finite difference techniques was selected to be used in this investigation. The reason for this selection was that implicit methods involve simultaneous solutions of all nodal data points and are more difficult to program for a digital computer than the straightforward explicit finite difference approach.

For some systems, implicit methods require less computer time, but implicit methods have not been successfully applied to viscous compressible flows. For viscous flow around a blunt body, coordinate transformations are often used which complicate the governing partial differential equation. The explicit finite difference technique lends itself to simple treatment of these complicated equations. Therefore, an explicit, time dependent, differencing technique was selected because of its greater flexibility and mathematical simplicity. Another advantage of finite differencing partial differential equations in time dependent form is that these equations are hyperbolic regardless of Mach number. This is especially advantageous for viscous compressible flows where there are regions of mixed subsonic and supersonic flow.

In the explicit time dependent technique selected for use in this investigation, dependent functionals, such as velocity and temperature, are determined only at a finite number of locations which are called nodes. A solution is started with initial values specified at all nodes. Later values are calculated by repeated application of the difference equations that are analogs of the governing partial differential equations for specific time increments. Boundary conditions must also be represented in finite difference form. Shock waves in the system may be represented by the difference equations which spread the wave over several nodes. Waves may also be represented as discontinuities in which the Rankine-Hugoniot equations apply.

Experimental results of previous investigations were studied for

comparison with those of this investigation. Only steady flow results from wind tunnel experiments were available. A special effort was made to obtain results for $2 \leq M \leq 4$ where gas properties are related by ideal gas equations.

2.2 Initial Values

2.2.1 Initial Bow Wave. Bow wave coordinates are required to specify initial values. Moretti, et al. [51, 1968; 52, 1968; 53, 1968] used relatively crude methods to initially estimate bow wave coordinates for an inviscid solution. Viscous systems require small nodal and time increments which result in long computing times for convergence. Therefore, a more accurate determination of the initial bow wave coordinates was desirable in the subject investigation. An accurate method of predicting bow wave coordinates was given by Moeckel [50, 1949] and Love [46, 1957]. Their techniques involve a combination of empirical and functional methods which are relatively simple to code for a digital computer.

2.2.2 Boundary Layer. A method for calculating laminar compressible boundary layers of a blunt body was needed in determining initial values. Many methods were reviewed and rejected as either being too complicated or too restrictive in flow conditions [32, 1955; 23, 1964; 27, 1953; 14, 1949]. The Cohen and Reshotko [19, 1955] results compared favorably with the experimental boundary layer velocities of Wells and Blumer [75, 1968]. Cohen and Reshotko present tables of a two dimensional solution for Prandtl Number = 1 and constant body temperature.

Pressure gradients are allowed from the infinitely favorable to the adverse gradients of separation. Results are given for body surface temperatures from absolute zero to twice the free stream stagnation value. Recently, their tables have been extended by Christian, Hankey and Petty [15, 1970]. The tables of both references involve the assumption that the inviscid velocity at the edge of the boundary layer is

$$u_e = \Gamma \lambda^m \quad (1)$$

Here Γ and m are constants and λ is the distance along the body surface. In utilizing the tables, segments of the boundary layer were matched to equation 1.

2.3 Differencing Techniques

2.3.1 Introduction. Basic theorems for stability and convergence of difference equations were derived by Courant, Fredricks and Lewy [20, 1928]. Von Neumann [73, 1944] suggested that hyperbolic partial differential equations representing mixed subsonic and supersonic flows could be solved by finite difference equations. Von Neumann and Richtmyer [74, 1950] added a stabilizing term to their difference equations to stabilize the numerical solution. Stabilizing terms have been developed which do not seriously degrade accuracy except in the vicinity of shock waves. Lax [44, 1954] systematically developed differencing techniques applicable to strong shock waves, but the waves are spread over several nodes. Rusanov [61, 1962] minimized the stabilizing term used by Lax to improve accuracy. However,

Emery [30, 1967] reported that computations using Rusanov's technique were unstable after long time periods. Aungier [1, 1970] developed simple stabilizing terms as a variation of Lax's method and his results for inviscid flows compared very favorably with those of experiments and with those of the method of characteristics. Lax and Wendroff [45, 1960] reported a differencing technique of second order accuracy which has been widely used both in its original and modified forms. Other time dependent differencing techniques have been introduced by Godunov [35, 1959], MacCormack [47, 1969] and Crocco [21, 1965].

After studying the available differencing techniques, the one of Lax-Wendroff was selected for differencing the field equations in this investigation. It was selected because successful applications have been reported for both inviscid and viscous flow systems.

2.3.2 Lax-Wendroff Differencing Technique. Lax and Wendroff truncated a Taylor expansion to yield difference equations of second order accuracy. The technique is described in detail in section 4.3.2.

Burstein [12, 1965] used the Lax-Wendroff technique to solve for the inviscid, two dimensional flow over a body with a square nose. In his solution, instabilities occurred near the detached shock and sonic line. Burstein eliminated the instabilities by adding stabilizing terms to the Lax-Wendroff difference equations. Lapidus [43, 1967] calculated the characteristics of inviscid flow over a two dimensional cylinder using a modified version of the Lax-Wendroff technique. Lapidus also experienced difficulties in stabilizing his solution.

However, he developed stabilizing terms which were less complicated than those of Burstein, and he succeeded in obtaining a solution. The stabilizing technique of Lapidus is described in section 4.5.2.

Skoglund, Cole and Staiano [65, 1967] developed methods for solving for the interaction of an oblique shock wave with a laminar boundary layer. Additional stabilizing terms were not necessary to achieve numerical stability for that system using the Lax-Wendroff technique. Later, Skoglund and Gay [66, 1969] extended the work to include separation of the boundary layer. Using the techniques of Skoglund, et al. [65, 1967], instabilities occurred in the separated region near the edge of the boundary layer. Numerical stabilization was accomplished by adding stabilizing terms that were derived from those of Lapidus [43, 1967].

Richtmyer and Morton [59, 1967], as well as Lapidus [43, 1967], proposed a two-step, Lax-Wendroff technique. Values are obtained at time $t + \frac{\Delta t}{2}$ using the first order technique of Lax [44, 1954]. Values at $t = t + \Delta t$ are calculated using centered time differences based on values at $t + \frac{\Delta t}{2}$. Erdos and Zakkay [31, 1969] used the two-step, Lax-Wendroff technique for solving an inviscid two dimensional flow in the near wake region. They added a stabilizing term to the difference equations of their second step in order to obtain a stable solution.

2.3.3 Aungier Differencing Technique. Aungier [1, 1970; 2, 1971; 3, 1968] developed a version of the Lax technique to solve for inviscid compressible flow about blunt bodies. His differencing technique is

described in section 4.3.2. The stabilizing term developed by Aungier is described in section 4.5.3.

2.4 Wave Fitting

As indicated by references [30, 1967; 39, 1954; 45, 1967; 65, 1967; 66, 1969; 74, 1950], representation of shock waves by difference equations results in spreading the wave over several nodes. For the blunt body system, it seems better to represent the bow wave as a discontinuity which satisfies the Rankine-Hugoniot equations. The latter technique is called wave fitting. An important problem of this technique is the coupling of the wave to the digitized field which is represented by difference equations. This technique was described by Richtmyer [64, 1961]. Moretti [52, 1966; 53, 1968; and 51, 1968] used a variation of Richtmyer's technique for blunt body systems. His method is explained in detail in [53, 1968].

2.5 Numerical Solutions of Blunt Body Systems

Solutions of blunt body systems using time dependent numerical techniques became feasible with the advent of high speed digital computers. An early paper of Burstein [12, 1965] was on inviscid compressible flow over a two dimensional, flat-nosed, blunt body. Free stream values were used for initial conditions, and the initial bow wave was at the body surface. The bow wave was represented by difference equations and was spread over several nodes. Burstein did not describe the techniques that he used for the body surface and at the downstream boundary. However, in an earlier paper [13, 1964], Burstein used a

reflection technique at the body surface and a backward differencing technique at the downstream boundary. Reflection techniques involve strings of nodes along the body surfaces and within the solid body. Absolute values at the nodes inside the body are set equal to the values at the first string of nodes outside of the body surface. Burstein used a variation of the two-step, Lax-Wendroff differencing technique for points in the field. Numerical instabilities occurred in the stagnation region, near the bow wave and near the downstream boundary. The solution was stabilized by adding stabilizing terms to the differencing equations.

Bohachevsky and Rubin [8, 1966] used a Lax differencing technique [44, 1954] to solve for the nonequilibrium inviscid flow over a variety of two dimensional and axisymmetrical bodies. The grid system was extended well beyond the expected bow wave into the free stream. The outer and downstream boundaries were treated in the following different ways: (1) first derivatives zero, (2) second derivatives zero, (3) reflection technique and (4) the boundary was left free. The results were approximately the same for all of these techniques. They concluded that the choice was unimportant as long as the flow at the boundary was supersonic. Body surface nodes were treated using the reflection techniques of Burstein [13, 1964]. Shock waves were represented by difference equations. Bohachevsky and Rubin did not report any trouble with numerical instabilities. However, their results were inaccurate in the stagnation region. Bohachevsky and Rubin ascribed

the errors to difficulties in differencing in spherical coordinates.

Later, Bohachevsky and Mates [7, 1966] extended the solution to include angles of attack. Additional problems were increased computer storage, further decrease in accuracy and large computer outputs. DeJarnette [24, 1966] also used the Lax technique to calculate inviscid nonequilibrium flow over a blunt body. DeJarnette limited his solution to supersonic regions and relied on some other solution to provide initial values downstream of the sonic line. Using a modified forward differencing technique at the body surface, he reported that results were more accurate than those of the reflection technique. However, DeJarnette's results show large perturbations downstream of the sonic line.

Although not reported by Bohachevsky and Rubin [8, 1966], according to an analysis by Moretti and Abbett [52, 1966], the required computer running time to calculate the flow around a step was approximately four hours on an IBM 7094. The number of nodes required to provide good resolution of the bow shock was 3588 and results after 650 cycles were presented in [8, 1966]; however, Moretti and Abbett maintained that in their opinion, convergence still had not occurred.

Moretti and Abbett represented the bow wave by a discontinuity. Since resolution near the wave was not a problem, the number of nodes in the field was reduced, and with fewer nodes, computational times were greatly reduced. Moretti and Abbett calculated inviscid flows over the forebody of various shapes. Initial values were obtained by

assuming a parabolic bow wave shape with the standoff distance being calculated on the basis of curvature. Initial values at the stagnation point were calculated by assuming isentropic flow behind the bow wave. Interpolations were used for values in the region between body surface and bow wave. Linear extrapolation was used at the downstream boundary. Values at the body surface were calculated using the method of characteristics. Mapping of the field into a rectangle was accomplished using a simple coordinate transformation. Moretti and Abbett used a Lax-Wendroff differencing technique. In order to speed convergence, the $\frac{\partial^2 f}{\partial t^2}$ term was arbitrarily multiplied by 2. Accurate results were obtained in the forebody region for two dimensional and axisymmetrical flows. Computer times varied from 15 seconds to 6 minutes on an IBM 7094 computer, depending on resolution. This vast improvement over the computational times of Bořachevsky and Rubin is due to a reduction in the number of nodes.

The foregoing report has served as a foundation for a series of reports by Moretti and others. Moretti and Bleich [53, 1968] extended the earlier techniques and obtained solutions for three dimensional inviscid flow around a blunt body. Their techniques were identical to those employed by Moretti and Abbett except that the need for a convergence term was not mentioned. A typical running time was thirty minutes on an IBM 7094 computer. A maximum of 594 nodes was used. From the results presented, it appears that convergence occurred within 300 to 500 cycles. Results were limited to the forebody region

because of limited computer storage. Later, Moretti [51, 1968] improved convergence and accuracy of the results of [53, 1968] by using spherical coordinates. This dependence of stability, convergence and accuracy on the coordinate system confirmed the findings of Bohachevsky and Rubin.

Moretti and Salas [54, 1969] extended the technique of Moretti and Abbett [52, 1966] to include viscosity and thermal conductivity. A nonlinear coordinate transformation was used to increase resolution of the boundary layer. The calculations of Moretti and Salas were limited to the forebody region of a two dimensional, circular cylinder. They used Lax-Wendroff differencing techniques in polar coordinates. In all cases, body temperature and viscosity were constant and Mach number was equal to 4. Reynolds numbers, that were referred to free stream conditions and body radius, ranged from 10^2 to 10^5 . A typical computing time was 4 minutes for 1000 cycles on a CDC 6600 computer. The number of cycles varied from 560 for $Re \leq 5000$ to 1500 for $Re > 5000$. In that time, convergence was not yet complete, but Moretti and Salas considered the results acceptable. Later, for the same system, Moretti and Salas [55, 1970] abandoned the Lax-Wendroff differencing technique in favor of the predictor-corrector one of MacCormack [47, 1969]. An equation written in terms of $\frac{\partial p}{\partial t}$ was used instead of the continuity equation. Even though coding was simplified, the reduction in computing time was not significant. Although no instabilities were reported, Moretti stated in a private communication that

instabilities occurred if the flow was not accelerating at the downstream boundary.

Scala and Gordon [62, 1968] obtained a solution for viscous compressible flow around a two dimensional cylinder using an explicit time dependent technique. Their technique involved a slight variation of the Crocco differencing technique [21, 1965]. The bow wave was represented by finite difference equations. The total number of computational nodes was large in order to achieve adequate resolution in the boundary layer. In one solution case, 637,000 nodal computations required twenty hours of IBM 7094 computer time.

Godunov [35, 1959] developed a time dependent technique which is supposedly an optimum combination of characteristic and difference equations. Godunov represented the bow wave by a discontinuity; however, in his calculations of the inviscid flow over a blunt body [36, 1961], the results were inaccurate near the stagnation point and the bow wave. Masson, Taylor and Foster [49, 1969] deduced that Godunov's treatment of the bow wave and body surface was incorrect. They obtained much better results using a slight variation of Moretti's technique for the bow wave and body surface. However, their results at and near the stagnation point were still in error. Aungier [1, 1970] also concluded that Godunov's technique does not properly represent physical conditions along stagnation streamlines of axisymmetric flows.

Lapidus [43, 1967] solved for the characteristics of inviscid flow over a two dimensional cylinder. Initial values including bow wave

coordinates were taken from the results of Swenson [69, 1964]. An unusual coordinate transformation was used to obtain a rectangular field. The bow wave was represented by difference equations. A two-step, Lax-Wendroff differencing technique was used for interior nodes. Instabilities occurred when linear extrapolation was used at the downstream boundary in early stages of the computation. Computations were stabilized by using an arbitrary technique for the initial 500 cycles. After 500 cycles, linear extrapolation was satisfactory. Instabilities also occurred near the stagnation point and near the bow wave that were similar to those reported by Burstein [12, 1965]. Lapidus used a simpler stabilizing term than the one used by Burstein. The difference of his results is as much as 30% from the more accurate ones of Swenson, even though Swenson's technique was used to calculate initial values.

Aungier [1, 1970] assumed that the initial bow wave was very close to the body and that its shape was the same as that of the body. Rankine-Hugoniot relationships and isentropic flow equations were used to obtain initial values in the field. Linear extrapolation was used at the downstream boundary. Forward differencing in terms of body related coordinates was used at the body surface. The field was segmented and a steady state was achieved in one segment before computing the next segment. The bow wave was represented by a discontinuity. Aungier was able to carry his time dependent inviscid solutions into the afterbody region. He reported that, within his knowledge, his time dependent solution was the first successful one for the afterbody region.

After deciding to use explicit, time dependent differencing techniques in this investigation, other numerical methods for blunt body systems were of little interest and are described only briefly. Van Dyke [72, 1958] gave a good survey of the early indirect inviscid methods in which the bow wave shape was assumed known and body shape was then part of the solution. A more accurate, but complicated, solution of a two dimensional, inviscid, blunt body system was given by Swenson [69, 1965]. Inouge and Lomax [39, 1962] solved for the inviscid flow over several blunt body shapes using an indirect method in the forebody region where the Mach number was less than 1.03. This solution was then used as a starting point for the method of characteristics for the remainder of the field. Calculated body pressures agreed closely with experiment in the forebody and afterbody regions. Slight deviations of calculated and experimental results occurred in the vicinity of the forebody-afterbody junction.

Dorodnitsyn [26, 1957] proposed a numerical method for non-linear flow equations which he called the method of integral relations. This method has been used by many investigators for inviscid flow [71, 1960; 70, 1963; 11, 1964; 6, 1965]. The method has an advantage of being direct, so that the bow wave coordinates are a part of the solution. Unfortunately, the method becomes extremely complex as the resolution in the shock layer is increased and, therefore, seems impractical for viscous systems.

2.6 Experimental Results

A large amount of experimental data has been collected for the flow over blunt bodies. However, reports containing data of both the body surface pressures and coordinates of the bow wave are scarce. Baer [4, 1961] conducted wind tunnel experiments on an AGARD Model E hemisphere cylinder configuration. Free stream Mach numbers ranged from 2 through 3 while Reynolds numbers varied from $.17 \times 10^6$ to $.51 \times 10^6$ per inch. In this report, coordinates of the bow wave are specified. In many other reports, only unscaled schlieren photographs are available.

Inouge and Lomax [39, 1962] summarized experimental results of Kendall [40, 1959], Kubota [42, 1957] and Baer [4, 1961]. Graphs of the bow wave, as well as body surface pressure distributions, for a hemisphere at $M = 4.76$, hemisphere cylinder at $M = 7.7$, sphere cone at $M = 4.95$, and a blunt ellipsoid-cylinder at $M = 5.12$ are presented.

Pressure distributions over hemisphere-cylinder bodies were given by Reichle [56, 1962] for Mach numbers varying from .4 to 5.0 and Reynolds numbers from $.36 \times 10^6$ to 1.2×10^6 . Unfortunately, bow wave coordinates are not available in this report. Cleary [17, 1965] measured pressures along several blunt cones at $M = 5.25$, 7.4, and 10.6. In addition, pitot pressures were measured in the shock layer for a 15° half angle blunt cone to study entropy layer thickness. Hasting, Parsh and Redman [37, 1957] measured body surface

pressures of flat faced cones and provided schlieren and shadow photographs of bow waves.

Experimental body pressures were compiled by Clark [16, 1966] for Mach numbers from 1.9 to 22 for spherical forebodies. Empirically correlated afterbody surface pressures were given by Eaves [29, 1968] for Mach numbers from 5 to 10.2. Forebody shapes consisted of hemispheres, flat faces, and round shouldered flat faces. Bow wave coordinates are not available in those reports.

Complete experimental boundary layer data are not available for axisymmetrical blunt bodies. Boundary layer velocities were measured by Wells and Blumer [75, 1968] for a hemisphere at $M = 2$, Reynolds number per inch from $.05 \times 10^6$ to $.5 \times 10^6$ and central body angles of 30, 50, 70 and 90 degrees. Total pressures were obtained with a pitot tube that was normal to the body surface. The reported uncertainty of the parameter $yD^{-1} \sqrt{Re_D}$ was ± 3 percent. Here, y is the distance normal to the body surface, D is the maximum diameter of the body and Re_D is a Reynolds number based on free stream static conditions and maximum body diameter. Body surface cooling was provided so that surface temperatures approximated the wind tunnel stagnation temperature to approximate an adiabatic body surface condition.

2.7 Summary

For inviscid flow, Aungier [1, 1970] was successful in obtaining time dependent solutions in the afterbody region of a blunt body. His results agree closely with measurements and those of the method of

characteristics. However, inviscid solutions of blunt body systems cannot provide boundary layer and heat transfer information.

Solutions of viscous flow about blunt bodies have been limited to two dimensional circular cylinders. In the case of Moretti and Salas [55, 1970], solutions were restricted to the forebody region with central angles less than 70° and with constant viscosity. Their treatment of bow waves as discontinuities reduced the computing time. The solutions of Scala and Gordon [62, 1968] required excessive computing times and were not verified by other methods. No viscous flow solutions were reported in the literature for the afterbody region of axisymmetrical bodies.

Experimental data are sparse and are not adequate for precise engineering. The most complete presentation of body pressures and bow wave coordinates was given by Baer [4, 1961] for a hemisphere cylinder. For blunt bodies, the only boundary layer experimental data found in the literature were those of Wells and Blumer [75, 1968].

3. THEORY

3.1 Introduction

3.1.1 System. For purposes of this investigation, a system is a specified section of matter that is being considered in a particular problem. The specifications of a system include initial values and boundary conditions.

Specifications for supersonic flow about a blunt body system are given in figure 1.

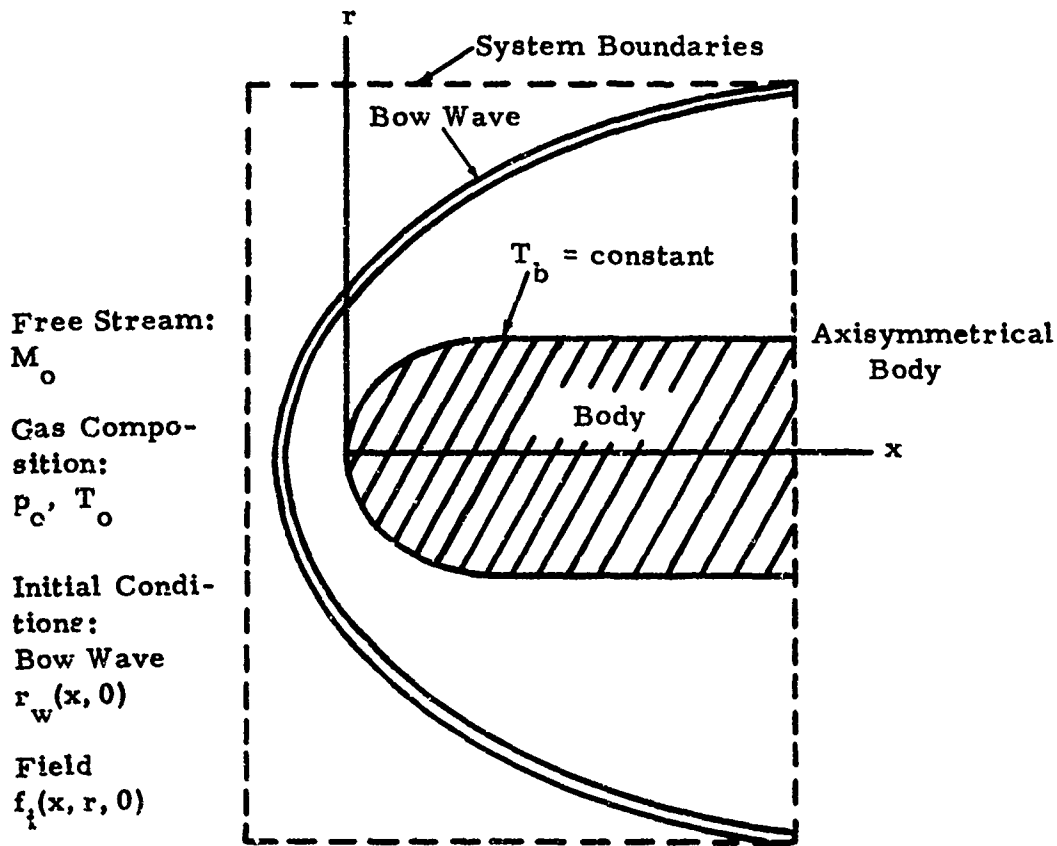


Figure 1. Specifications of the Blunt Body System

In developing time dependent numerical techniques, independent variables were x , r , t , and dependent variables were the radius of the bow wave $r_w(x, t)$ and field variables $f_i(x, r, t)$. Boundary conditions were those of the free stream and body surface. Initial values $r_w(x, 0)$ and $f_i(x, r, 0)$ were estimated to approximate steady values.

3.1.2 Scope. The problem was to calculate $r_w(x, t)$ and $f_i(x, r, t)$ as $t \rightarrow \infty$. The viscous compressible flow equations were the basis of calculations. The purpose of this chapter is to present the theory that was used in developing numerical techniques, including the basic differential equations, coordinate transformations and the method of characteristics.

3.2 Basic Differential Equations

From [64], the vector form of the basic, viscous, compressible flow equations are:

$$\frac{\partial \rho}{\partial t} + \nabla \cdot (\rho \mathbf{V}) = 0 \quad (2)$$

$$\rho \dot{\mathbf{V}} = \mathbf{B} + \nabla \cdot \mathbf{\Sigma} \quad (3)$$

$$\rho T \dot{s} = - \nabla \cdot \mathbf{Q} + \mathbf{\Phi} : \nabla \mathbf{V} \quad (4)$$

where: ρ is density

t is time

\mathbf{V} is velocity

$$\dot{\mathbf{V}} = \frac{\partial \mathbf{V}}{\partial t} + \mathbf{V} \cdot \nabla \mathbf{V}$$

\mathbf{B} is specific body force per unit volume which is negligible in systems of this investigation.

$\underline{\Sigma} = -p \underline{I} + \underline{\Phi}$ is stress dyad

$p = \rho RT$ is pressure

R is a gas constant

T is temperature

\underline{I} is idemfactor

$\underline{\Phi} = [(\eta - \frac{2}{3}\mu) \nabla \cdot \underline{V}] \underline{I} + 2\mu \underline{\Xi}$ is the viscous stress dyad

η is bulk viscosity which is negligible in systems of this investigation, [10]

μ is shearing viscosity

$\underline{\Xi} = \frac{1}{2} (\nabla \underline{V} + \underline{V} \nabla)$ is a rate of strain dyad

$\underline{V} \nabla$ is the transpose of $\nabla \underline{V}$

s is entropy

$\underline{Q} = -k \nabla T$ is heat flux

k is thermal conductivity.

Conversion from vector form into orthogonal curvilinear coordinates was accomplished using the following equations:

$$\nabla = \frac{\hat{x}_i}{h_i} \frac{\partial}{\partial x_{(i)}} \quad (5)$$

$$\nabla \underline{V} = \frac{\hat{x}_i}{h_i} (\hat{x}_j v_j)_{, (i)} \quad (6)$$

$$\nabla \cdot \underline{V} = \frac{1}{h_1 h_2 h_3} \frac{\partial}{\partial x_i} (h_j h_k v_i) \quad (7)$$

$$\frac{\partial \hat{\chi}_\alpha}{\partial x_\beta} = \frac{\hat{\chi}_\beta}{h_\alpha} \frac{\partial h_\beta}{\partial x_\alpha} - \delta_{\alpha\beta} \nabla h_\alpha \quad (8)$$

where: repetition of the English indices i or j without parenthesis

implies a summation of that term with indices 1, 2, 3

h_i is a scale factor of the coordinates

χ_i is an orthogonal curvilinear coordinate

$\delta_{\alpha\beta}$ is the kronecker delta.

3.3 Coordinate Transformations

3.3.1 Introduction. To simplify the solution of the blunt body system, body related coordinates λ and ω were used. In terms of them, the entire surface of any body is specified by $\omega_b = 0$. In the numerical solution of equations 2, 3 and 4, a concentration of nodes in the boundary layer and near the stagnation point is desirable for accurate resolution of those regions. This was accomplished with nonlinear coordinate transformations. In addition, treatment of the bow wave as a discontinuity was simplified by representing the bow wave as a grid line.

3.3.2 Body Related Coordinates. The body related coordinates λ and ω are shown in figure 2, where λ is the distance along the body from its nose and ω is the perpendicular distance from the body surface to a point in the system.

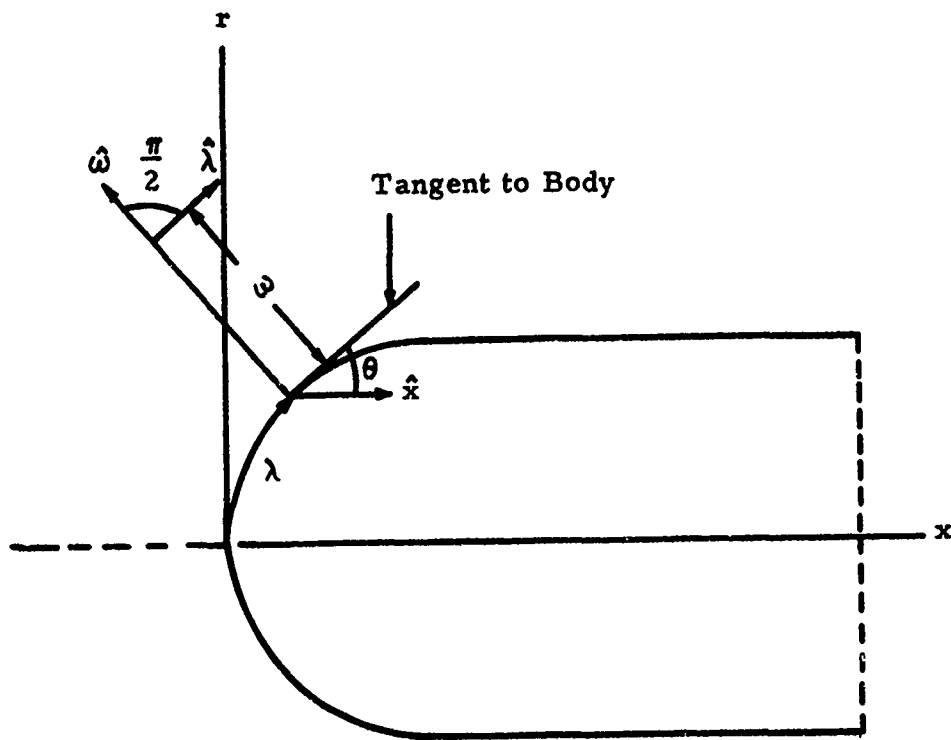


Figure 2. Body Related Coordinate System

At any point, the lines $\lambda = \text{constant}$ and $\omega = \text{constant}$ are perpendicular.

θ is the angle between the unit vectors $\hat{\lambda}$ and \hat{x} . The body curvature is

$$\kappa(\lambda) = -\frac{d\theta}{d\lambda} \quad (9)$$

The scale factors are:

$$\begin{aligned} h = h_{\lambda} &= 1 + \kappa\omega \\ h_{\omega} &= 1 \\ h_{\phi} &= r \end{aligned} \quad (10)$$

From figure 2,

$$r(\lambda, \omega) = \int_0^\lambda \sin \theta \, d\lambda + \omega \cos \theta \quad (11)$$

$$x(\lambda, \omega) = \int_0^\lambda \cos \theta \, d\lambda - \omega \sin \theta$$

In an axisymmetrical system, velocity

$$\vec{v} = u\hat{\lambda} + v\hat{\omega} \quad (12)$$

3.3.3 Nonlinear Coordinate Transformations. In the numerical analysis of a blunt body system, greater resolution is required near the stagnation point and body surface.

Skoglund, Cole and Staiano [65] and Staiano [67] demonstrated that nonlinear coordinate transformations of the differential equations yield satisfactory results for the interaction of an oblique shock wave and laminar boundary layer. The logarithmic transformations of Skoglund, Cole and Staiano were tried for the blunt body system. They were later modified, so that the bow wave was represented by a grid line. This simplified coupling of the bow wave to the digitized field.

The coordinate transformations that were used in the solution phase of the subject investigation are:

$$\zeta = \ln(\alpha\lambda + 1) \quad (13)$$

$$\nu = \ln \left[\beta \frac{\omega}{\omega_w(\lambda, t)} + 1 \right] \quad (14)$$

$$\tau = t \quad (15)$$

where: $\omega_w(\lambda, t)$ is the bow wave coordinate

α and β are constants

$$f_{i,t} = (f_{i,t})_{\lambda \omega}$$

$$f_{i,\tau} = (f_{i,\tau})_{\zeta \nu}$$

For equal increments of $\Delta\zeta$ and $\Delta\nu$, these transformations concentrate the grid lines near the stagnation point and body surface. The grid lines are represented by the grid line $\nu = \nu_w = \text{constant}$.

3.4 Transformation of Differential Equations

3.4.1 Introduction. The basic flow equations with diffusion were not available in the literature in terms of body related coordinates. The simplest method of expressing equations 2, 3 and 4 in body related coordinates is to use the scale factors of equation 10. A more tedious method is to use the chain rule for a total derivative. As a check, both methods were used. In these derivations, the inviscid and diffusion parts were treated separately. After expressing equations 2, 3 and 4 in terms of body related coordinates λ , ω and t , they were transformed into ζ , ν and τ using equations 13, 14 and 15.

3.4.2 Inviscid Equations. For inviscid flow, $\Phi = 0$ and $\Omega = 0$. In transforming equations 2 through 4 to a dimensionless form, reference variables are the maximum body radius r_0 , free stream acoustic

speed a_0 , density ρ_0 , temperature T_0 and dynamic viscosity μ_0 . In previous investigations [13, 43, 65, 66, 67], numerical stability was improved by using the following variables:

$$\begin{aligned} \rho & \\ m &= \rho u \\ n &= \rho v \\ E &= \rho \left[\frac{T}{\gamma(\gamma - 1)} + \frac{u^2 + v^2}{2} \right] \end{aligned} \tag{16}$$

where E is energy per unit volume.

In this investigation, an entropy equation was used instead of an energy equation. In that equation, the specific entropy per unit volume $S = \rho s$. By combining equations 2 through 12 and eliminating the reference variables, the axisymmetrical, dimensionless, inviscid flow equations are of the form:

$$f_{i,t} = \frac{1}{h} G_{i,\lambda} + H_{i,\omega} + B_i, \quad i = 1, 2, 3, 4 \tag{17}$$

where

$$f = \begin{vmatrix} \rho \\ m \\ n \\ S \end{vmatrix} \quad G = \begin{vmatrix} -m \\ -\frac{m^2}{\rho} - \frac{\rho\gamma}{\gamma} \exp\left(\frac{S}{\rho}\right) \\ -\frac{nm}{\rho} \\ -\frac{mS}{\rho} \end{vmatrix}$$

$$H = \begin{vmatrix} -n \\ -\frac{mn}{\rho} \\ -\frac{n^2}{\rho} - \frac{\rho\gamma}{\gamma} \exp\left(\frac{S}{\rho}\right) \\ -\frac{nS}{\rho} \end{vmatrix} \quad B = \begin{vmatrix} -\frac{\kappa n}{h} - \rho e_{\varphi\varphi} \\ -\frac{2\kappa}{\rho h} mn - m e_{\varphi\varphi} \\ -\frac{\kappa}{\rho h} (n^2 - m^2) - n e_{\varphi\varphi} \\ -\frac{\kappa n S}{\rho h} - S e_{\varphi\varphi} \end{vmatrix}$$

$$e_{\varphi\varphi} = \frac{1}{\rho r} (m \sin \theta + n \cos \theta).$$

The symbol $e_{\varphi\varphi}$ is used because this term appears in the rate of strain tensor.

In cartesian coordinates, the conservative form of the flow equations is $f_{i,t} = g_{i,x} + h_{i,y}$. Lax and Wendroff [45] demonstrated that the difference form of that equation satisfies the Rankine-Hugoniot relationships for a finite element and that truncation errors of these difference equations are dissipative. Equation 17 is in conservative form except for the B_i term.

From equations 13 through 15,

$$f_{,t} = -k_1 f_{,v} + f_{,r} \quad (18)$$

$$f_{,\lambda} = k_2 f_{,\zeta} - k_3 f_{,v} \quad (19)$$

$$f_{,\omega} = k_4 f_{,v} \quad (20)$$

$$\text{where: } k_1 = \beta e^{-\nu} \frac{\omega}{\omega_w} \omega_{w,t} \quad (21)$$

$$k_2 = \alpha e^{-\zeta} \quad (22)$$

$$k_3 = \alpha \beta e^{-(\zeta+\nu)} \frac{\omega}{\omega_w} \omega_{w,\zeta} \quad (23)$$

$$k_4 = \frac{\beta e^{-\nu}}{\omega_w} \quad (24)$$

From equations 17 through 24

$$f_{i,\tau} = k_1 f_{i,\nu} + \frac{k_2}{h} G_{i,\zeta} - \frac{k_3}{h} G_{i,\nu} + k_4 H_{i,\nu} + B_i \quad (25)$$

3.4.3 Viscous Equations. Viscous flow equations 2 through 4 have the form

$$f_{i,\tau} = k_1 f_{i,\nu} + \frac{k_2}{h} C_{i,\zeta} - \frac{k_3}{h} G_{i,\nu} + k_4 H_{i,\nu} + B_i + \varphi_i \quad (26)$$

where $\varphi_1 = 0$

$$\hat{\lambda} \varphi_2 + \hat{\omega} \varphi_3 = \nabla \cdot \Phi$$

$$\varphi_4 = -\nabla \cdot \underline{\underline{Q}} + \underline{\underline{\Phi}} : \nabla \underline{\underline{V}}$$

The derivation of these terms in body related coordinates was lengthy.

A few examples of the procedures are presented here. From equation 6,

$$\begin{aligned}
\nabla_{\sim} V &= \hat{\lambda} \frac{1}{h} (u\hat{\lambda} + v\hat{\omega})_{,\lambda} + \hat{\omega} (u\hat{\lambda} + v\hat{\omega})_{,\omega} + \frac{\hat{\phi}}{r} (u\hat{\lambda} + v\hat{\omega})_{,\phi} \\
&= \frac{1}{h} (u_{,\lambda} + \kappa v) \hat{\lambda} \hat{\lambda} + \left(\frac{1}{h} v_{,\lambda} - \frac{\kappa u}{h} \right) \hat{\lambda} \hat{\omega} + \\
&\quad (u_{,\omega}) \hat{\omega} \hat{\lambda} + (v_{,\omega}) \hat{\omega} \hat{\omega} + \frac{1}{r} (u \sin \theta + v \cos \theta) \hat{\phi} \hat{\phi}
\end{aligned}$$

Using the transpose of equation 27, the elements of the rate of strain tensor are:

$$e_{\lambda\lambda} = \frac{1}{h} (u_{,\lambda} + \kappa v) \quad (28)$$

$$e_{\lambda\omega} = e_{\omega\lambda} = \frac{1}{2} \left(\frac{1}{h} v_{,\lambda} + u_{,\omega} - \frac{\kappa u}{h} \right) \quad (29)$$

$$e_{\omega\omega} = v_{,\omega}$$

$$e_{\phi\phi} = \frac{1}{r} (u \sin \theta + v \cos \theta) \quad (31)$$

From equations 7 and 8,

$$\begin{aligned}
\nabla \cdot (\underline{T} \underline{\Xi}) &= \frac{1}{h} [T(e_{\lambda\lambda} \hat{\lambda} + e_{\lambda\omega} \hat{\omega})]_{,\lambda} \\
&+ [T(e_{\omega\lambda} \hat{\lambda} + e_{\omega\omega} \hat{\omega})]_{,\omega} + \frac{1}{r} (Te_{\varphi\varphi} \hat{\varphi})_{,\varphi} \\
&= \left[\frac{1}{h} (Te_{\lambda\lambda})_{,\lambda} + \frac{2\kappa e_{\lambda\omega} T}{h} + (Te_{\lambda\omega})_{,\omega} \right. \\
&\quad \left. + \frac{T}{r} (e_{\lambda\lambda} \sin \theta + e_{\lambda\omega} \cos \theta - e_{\varphi\varphi} \sin \theta) \right] \hat{\lambda} \\
&+ \left[\frac{1}{h} (Te_{\lambda\omega})_{,\lambda} + (Te_{\omega\omega})_{,\omega} + \frac{\kappa T}{h} (e_{\omega\omega} - e_{\lambda\lambda}) \right. \\
&\quad \left. + \frac{T}{r} (e_{\lambda\omega} \sin \theta + e_{\omega\omega} \cos \theta - e_{\varphi\varphi} \cos \theta) \right] \hat{\omega} \quad (32)
\end{aligned}$$

By similar methods, the diffusion terms of equation 26 are:

$$\varphi_1 = 0 \quad (33)$$

$$\begin{aligned}
\varphi_2 &= \frac{M_o C}{Re_o} \left\{ \frac{1}{h} \left[\frac{4}{3} (Te_{\lambda\lambda})_{,\lambda} - \frac{2}{3} (Te_{\omega\omega})_{,\lambda} - \frac{2}{3} (Te_{\varphi\varphi})_{,\lambda} \right. \right. \\
&\quad \left. \left. + 4 Te_{\lambda\omega} \kappa \right] + 2 (Te_{\lambda\omega})_{,\omega} + \frac{2T}{r} (\sin \theta e_{\lambda\lambda} + \cos \theta e_{\lambda\omega} \right. \\
&\quad \left. - \sin \theta e_{\varphi\varphi}) \right\} \quad (34)
\end{aligned}$$

$$\begin{aligned}
\varphi_3 &= \frac{M_o C}{Re_o} \left\{ -\frac{2}{3} (Te_{\lambda\lambda})_{,\omega} + \frac{4}{3} (Te_{\omega\omega})_{,\omega} - \frac{2}{3} (Te_{\varphi\varphi})_{,\omega} \right. \\
&\quad \left. + \frac{2}{h} (Te_{\lambda\omega})_{,\lambda} + \frac{2\kappa T}{h} (e_{\omega\omega} - e_{\lambda\lambda}) + \frac{2T}{r} (\sin \theta e_{\lambda\omega} \right. \\
&\quad \left. + \cos \theta e_{\omega\omega} - \cos \theta e_{\varphi\varphi}) \right\} \quad (35)
\end{aligned}$$

$$\begin{aligned}
\varphi_4 = \frac{M_o C_\ell}{T Re_o} & \left\{ \frac{\gamma}{Pr} \left[\frac{1}{h^2} (T T_{,\lambda})_{,\lambda} + (T T_{,\omega})_{,\omega} \right. \right. \\
& + \frac{1}{h} (T T_{,\lambda})_{,\lambda} \left(\frac{1}{h} \right)_{,\lambda} + \frac{\kappa T}{h} T_{,\omega} + \frac{T}{hr} (T_{,\lambda} \sin \theta \\
& + T_{,\omega} \cos \theta) \left. \right] + \gamma(\gamma - 1) T \left[\frac{4}{3} (e_{\lambda\lambda}^2 + e_{\omega\omega}^2 + e_{\varphi\varphi}^2 \right. \\
& \left. \left. - e_{\lambda\lambda} e_{\omega\omega} - e_{\lambda\lambda} e_{\varphi\varphi} - e_{\omega\omega} e_{\varphi\varphi}) + 4 e_{\lambda\omega}^2 \right] \right\} \quad (36)
\end{aligned}$$

where: M_o = free stream Mach number

$Re_o = \frac{\rho_o v_o r_c}{\mu_o}$ is free stream Reynolds number

$Pr = \frac{\mu c_p}{k}$ is Prandtl number

$\mu = C_\ell T$

$C_\ell = 1$ in this investigation.

From Sutherland's equation [63],

$$C_\ell = \frac{T_s + \kappa_{su}}{T_b + \kappa_{su}} \sqrt{\frac{T_b}{T_s}}$$

κ_{su} = Sutherland constant = 198.6° R for air

T_s = stagnation temperature

T_b = body temperature

In transforming equations 33 through 36 into coordinates ζ and

ν of equations 13 and 14, the second derivatives are:

$$\begin{aligned}
f_{i,\lambda\lambda} = k_3^2 (f_{i,\nu\nu} - f_{i,\nu}) - 2k_2 k_3 f_{i,\zeta\nu} - k_5 f_{i,\nu} \\
+ k_2^2 (f_{i,\zeta\zeta} - f_{i,\zeta}) \quad (37)
\end{aligned}$$

$$f_{i, \omega\omega} = k_4^2 (f_{i, \nu\nu} - f_{i, \nu}) \quad (38)$$

$$f_{i, \omega\lambda} = k_2 k_4 \left(f_{i, \zeta\nu} - \frac{\omega_w \zeta}{\omega_w} f_{i, \nu} \right) + k_3 k_4 (f_{i, \nu\nu} - f_{i, \nu}) \quad (39)$$

where: k_2, k_3, k_4 are given in equations 21 through 24.

$$k_5 = \frac{\omega}{\omega_w^2} \beta \alpha^2 e^{-(2\zeta+\nu)} \left[\omega_w \zeta \zeta - \omega_w \zeta - \frac{2}{\omega_w} (\omega_w \zeta)^2 \right]. \quad (40)$$

Complete difference equations were not derived. It was simpler to use equations 18 through 40 directly in computer codes.

3.4.4 Equations Along the Stagnation Streamline. Equation 26 is indeterminate along the stagnation streamline where $\lambda = 0$ because B_i and φ_i approach ∞ as r approaches 0. For symmetry about the stagnation streamline,

$$f_i \neq 0, \quad f_{i, \lambda} = 0, \quad f_{i, \lambda\lambda} \neq 0, \quad f_{i, \lambda\omega} = 0, \quad i = 1, 3, 4 \quad (41)$$

For $i = 2$,

$$u = 0, \quad u_{, \lambda} \neq 0, \quad u_{, \lambda\lambda} = 0, \quad u_{, \lambda\omega} \neq 0 \quad (42)$$

L'Hospital's rule is that if $f_1(\lambda)$ and $f_2(\lambda) \rightarrow 0$ as $\lambda \rightarrow 0$, then

$$\lim_{\lambda \rightarrow 0} \left[\frac{f_1(\lambda)}{f_2(\lambda)} \right] = \lim_{\lambda \rightarrow 0} \left[\frac{f_{1, \lambda}}{f_{2, \lambda}} \right] \quad (43)$$

In the following example of the application of L'Hospital's rule, at

$\lambda \neq 0$, $e_{\varphi\varphi} = \frac{1}{r} (u \sin \theta + v \cos \theta)$. At $\lambda = 0$, $r = 0$, $u = 0$, $\theta = \pi/2$ and

$$\lim_{\lambda \rightarrow 0} \left[\frac{u_{,\lambda} \sin \theta + u \cos \theta \frac{d\theta}{d\lambda} + v_{,\lambda} \cos \theta - v \sin \theta \frac{d\theta}{d\lambda}}{\sin \theta - \omega \sin \theta \frac{d\theta}{d\lambda}} \right] = e_{\varphi\varphi} \lambda = 0$$

From $h = 1 + \kappa\omega = 1 - \left(\frac{d\theta}{d\lambda}\right)\omega$,

$$\lim_{\lambda \rightarrow 0} \left[\frac{(u_{,\lambda} + \kappa v) \sin \theta + (v_{,\lambda} - \kappa u) \cos \theta}{h \sin \theta} \right] = e_{\lambda\lambda} \lambda = 0$$

By similar modifications of equations 17 and 26, at $\lambda = 0$

$$G = \begin{vmatrix} 0 \\ -\frac{\rho\gamma}{\gamma} \exp\left(\frac{S}{\rho}\right) \\ 0 \\ 0 \end{vmatrix} \quad H = \begin{vmatrix} -n \\ 0 \\ -\frac{n^2}{\rho} - \frac{\rho\gamma}{\gamma} \exp\left(\frac{S}{\rho}\right) \\ -\frac{Sn}{\rho} \end{vmatrix} \quad (44)$$

$$B = \begin{vmatrix} -\frac{\kappa n}{h} - \rho e_{\lambda\lambda} \\ 0 \\ -\frac{\kappa n^2}{\rho h} - n e_{\lambda\lambda} \\ -\frac{\kappa Sn}{\rho h} - S e_{\lambda\lambda} \end{vmatrix} \quad G_{,\lambda} = \begin{vmatrix} -\rho u_{,\lambda} \\ 0 \\ -n u_{,\lambda} \\ -S u_{,\lambda} \end{vmatrix}$$

$$\varphi_1 = 0$$

$$\varphi_2 = 0$$

$$\varphi_3 = \frac{M_o C}{Re_o} \ell \left\{ \frac{4}{3} [(Te_{\omega\omega})_{,\omega} - (Te_{\lambda\lambda})_{,\omega}] \right. \\ \left. + \frac{2T}{h} \left(\frac{1}{h} v_{,\lambda\lambda} - u_{,\lambda} \frac{\kappa}{h} + u_{,\omega\lambda} \right) + \frac{4\kappa T}{h} (e_{\omega\omega} - e_{\lambda\lambda}) \right\} \quad (45)$$

$$\varphi_4 = \frac{M_o C}{TRe_o} \ell \left\{ \frac{\gamma}{Pr} \left[\frac{2T}{h^2} T_{,\lambda\lambda} + T_{,\omega}^2 + T T_{,\omega\omega} + \frac{\kappa T}{h} T_{,\omega} \right. \right. \\ \left. \left. \left(1 + \frac{1}{h} \right) \right] + \frac{4}{3} \gamma (\gamma - 1) T (e_{\omega\omega} - e_{\lambda\lambda})^2 \right\}$$

Other terms of equation 26 do not require special treatment.

3.5 Method of Characteristics

Since the system is time dependent, the bow wave moves. In determining bow wave speed, one equation is needed in addition to the Rankine-Hugoniot relationships. The additional equation was obtained by the method of characteristics. In the following, the technique of Moretti and Abbett [52] is adapted to body related coordinates.

Let $\omega_w(\lambda, t + \Delta t)$ be the point where the ω coordinate intersects the bow wave at time $t + \Delta t$. In this section, the orthogonal coordinate frame of figure 3 with origin at $\omega_w(\lambda, t + \Delta t)$ is used.

As shown in figure 4, the boundaries of the blunt body system are A B C D E F A. As indicated, the coordinate ω_w of the bow wave varies with respect to λ and t . Equation 14 implies that the bow wave coordinate ν_w is a constant and is not a function of ζ or τ . In the digitized field of figure 5, $\nu_w = \text{constant}$ is one of the boundaries. Transformations of cylindrical coordinates to ζ and ν were specified in equations 11, 13 and 14. The determination of α and β of equations 13 and 14 is described in section 4.2.2 because of their dependence on initial values.

4.2 Initial Values

4.2.1 Initial Bow Wave Coordinates. Initial values of bow wave coordinates were calculated using the method of Love [46]. The method involves a combination of functional and empirical analysis which assumes that the bow wave is hyperbolic, so that

$$r_w(x, 0) = \left[\frac{(\xi_w + x)^2 - \xi_a^2}{M_o - 1} \right]^{1/2} \quad (64)$$

where: ξ_a = distance from the most forward point on the bow wave to an intercept of its asymptote with the x-axis

ξ_w = distance from stagnation point to an intercept of the bow wave asymptote with the x-axis

M_o = free stream Mach number.

A characteristic variable $\beta(\eta, t)$ is introduced so that

$$f_{,t} = \frac{df}{d\beta} \beta_{,t} \quad (52)$$

$$f_{,\eta} = \frac{df}{d\beta} \beta_{,\eta} \quad (53)$$

Substituting equations 52 and 53 into 50 and 51,

$$\beta_{,t} \frac{dp}{d\beta} + v_{\eta} \beta_{,\eta} \frac{dp}{d\beta} + p\gamma \beta_{,\eta} \frac{dv}{d\beta} = c_1 \quad (54)$$

$$\beta_{,t} \frac{dv}{d\beta} + v_{\eta} \beta_{,\eta} \frac{dv}{d\beta} + \frac{1}{\rho\gamma} \beta_{,\eta} \frac{dp}{d\beta} = c_2 \quad (55)$$

where: $c_1 = -p\gamma v_{\xi, \xi} - v_{\xi} p_{,\xi}$

$$c_2 = -v_{\xi} v_{\eta, \xi}$$

The determinant form is

$$\begin{vmatrix} (\beta_{,t} + v_{\eta} \beta_{,\eta}) & p\gamma \beta_{,\eta} \\ \frac{1}{\rho\gamma} \beta_{,\eta} & (\beta_{,t} + v_{\eta} \beta_{,\eta}) \end{vmatrix} \begin{vmatrix} \frac{dp}{d\beta} \\ \frac{dv}{d\beta} \end{vmatrix} = \begin{vmatrix} c_1 \\ c_2 \end{vmatrix} \quad (56)$$

In accordance with the usual method of characteristics [33], the left determinant is set equal to zero. The result is

$$\beta_{,t} + (v_{\eta} \pm a) \beta_{,\eta} = 0 \quad (57)$$

One solution of equation 57 is the characteristic

$$\beta = \eta - (v_{\eta} - a)t \quad (58)$$

For β constant,

$$\left(\frac{d\eta}{dt}\right)_{\beta} = v_{\eta} - a \quad (59)$$

From equations 50, 51 and 59 a compatibility equation is

$$\left(\frac{dp}{dt}\right)_{\beta} - \gamma \rho a \left(\frac{dv}{dt}\right)_{\beta} = \sigma_{\eta} \quad (60)$$

where $\sigma_{\eta} = -\rho \gamma v_{\xi, \xi} - v_{\xi} p_{, \xi} + \gamma \rho a v_{\xi} v_{\eta, \xi}$

In chapter 4, equations 117 through 127 are the basis of a wave fitting technique which couples the bow wave to the digitized field.

In this investigation, the method of characteristics was also used to derive an inviscid boundary equation at the body surface in terms of body related coordinates. With ω normal to the body surface, ω replaces η and v replaces v_{η} in equations 59 and 60 so that

$$\left(\frac{d\omega}{dt}\right)_{\beta} = v - a \quad (61)$$

$$\left(\frac{dp}{dt}\right)_{\beta} - \gamma \rho a \left(\frac{dv}{dt}\right)_{\beta} = \sigma_{\omega} \quad (62)$$

where $\sigma_{\omega} = \gamma \rho a \left(\frac{u}{h} v_{, \lambda} - \frac{\kappa u^2}{h}\right) - \frac{u}{h} p_{, \lambda} - \gamma p (e_{\lambda \lambda} + e_{\varphi \varphi})$

The value of σ_{ω} in equation 62 is indeterminate along the stagnation streamline. Using the technique of section 3.4.4, at $\lambda = 0$

$$\sigma_{\omega} = -2\gamma p e_{\lambda \lambda} \quad (63)$$

4. NUMERICAL TECHNIQUES

4.1 Introduction

In this investigation, the transformed, viscous, compressible flow equations of section 3.4 were solved numerically by converting them into a set of difference equations. The solution was started with initial values at all nodes and involved boundary values, equations for interior nodes and equations along the stagnation streamline. Those equations are presented in this section. The sequence and relationship of computer operations are presented in section 5.

The following terms are used in the description of numerical techniques. A system is the specified section of matter that is being considered in a particular problem. The specifications of a system include initial values and boundary conditions. A field is the interior part of a system at a specified time. It does not include boundaries. The dimensionless, independent variables are ζ , ν and τ as defined in equations 13 through 15. Nodes are defined by specified values of ζ and ν . The increments $\Delta\zeta$ and $\Delta\nu$ between nodes are constant. Intervals are changes in time $\Delta\tau$ which are approximately constant. A cycle is a set of computations for all nodes at a single time. An iteration is one step of a successive approximation at a single node and time.

As shown in figure 4, the boundaries of the blunt body system are A B C D E F A. As indicated, the coordinate ω_w of the bow wave varies with respect to λ and t . Equation 14 implies that the bow wave coordinate ν_w is a constant and is not a function of ζ or τ . In the digitized field of figure 5, $\nu_w = \text{constant}$ is one of the boundaries. Transformations of cylindrical coordinates to ζ and ν were specified in equations 11, 13 and 14. The determination of α and β of equations 13 and 14 is described in section 4.2.2 because of their dependence on initial values.

4.2 Initial Values

4.2.1 Initial Bow Wave Coordinates. Initial values of bow wave coordinates were calculated using the method of Love [46]. The method involves a combination of functional and empirical analysis which assumes that the bow wave is hyperbolic, so that

$$r_w(x, 0) = \left[\frac{(\xi_w + x)^2 - \xi_a^2}{M_o - 1} \right]^{1/2} \quad (64)$$

where: ξ_a = distance from the most forward point on the bow wave to an intercept of its asymptote with the x-axis

ξ_w = distance from stagnation point to an intercept of the bow wave asymptote with the x-axis

M_o = free stream Mach number.

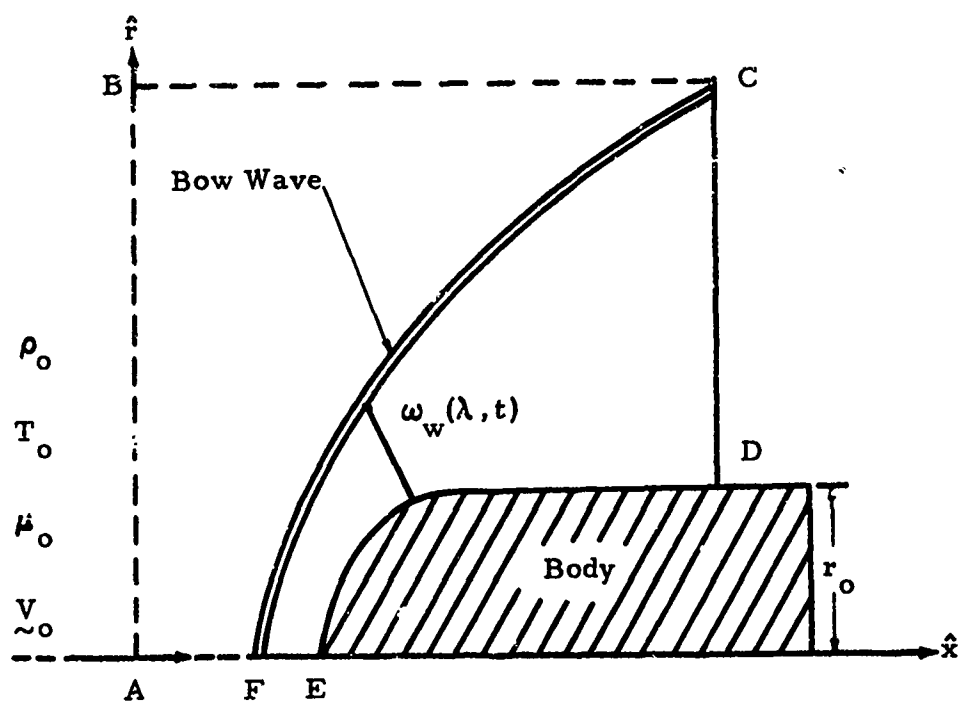


Figure 4. Blunt Body System

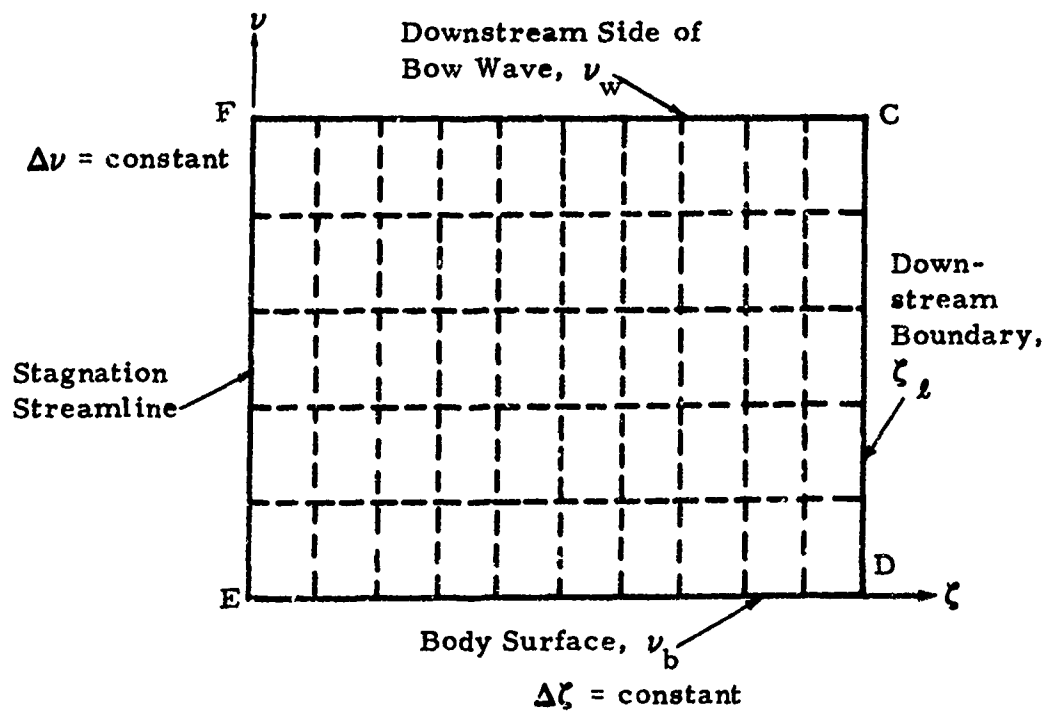


Figure 5. Digitized System

Love empirically determined the parameters ξ_a and ξ_w and tabulated them as functions of body shape and free stream Mach number.

4.2.2 Coordinates of Nodes. Equal increments of $\Delta\zeta$ and $\Delta\nu$ were used in computations to establish the location of nodes. The relationships between ζ , ν , τ and indices I, J, K are:

$$\zeta = (I - 1)\Delta\zeta \quad (65)$$

$$\nu = (J - 1)\Delta\nu \quad (66)$$

$$\tau_{K+1} = \tau_K + \Delta\tau_K \quad (67)$$

Cylindrical coordinates $x(I, J)$ and $r(I, J)$ of nodes were determined from equations 11, 13 and 14.

In starting a viscous flow calculation, the number of nodes in the boundary layer and the total number of nodes between the body surface and bow wave were selected. Staiano [67] found that at least six nodes were required in the boundary layer for acceptable accuracy. The minimum boundary layer thickness is at the stagnation point. From [67] the boundary layer displacement thickness at the stagnation point for axisymmetrical flow about a blunt body is

$$\delta^* = \Lambda(g_b) \left(\frac{\mu_b}{Re_a \rho_b u_{e,\lambda}} \right)^{1/2} \frac{T_s}{T_b} \quad (68)$$

where: $\Lambda(g_b)$ = the tabulated function of [18]

$$g_b = \left(\frac{T_b}{T_s} - 1 \right)$$

$$Re_a = \frac{\rho_o a r_o}{\mu_o}$$

subscript s is for free stream stagnation conditions

subscript b is for the body surface

subscript e is for the edge of the boundary layer.

Using experimental data, Boison and Curtiss [9] derived an empirical equation for the stagnation point velocity gradient $u_{e,\lambda}$. Combining it with equation 68, the stagnation point boundary layer displacement thickness is

$$\delta^* = \Lambda(g_b) \left(\frac{C_\ell \lambda'}{.269 \rho_b Re_a} \right)^{1/2} T_s^{1/4} \quad (69)$$

where: $\lambda' =$ value of λ for $p_e/p_s = .95$

$p_s =$ stagnation point pressure

$\mu = C_\ell T_s$.

From Schlichting [63],

$$\omega_e \approx 3\delta^* \quad (70)$$

where ω_e is velocity thickness of the boundary layer.

Using the Newton-Raphson iteration technique, the parameter β of equation 14 was calculated from

$$e_1 \ln(\beta + 1) - e_2 \ln\left(\beta \frac{\omega_o}{d_w} + 1\right) = 0 \quad (71)$$

where: e_1 = number of increments in the boundary layer at the stagnation point

e_2 = number of increments for the stagnation streamline

d_w = standoff distance of bow wave.

In a similar manner, the parameter α was calculated using

$$e_j \ln(\alpha \lambda_j + 1) - e_l \ln(\alpha \lambda_l + 1) = 0 \quad (72)$$

where: λ_j = value of λ at the junction of the forebody and afterbody

λ_l = value of λ at the downstream boundary

e_j = number of increments for the forebody

e_l = number of increments for the entire body surface.

4.2.3 Boundary Layer. A simple method was not available in the literature for calculating initial values in the boundary layer of an axisymmetrical body. From an extensive review of the literature, the two dimensional, similarity solution of Cohen and Reshotko [19] was selected as the best available basis for calculating initial values in the boundary layer. The transformation of Mangler [48] was used to adapt the two dimensional solution to axisymmetrical flows. The necessary boundary values were u_e , ρ_e , p_e and T_e . The pressure $p_e(\lambda)$ was approximated using the results of Clark [16]. Assuming isentropic flow along the outer edge of the boundary layer, $u_e(\lambda)$, $\rho_e(\lambda)$ and $T_e(\lambda)$ were easily calculated for each value of $\lambda(I)$. The results of Cohen and Reshotko [19] are tabulated in terms of a

compressibility factor β_c and the body surface temperature factor g_b of equation 68.

$$\beta_c(\text{IF}) = \frac{2\alpha_c}{\alpha_c + 1} \quad (73)$$

where: IF = nodal index of the forebody

$$\alpha_c = \frac{\dot{m}_e T_s (r_b^2 a_e p_e T_e u_e)^{-1} \int_0^\lambda a_e p_e r_b^2 d\lambda$$

$r_b(x)$ = body radius

The assumption in the afterbody region was that $\beta_c = 0$. Having computed β_c and g_b , values of η , $f(\eta)$, $f'(\eta)$ and $g(\eta)$ were obtained from the tables of [19]. In terms of them, initial values in the boundary layer were:

$$\frac{u}{u_0} = f'(\eta) \quad (74)$$

$$v = r_b v_y - \frac{dr_b}{d\lambda} \frac{\omega u}{r_b} \quad (75)$$

$$\frac{T}{T_0} = (1 + \frac{\gamma-1}{2} M_e^2) [1 + g(\eta)] - \frac{\gamma-1}{2} [M_e f'(\eta)]^2 \quad (76)$$

$$\text{where: } \omega = \frac{1}{r_b} \left(\frac{p_s}{p_e a_e} \right) \left[\left(\frac{2}{\alpha_c + 1} \right) \frac{\mu_s a_s X}{M_e Re_a \rho_s} \right]^{1/2} \int_0^\eta \left(\frac{T}{T_0} \right) d\eta \quad (77)$$

$$v_y = C \left(\frac{a_e p_e}{\rho p_s} \right) \frac{1}{2} \left[\frac{2\mu_s M_e \rho_s}{a_s Re_a (\alpha_c + 1) X} \right]^{1/2} [\eta f'(\eta) - f(\eta)] \quad (78)$$

$$X = C_{\ell} (a_s p_s)^{-1} \int_0^{\lambda} a_e p_e r_b^2 d\lambda \quad (79)$$

$$f'(\eta_e) = .9995$$

M_e = Mach number at ω_e .

Equation 79 is a combination of transformations of Mangler [48] and Stewartson [68]. In the computations, derivatives were approximated by centered differences, and integrals were approximated by Simpson's rule. Values at nodes were determined by linear interpolation with respect to ω .

4.2.4 Initial Field Values. The initial bow wave coordinates were calculated using equation 64. The Rankine-Hugoniot relationships were used to compute initial values of $f_i(\lambda, \omega_w, 0)$, assuming wave speed equaled zero. This provided initial values for $f_i(\lambda, \omega_w, 0)$. Utilizing initial values at ω_e and ω_w , by linear interpolation

$$f_i(\lambda, \omega, 0) = f_i(\lambda, \omega_e, 0) + C_{\omega} [f_i(\lambda, \omega_w, 0) - f_i(\lambda, \omega_e, 0)] \quad (80)$$

where $C_{\omega} = (\omega - \omega_e) / (\omega_w - \omega_e)$.

For viscous flows ω_e was at the edge of the boundary layer. For inviscid flow $\omega_e = 0$.

4.3 Field Equations

4.3.1 Introduction. Implicit and explicit numerical solutions of equations 2 through 4 are often complicated by instabilities. Many techniques for solving them are available in the literature [1, 5, 8,

21, 45, 47]. All of the techniques that were used in this investigation were explicit and time dependent. No previous solutions were available in the special coordinates of this investigation. The differencing techniques that were used were patterned after those which had been satisfactory for blunt body systems. All of the techniques of this investigation were of the form

$$f_i(\zeta, \nu, \tau + \Delta\tau) = f_i(\zeta, \nu, \tau) + \Delta\tau f_{i,\tau}(\zeta, \nu, \tau) + \frac{\Delta\tau^2}{2} f_{i,\tau\tau}(\zeta, \nu, \tau) + \psi_i \quad (81)$$

where: ψ_i is an arbitrary stabilizing term that is described in section 4.5

$f_{i,\tau}(\zeta, \nu, \tau)$ is given by equation 26

$f_{i,\tau\tau}(\zeta, \nu, \tau)$ is derived in section 4.3.2

Depending upon the particular technique, some of the terms of equation 81 may be zero.

4.3.2 Lax-Wendroff Technique. On the basis of previous results [54, 65, 66] and those of this investigation, an extension of the Lax-Wendroff differencing technique [45] was used to solve viscous compressible flow around a system with an afterbody. The main feature of the technique is the approximation of $f_{i,\tau\tau}$ in equation 81. Since $\nu = \nu(\lambda, \omega, t)$,

$$(f_{i, \tau\tau})_{\zeta\nu} = (f_{i, tt})_{\lambda\omega} - k_1^2(f_{i, \nu\nu} - f_{i, \nu}) - k_6 f_{i, \nu} + 2k_1 f_{i, \nu\tau} \quad (82)$$

$$\text{where: } k_6 = \frac{\beta e^{-\nu} \omega}{\omega_w^2} \left(\frac{2}{\omega_w} \omega_{w, t}^2 - \omega_{w, tt} \right) f_{i, \nu}$$

$$f_{i, \nu\tau} = k_1(f_{i, \nu\nu} - f_{i, \nu}) + \frac{\omega_{w, t}}{\omega_w} f_{i, \nu}$$

$$+ \frac{k_2}{h} \left(G_{i, \zeta\nu} - \frac{G_{i, \zeta^h, \nu}}{h} \right) - \frac{k_3}{h} (G_{i, \nu\nu} - G_{i, \nu})$$

$$+ \frac{k_3}{h^2} G_{i, \nu^h, \nu} + k_4 (H_{i, \nu\nu} - H_{i, \nu})$$

$$+ B_{i, \nu} - \frac{k_2}{h} \frac{\omega_{w, \zeta}}{\omega_w} G_{i, \nu}$$

Based upon the results of [65], an adequate approximation of $f_{i, tt}$ is obtained with $\varphi_i = 0$. From equation 17

$$(f_{i, tt})_{\lambda\omega} = \frac{1}{h} (a_{ij} f_{j, t})_{, \lambda} + (b_{ij} f_{j, t})_{, \omega} + c_{ij} f_{j, t} \quad (83)$$

$$\text{where: } a_{ij} = \frac{\partial G_i}{\partial f_j}; \quad b_{ij} = \frac{\partial H_i}{\partial f_j}; \quad c_{ij} = \frac{\partial B_i}{\partial f_j}$$

By expanding

$$a_{ij} = \begin{vmatrix} 0 & -1 & 0 & 0 \\ u^2 + \frac{T}{\gamma}(s - \gamma) & -2u & 0 & -\frac{T}{\gamma} \\ uv & -v & -u & 0 \\ su & -s & 0 & -u \end{vmatrix} \quad (84)$$

$$b_{ij} = \begin{vmatrix} 0 & 0 & -1 & 0 \\ uv & -v & -u & 0 \\ v^2 + \frac{T}{\gamma}(s - \gamma) & 0 & -2v & -\frac{T}{\gamma} \\ sv & 0 & -s & -v \end{vmatrix} \quad (85)$$

$$c_{ij} = \begin{array}{c|ccc} & & -\frac{\sin \theta}{r} & -\left(\frac{x}{h} + \frac{\cos \theta}{r}\right) & 0 \\ \hline & 0 & & & \\ \frac{2xuv}{h} + ue \varphi \varphi & & -\left(\frac{2x}{h} + \frac{\sin \theta}{r} + e \varphi \varphi\right) & -\left(\frac{2xu}{h} - \frac{u \cos \theta}{r}\right) & 0 \\ \frac{x}{h}(v^2 - u^2) + ve \varphi \varphi & & \left(\frac{2xu}{h} - \frac{v \sin \theta}{r}\right) & -\left(\frac{2xv}{h} + \frac{v \cos \theta}{r} + e \varphi \varphi\right) & 0 \\ \frac{xvs}{h} + se \varphi \varphi & & -\left(\frac{\sin \theta}{r}\right)s & -\left(\frac{x}{h} + \frac{\cos \theta}{r}\right)s & -\frac{xv}{h} - e \varphi \varphi \end{array} \quad (86)$$

By expanding equation 83,

$$\begin{aligned}
 f_{i,tt} = & \left(\frac{1}{h} a_{ij,\lambda} + b_{ij,\omega} + c_{ij} \right) f_{j,t} \\
 & + \frac{a_{ij}}{h} \left(\frac{1}{h} G_{j,\lambda\lambda} - \frac{1}{h^2} G_{j,\lambda} h_{,\lambda} + H_{j,\omega\lambda} + B_{j,\lambda} \right) \\
 & + b_{ij} \left(\frac{1}{h} G_{j,\lambda\omega} - \frac{1}{h^2} G_{j,\lambda} h_{,\omega} + H_{j,\omega\omega} + B_{j,\omega} \right)
 \end{aligned} \tag{87}$$

The jacobians a_{ij} , b_{ij} and c_{ij} were differentiated explicitly to avoid storing them during computations. For example, from equations 19 and 84

$$a_{31,\lambda} = v(k_{2,u,\zeta} - k_{3,u,\nu}) + u(k_{2,v,\zeta} - k_{3,v,\nu})$$

An example of the differentiation of G, H and B is that

$$G_{3,\lambda} = k_2 G_{3,\zeta} - k_3 G_{3,\nu}$$

4.3.3 Aungier Technique. The differencing technique of Aungier [1] was used to check the derivation and computer coding of boundary and field equations. The technique is a variation of one proposed by Lax [44] and is of first order accuracy. In it, $f_{i,\tau\tau} = 0$ and $\psi_i \neq 0$ in equation 82.

4.3.4 Approximations of Derivatives. Approximations of the derivatives that evolve from equation 81 were those of equations 18 through 24, 37 through 40 and the following:

$$f_{i, \zeta}(\zeta, \nu, \tau) = \frac{1}{2\Delta\zeta} [f_i(\zeta + \Delta\zeta, \nu, \tau) - f_i(\zeta - \Delta\zeta, \nu, \tau)] \quad (88)$$

$$f_{i, \nu} = \frac{1}{2\Delta\nu} [f_i(\zeta, \nu + \Delta\nu, \tau) - f_i(\zeta, \nu - \Delta\nu, \tau)] \quad (89)$$

$$f_{i, \zeta\zeta}(\zeta, \nu, \tau) = \frac{1}{\Delta\zeta^2} [f_i(\zeta + \Delta\zeta, \nu, \tau) - 2f_i(\zeta, \nu, \tau) + f_i(\zeta - \Delta\zeta, \nu, \tau)] \quad (90)$$

$$f_{i, \nu\nu} = \frac{1}{\Delta\nu^2} [f_i(\zeta, \nu + \Delta\nu, \tau) - 2f_i(\zeta, \nu, \tau) + f_i(\zeta, \nu - \Delta\nu, \tau)] \quad (91)$$

$$f_{i, \zeta\nu}(\zeta, \nu, \tau) = \frac{1}{4\Delta\zeta\Delta\nu} [f_i(\zeta + \Delta\zeta, \nu + \Delta\nu, \tau) - f_i(\zeta + \Delta\zeta, \nu - \Delta\nu, \tau) - f_i(\zeta - \Delta\zeta, \nu + \Delta\nu, \tau) + f_i(\zeta - \Delta\zeta, \nu - \Delta\nu, \tau)] \quad (92)$$

$$\omega_{w, t} = \frac{1}{\Delta t} [\omega_w(\lambda, t + \Delta t) - \omega_w(\lambda, t)] \quad (93)$$

$$\omega_{w, tt} = \frac{1}{\Delta t} [\omega_{w, t}(\lambda, t + \Delta t) - \omega_{w, t}(\lambda, t)] \quad (94)$$

Because $\kappa = -\frac{d\theta}{d\lambda}$ is discontinuous at the junction of a hemisphere-cylinder, the approximations of derivatives at the junction were not compatible with those at nearby nodes. To avoid this problem, an average curvature

$$\begin{aligned} \kappa_a(\zeta) = & \frac{1}{8} [\kappa(\zeta - 2\Delta\zeta) + \kappa(\zeta - \Delta\zeta) + 4\kappa(\zeta) + \kappa(\zeta + \Delta\zeta) \\ & + \kappa(\zeta + 2\Delta\zeta)] \end{aligned} \quad (95)$$

was used at all nodes.

As illustrated by figure 6, there is no discontinuity in κ_a .

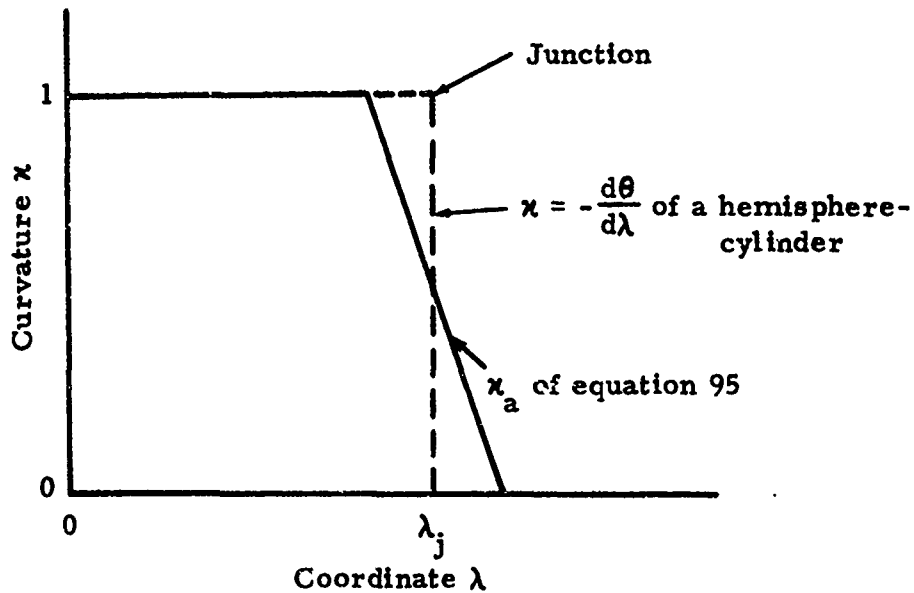


Figure 6. Curvature κ of a Hemisphere-Cylinder

4.4 Equations Along the Stagnation Streamline

Along the stagnation streamline where $u = 0$, special equations are:

$$f_{i,\tau}(0, \nu, \tau) = k_1 f_{i,\nu} + \frac{1}{h} G_{i,\lambda} + k_4 H_{i,\nu} + B_i + \phi_i \quad (96)$$

$$\begin{aligned} f_{i,\nu\tau} = & k_1 (f_{i,\nu\nu} - f_{i,\nu}) + \frac{\omega_{w,t}}{\omega_w} f_{i,\nu} \\ & + \frac{1}{h} (G_{i,\lambda\nu} - \frac{G_{i,\lambda} h}{h}) + k_4 (H_{i,\nu\nu} - H_{i,\nu}) + B_{i,\nu} \end{aligned} \quad (97)$$

$$\begin{aligned}
(f_{i,tt})_{\lambda\omega} &= \left(\frac{1}{h}a_{ij,\lambda} + b_{ij,\omega} + c_{ij}\right)f_{j,t} \\
&\quad - \frac{f_i}{\rho h}m_{,\lambda\tau} + \frac{a_{ij}}{h}\left(\frac{1}{h}G_{j,\lambda\lambda} - \frac{1}{h^2}G_{j,\lambda}{}^h{}_{,\lambda}\right. \\
&\quad \left.+ H_{j,\omega\lambda} + B_{j,\lambda}\right) + b_{ij}\left(\frac{1}{h}G_{j,\lambda\omega}\right. \\
&\quad \left.- \frac{1}{h^2}G_{j,\lambda}{}^h{}_{,\omega} + H_{j,\omega\omega} + B_{j,\omega}\right) \quad (98)
\end{aligned}$$

$$m_{,\lambda\tau} = -\frac{1}{\gamma h}p_{,\lambda\lambda} - u_{,\lambda}n_{,\omega} - nu_{,\lambda\omega} - 3\rho u_{,\lambda}e_{\lambda\lambda} \quad (99)$$

$$c_{ij} = \begin{vmatrix} 0 & 0 & \frac{-2\kappa}{h} & 0 \\ 0 & 0 & 0 & 0 \\ v\left(\frac{\kappa v}{h} + e_{\lambda\lambda}\right) & 0 & -\left(\frac{3\kappa v}{h} + e_{\lambda\lambda}\right) & 0 \\ s\left(\frac{\kappa v}{h} + e_{\lambda\lambda}\right) & 0 & -\frac{2\kappa s}{h} & -\left(\frac{\kappa v}{h} + e_{\lambda\lambda}\right) \end{vmatrix} \quad (100)$$

The jacobians a_{ij} and b_{ij} of equations 84 and 85 are unchanged. The derivatives $f_{i,\nu}$ and $f_{i,\nu\nu}$ were approximated with the centered differences of equations 89 and 91. The derivatives $f_{i,\lambda}$, $f_{i,\lambda\lambda}$ and $f_{i,\lambda\omega}$ were approximated using the symmetry conditions of equations 41 and 42, so that for all variables except m and u ,

$$f_{i,\lambda} = f_{i,\lambda\omega} = 0 \quad (101)$$

$$f_{i,\lambda\lambda} = \frac{2}{\Delta\lambda} [f_i(\Delta\lambda, \nu, \tau) - f_i(0, \nu, \tau)] \quad (102)$$

where $\Delta\lambda = [\exp(\Delta\xi) - 1]/\alpha$.

For u ,

$$u_{,\lambda} = \frac{1}{\Delta\lambda} u(\Delta\lambda, \nu, \tau) \quad (103)$$

$$u_{,\lambda\lambda} = 0 \quad (104)$$

$$u_{,\lambda\omega} = \frac{k_4}{2\Delta\lambda\Delta\nu} [u(\Delta\lambda, \nu + \Delta\nu, \tau) - u(\Delta\lambda, \nu - \Delta\nu, \tau)] \quad (105)$$

Derivatives of m have the same form.

4.5 Stabilizing Terms

4.5.1 Introduction. Linear stability theory is extensive and complicated and is beyond the scope of this investigation. For linearized one dimensional equations, Richtmyer and Morton [59] derived the following criterion for numerical stability of the Lax-Wendroff differencing technique when $\psi_i = 0$:

$$(|v_x| + a) \frac{\Delta t}{\Delta x} < 1 \quad (106)$$

where: v_x = the x component of velocity

a = sonic speed

Equation 106 is the Courant-Fredricks-Lewy criterion for stability.

For linearized two dimensional equations in which $\Delta x = \Delta y$, Richtmyer [58] derived the criterion that

$$\left(\sqrt{v_x^2 + v_y^2} + a \right) \frac{\Delta t}{\Delta x} \leq \frac{1}{\sqrt{2}} \quad (107)$$

where v_y = the y component of velocity.

Numerical experiments by Emery [30], Gary [34] and others have demonstrated that the stability criterion of equation 107 is necessary for many systems. It was used with the equality sign in this investigation to determine the upper limit

$$\Delta t_l = \frac{\Delta x}{\sqrt{2}(\sqrt{u^2 + v^2} + a)} \quad (108)$$

where Δx = minimum of $\Delta \lambda$ and $\Delta \omega$.

Many investigations [12, 30, 31, 43, 66] have shown that linear stability criteria, such as equation 107, are necessary but not sufficient. In previous numerical solutions of blunt body systems in which equations 106 or 107 were satisfied, numerical instabilities have occurred near the stagnation point, sonic line and downstream boundary. In some of these cases, stabilizing terms were added to the basic difference equations. A stabilizing term is an artificial, mathematical term that is added to a difference equation to improve numerical stability. Satisfactory stabilizing terms must not introduce unacceptable errors in the results. In this investigation, stabilizing terms of Lapidus [43] and Aungier [1] were modified and used in numerical experiments because they were satisfactory in previous solutions of inviscid flow about blunt bodies.

4.5.2 Lapidus Stabilizing Term. Skoglund and Gay [66] demonstrated that the addition of the Lapidus stabilizing term had a negligible effect

in the boundary layer of a flat plate. For two dimensional inviscid flow, Lapidus [43] analytically demonstrated that his stabilizing term was conservative and was of third order accuracy. By expressing the Lapidus stabilizing term of [43] in ζ and ν coordinates, one of the stabilizing terms that was used in equation 81 is

$$\begin{aligned} \psi_i = & \frac{\Delta\tau}{2} \left\{ L_{ij}(\zeta + \frac{\Delta\zeta}{2}, \nu, \tau) \left[\frac{k_2}{h} \vec{f}_{j, \zeta} - \frac{k_3}{h} \vec{f}_{j, \nu} \right] \right. \\ & + L_{ij}(\zeta - \frac{\Delta\zeta}{2}, \nu, \tau) \left[\frac{k_2}{h} \vec{f}_{j, \zeta} - \frac{k_3}{h} \vec{f}_{j, \nu} \right] \\ & \left. + L_{ij}(\zeta, \nu + \frac{\Delta\nu}{2}, \tau) [k_4 \vec{f}_{j, \nu}] + L_{ij}(\zeta, \nu - \frac{\Delta\nu}{2}, \tau) [k_4 \vec{f}_{j, \nu}] \right\} \end{aligned} \quad (109)$$

where: $\vec{f}_{j, \zeta}(\zeta, \nu, \tau) = \frac{1}{\Delta\zeta} [f_j(\zeta + \Delta\zeta, \nu, \tau) - f_j(\zeta, \nu, \tau)]$

$$\vec{f}_{j, \zeta}(\zeta, \nu, \tau) = \frac{1}{\Delta\zeta} [f_j(\zeta, \nu, \tau) - f_j(\zeta - \Delta\zeta, \nu, \tau)]$$

$$L_{ij}(\zeta + \frac{\Delta\zeta}{2}, \nu, \tau) = C_1 |u(\zeta + \Delta\zeta, \nu, \tau) - u(\zeta, \nu, \tau)| \delta_{ij}$$

$$L_{ij}(\zeta, \nu + \frac{\Delta\nu}{2}, \tau) = C_2 |v(\zeta, \nu + \Delta\nu, \tau) - v(\zeta, \nu, \tau)| \delta_{ij}$$

C_1 and C_2 are arbitrary constants. Acceptable values were determined by numerical experiment

δ_{ij} is the kronecker delta = 1 if $i = j$; = 0 if $i \neq j$

4.5.3 Aungier Stabilizing Term. The derivation of the Aungier stabilizing term [1] begins with the following linearized flow equation:

$$f_{,t} = -\alpha_1 f_{,x} + \frac{\alpha_2}{2} \frac{\Delta x^2}{\Delta t} f_{,xx} \quad (110)$$

where $\alpha_1, \alpha_2 = \text{constant}$.

By substituting a solution of the form

$$f = f_0 + f_\delta \exp(bt + cx) \quad (111)$$

into a difference form of equation 110 and requiring $|\exp(b\Delta t)| \leq 1$,

the limiting

$$\frac{\Delta t}{\Delta x} = \frac{\sqrt{\alpha_2}}{\alpha_1} \quad (112)$$

where: $f_0 = \text{constant}$

$f_\delta = \text{constant} \ll f_0$

b and c are constants.

Aungier reasoned that the Courant-Fredricks-Lewy stability criterion should be satisfied. From equations 106 and 110, $\alpha_1 = u + a$. This yielded

$$\frac{\Delta t}{\Delta x} = \frac{\sqrt{\alpha_2}}{u + a} \quad (113)$$

For two dimensional systems, Aungier assumed a stabilizing term of the form

$$\psi_a = \frac{(u + a)^2}{2} \Delta t^2 f_{,xx} + \frac{(v + a)^2}{2} \Delta t^2 f_{,yy} \quad (114)$$

By simple replacement for inviscid flow in the subject investigation, a stabilizing term that was used in equation 81 was:

$$\psi_i = C_3(u+a)^2 \frac{\Delta t^2}{2} f_{i,\lambda\lambda} + C_4(v+a)^2 \frac{\Delta t^2}{2} f_{i,\omega\omega} \quad (115)$$

where C_3 and C_4 are arbitrary constants.

This equation was satisfactory for inviscid flow but yielded inaccurate results for viscous flow. An accurate solution for viscous flow was obtained using

$$\psi_i = C_5(u+ba)^2 \frac{\Delta t^2}{2} f_{i,\lambda\lambda} + C_6(v+ba)^2 \frac{\Delta t^2}{2} f_{i,\omega\omega} \quad (116)$$

where $b = \exp[-C_7(J_e - J)\Delta\nu]$ for $J \leq J_e$

$= 1$ for $J > J_e$

C_7 is an arbitrary constant

J = index of nodes in the ω direction

J_e is a node near the edge of the boundary layer.

4.6 Bow Wave Technique

4.6.1 Bow Wave Equations. At the upstream boundary AB of figure 4, the free stream values are constant. Since the governing equations are time dependent, the bow wave may move. In figure 3 of section 3.5, the speed of the bow wave in the $\hat{\eta}$ direction is designated as w . The Rankine-Hugoniot relationships for a moving wave are

$$v_{i+2} = \frac{\frac{\gamma-1}{2}(v_{\eta 1} - w)^2 + 1}{\frac{\gamma+1}{2}(v_{\eta 1} - w)} + w \quad (117)$$

$$v_{\xi 2} = v_{\xi 1} \quad (118)$$

$$\rho_2 = (v_{\eta 1} - w) / (v_{\eta 2} - w) \quad (119)$$

$$p_2 = 1 + \frac{2\gamma}{\gamma + 1} [(v_{\eta 1} - w)^2 - 1] \quad (120)$$

where: $v_{\eta 1} = \frac{v_1}{\Gamma} \left[\frac{\omega_{w, \lambda}}{h} \cos \theta + \sin \theta \right]$

$$v_{\xi 1} = \frac{v_1}{\Gamma} \left[\cos \theta - \frac{\omega_{w, \lambda}}{h} \sin \theta \right]$$

v_1 = freestream velocity in x direction

$$\Gamma = \left[\left(\frac{\omega_{w, \lambda}}{h} \right)^2 + 1 \right]^{1/2}$$

subscripts 1 and 2 refer to values at upstream and downstream sides of the bow wave.

Unit vectors are:

$$\hat{\eta} = \left(\frac{\omega_{w, \lambda}}{h} \hat{\lambda} - \hat{\omega} \right) / \Gamma \quad (121)$$

$$\hat{\xi} = \left(\hat{\lambda} - \frac{\omega_{w, \lambda}}{h} \hat{\omega} \right) / \Gamma \quad (122)$$

In the above set of equations $\omega_{w, \lambda}$ was approximated by

$$\begin{aligned}\omega_{w,\lambda}(\lambda, t + \Delta t) &= \frac{1}{3} [\vec{\omega}_{w,\lambda}(\lambda, t + \Delta t) + 2\overleftarrow{\omega}_{w,\lambda}(\lambda, t + \Delta t)] \\ &= \frac{k_2}{3\Delta\zeta} [\omega_w(\zeta + \Delta\zeta, \tau + \Delta\tau) \\ &\quad + \omega_w(\zeta, \tau + \Delta\tau) - 2\omega_w(\zeta - \Delta\zeta, \tau + \Delta\tau)]\end{aligned}\tag{123}$$

$$\text{where: } \vec{\omega}_{w,\lambda}(\lambda, t + \Delta t) = \frac{1}{\Delta\zeta} [\omega_w(\zeta + \Delta\zeta, \tau + \Delta\tau) - \omega_w(\zeta, \tau + \Delta\tau)]$$

$$\overleftarrow{\omega}_{w,\lambda}(\lambda, t + \Delta t) = \frac{1}{\Delta\zeta} [\omega_w(\zeta, \tau + \Delta\tau) - \omega_w(\zeta - \Delta\zeta, \tau + \Delta\tau)]$$

Aungier [1] found that the technique of equation 123 inhibited oscillations of ω_w with respect to λ .

Equation 59 was used to obtain the characteristic slope of figure 7.

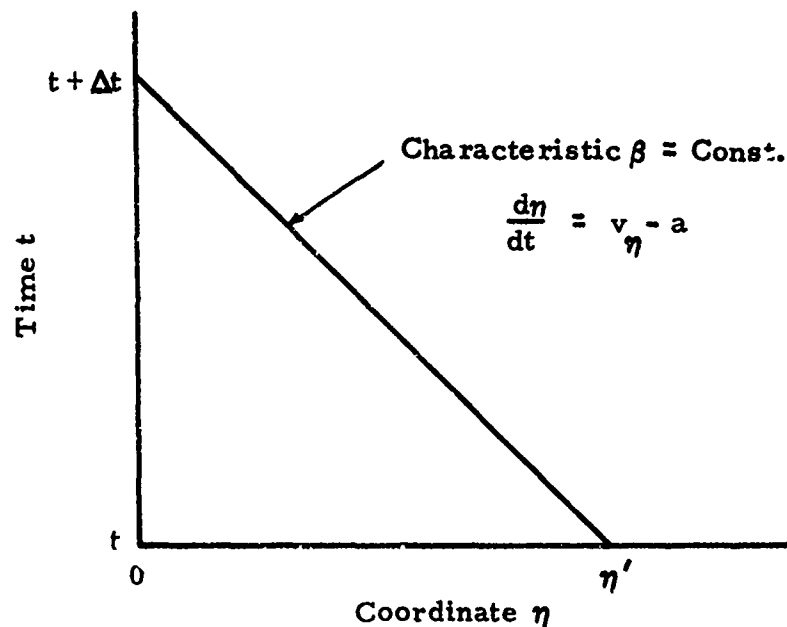


Figure 7. Characteristic at the Bow Wave

The intersection of the characteristic with the η axis at time t is symbolized by η' and was calculated by a method that is outlined in

the next section. Along the characteristic, an approximation of equation 60 is

$$v_{\eta 2} = v'_{\eta} + [p_2 - p' - \sigma'_{\eta} \Delta t] / \overline{\gamma \rho a} \quad (124)$$

where: $\overline{\gamma \rho a} = .5[\gamma \rho_2 a_2 + \gamma \rho' a']$

primes refer to values at η' and time t

subscript 2 refers to values on the downstream side of the

bow wave at time $t + \Delta t$.

In evaluating σ'_{η} , known values at nodes were interpolated to determine value at η' . Using the chain rule yielded,

$$f_{i, \xi} = \frac{\partial f_i}{\partial \lambda'} \alpha_3 + \frac{\partial f_i}{\partial \omega'} \alpha_4 \quad (125)$$

where: $\alpha_3 = \left[\cos(\theta - \theta') - \frac{\omega_w \lambda}{h} \sin(\theta - \theta') \right] / \Gamma$

$\alpha_4 = \left[\sin(\theta - \theta') + \frac{\omega_w \lambda}{h} \cos(\theta - \theta') \right] / \Gamma$.

At η' ,

$$v'_{\eta} = u' \alpha_4 - v' \alpha_3 \quad (126)$$

$$v'_{\xi} = u' \alpha_3 + v' \alpha_4 \quad (127)$$

The values of λ' , ω' and θ' at η' were determined using the Newton-Raphson iteration technique.

The bow wave coordinates at time $t + \Delta t$ were calculated using

$$\omega_w(\lambda, t + \Delta t) = \omega_w(\lambda, t) - \Gamma w(t)\Delta t \quad (128)$$

and held constant during a cycle.

4.6.2 Iteration Techniques. To calculate $f_{i2}(\lambda, \omega_w, t + \Delta t)$, equations of the preceding section were solved by an iteration technique. As a first approximation of $w(t + \Delta t)$, $w(1) = w(t)$ where the number in parentheses refers to the approximation number. Having the approximate value of $w(1)$, equations 117, 119 and 120 were solved for $v_{\eta 2}(1)$, $p_2(1)$ and $\rho_2(1)$. With $v_{\eta 2}(1)$ available, the first approximation of η' was

$$\eta'(1) = |v_{\eta 2}(1) - a_2(1)|\Delta t \quad (129)$$

where $a_2(1) = \sqrt{T_2(1)}$.

Using the Newton-Raphson iteration technique and linear interpolation, a' was determined and equation 126 was solved for v'_η . The second approximation of η' was

$$\eta'(2) = |v_{\eta 2}(1) - a_2(1) + v'_\eta - a'|\Delta t/2 \quad (130)$$

The above process was repeated until

$$|\eta'(n) - \eta'(n-1)| < 10^{-5} \quad (131)$$

Once an accurate location of η' was obtained, σ'_η was calculated and equation 124 was solved for $v_{\eta 2}(2)$.

If

$$|v_{\eta 2}(1) - v_{\eta 2}(2)| > 10^{-5} \quad (132)$$

a new value of $w(2)$ was estimated from

$$w^2(2) + \left[\frac{\gamma - 3}{2} v_{\eta 1} - \frac{\gamma + 1}{2} v_{\eta 2}(1) \right] w(2) + \frac{\gamma + 1}{2} v_{\eta 1} v_{\eta 2}(1) - \frac{\gamma - 1}{2} v_{\eta 1}^2 - 1 = 0 \quad (133)$$

The value of $w(2)$ was used in equations 117, 119 and 120 to estimate $v_{\eta 2}(2)$, $p_2(2)$ and $\rho_2(2)$. A new value of η' corresponding to $v_{\eta 2}(2)$ and $a_2(2)$ was determined from equations 129 through 131. Equation 124 was again solved for $v_{\eta 2}(3)$. This process was continued until

$$|v_{\eta 2}(n) - v_{\eta 2}(n - 1)| < 10^{-5} \quad (134)$$

Only a few iterations were required to satisfy equation 134.

After satisfying equation 134, the downstream λ and ω components of velocity were computed from

$$u(\lambda, \omega_w, t + \Delta t) = \left[v_{\eta 2} \frac{\omega_w, \lambda}{h} + v_{\xi 2} \right] / \Gamma \quad (135)$$

$$v(\lambda, \omega_w, t + \Delta t) = \left[-v_{\eta 2} + v_{\xi 2} \frac{\omega_w, \lambda}{h} \right] / \Gamma \quad (136)$$

4.7 Boundary Equations

4.7.1 At the Downstream Boundary. The difference equations at the downstream boundary λ_{ℓ} were the same as those in the field of section

4.3. Values at $\lambda_{\ell+1}$ were required in the approximations of derivatives

at λ_ℓ . In finding the location of nodes at $\lambda_{\ell+1}$, an approximation for shock wave coordinate $\omega_w(\lambda_{\ell+1})$ was needed. From figure 8, the extrapolated value of $\omega_w(\lambda_{\ell+1})$ was determined by finding the intersection of a line drawn through the points $\omega_w(\lambda_{\ell-1})$ and $\omega_w(\lambda_\ell)$ with a line extended in the $\hat{\omega}$ direction at $\lambda_{\ell+1}$.

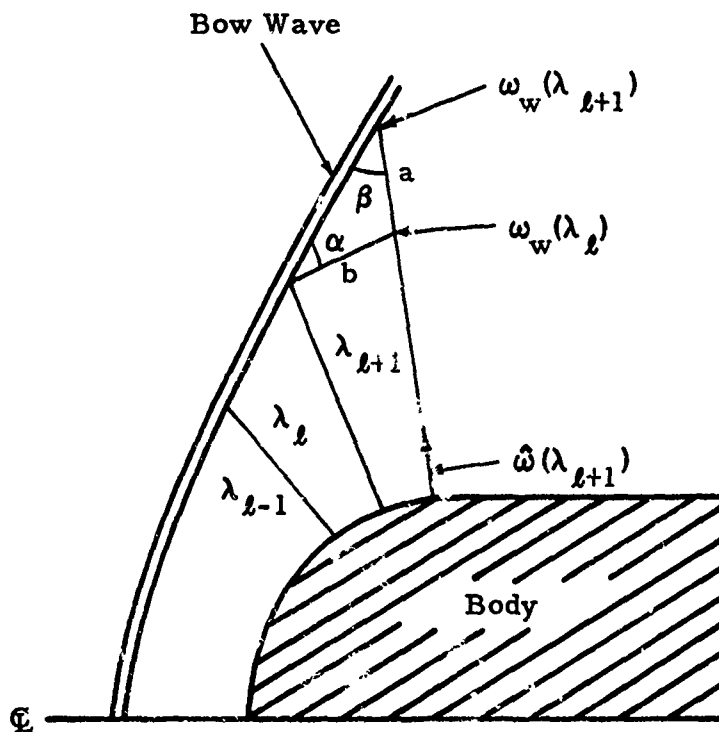


Figure 8. Location of $\omega_w(\lambda_{\ell+1})$

From the law of sines,

$$\omega_w(\lambda_{\ell+1}) = \omega_w(\lambda_\ell) + b \sin \alpha / \sin \beta \quad (137)$$

By linear extrapolation,

$$f_i(\lambda_{\ell+1}, \omega, t) = f_i(\lambda_{\ell-1}, \omega, t) + C_\lambda [f_i(\lambda_\ell, \omega, t) - f_i(\lambda_{\ell-1}, \omega, t)] \quad (138)$$

where $C_\lambda = (\lambda_{\ell+1} - \lambda_{\ell-1}) / (\lambda_\ell - \lambda_{\ell-1})$

4.7.2 At the Body Surface with Viscous Flow. The boundary conditions for viscous flow at the body surface were $u(\lambda, 0, t) = v(\lambda, 0, t) = 0$ and $T(\lambda, 0, t) = T_b = \text{constant}$. Using $s = \ln(p/\rho^\gamma)$ to combine equations for $i = 1$ and 4 in equation 26,

$$p_{,t} = -\gamma p v_{, \omega} + \varphi_4 \quad (139)$$

$$\text{where: } \varphi_4 = \frac{M_o C_\ell}{Re_o} \left\{ \frac{\gamma}{Pr} \left[T_{, \omega}^2 + T_b T_{, \omega \omega} + \kappa T_b T_{, \omega} \right. \right. \\ \left. \left. + \frac{T_b T_{, \omega}}{r} \cos \theta \right] + \gamma(\gamma - 1) T_b \left[\frac{4}{3} e^2_{\omega \omega} + u_{, \omega}^2 \right] \right\}$$

At the stagnation point

$$\varphi_4 = \frac{M_o C_\ell}{Re_o} \left\{ \frac{\gamma}{Pr} [T_{, \omega}^2 + T_b T_{, \omega \omega} + 2\kappa T_b T_{, \omega}] \right. \\ \left. + \frac{4}{3} \gamma(\gamma - 1) T_b e^2_{\omega \omega} \right\} \quad (140)$$

Using a Taylor series, the pressure at the body surface is

$$p(\lambda, 0, t + \Delta t) = p(\lambda, 0, t) + \Delta t p_{,t}(\lambda, 0, t) \quad (141)$$

$$+ \frac{\Delta t^2}{2} p_{,tt}(\lambda, 0, t)$$

where: $p_{,tt} = -\gamma p_{,t} v_{, \omega} - \gamma p v_{, \omega t}$

$$v_{, \omega t} = -v_{, \omega}^2 + \rho_{, \omega} p_{, \omega} / \gamma \rho^2 - p_{, \omega \omega} / \gamma \rho$$

$\varphi_{3, \omega} = \varphi_{4, t} = 0$ as an approximation

$$f_{i, \omega} = \frac{1}{\Delta\omega} [f_i(\lambda, \Delta\omega, t) - f_i(\lambda, 0, t)] \quad (142)$$

$$\Delta\omega = \omega_w [\exp(\Delta\nu) - 1] / \beta$$

$p_{, \omega\omega}(\lambda, 0, t)$ was approximated by equation 38 for $\omega = \Delta\omega$.

The density at the body surface

$$\rho(\lambda, 0, t + \Delta t) = \rho(\lambda, 0, t + \Delta t) / T_b \quad (143)$$

4.7.3 At the Body Surface with Inviscid Flow. Boundary conditions at

the body surface for inviscid flow are $v(\lambda, 0, t) = 0$, $u(\lambda, 0, t) \neq 0$ and

$T(\lambda, 0, t)$ is not constant. For inviscid flow,

$$u_{,t} = -uu_{, \lambda} - p_{, \lambda} / \gamma \rho \quad (144)$$

$$s_{,t} = -us_{, \lambda} \quad (145)$$

Equation 61 was used to establish the characteristic of figure 9.

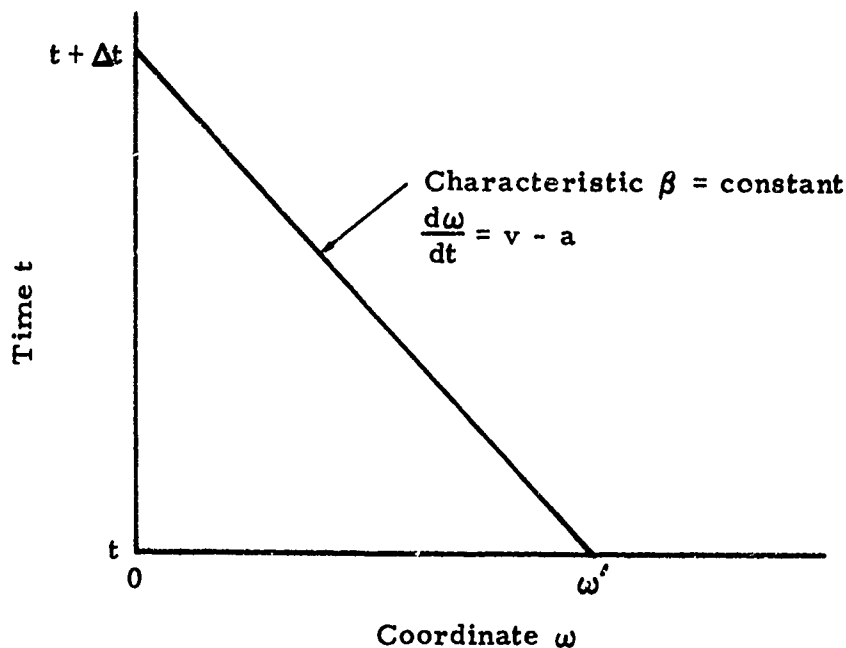


Figure 9. Characteristic at Body Surface

The intersection ω' on the ω axis at time t was found using the iteration techniques of section 4.6.2. Equation 62 was approximated by

$$p(\lambda, 0, t + \Delta t) = \sigma'_{\omega} \Delta t + p' - \overline{\gamma \rho a} v' \quad (146)$$

where: $\overline{\gamma \rho a} = .5\gamma [\rho(\lambda, 0, t)a(\lambda, 0, t) + \rho'a']$

primes refer to values at ω' .

Equations 144 and 145 were solved in the same manner as equation 141.

The derivative $f_{i, \omega}$ was approximated by equation 142, and the derivative $f_{i, \omega\omega}$ was approximated by equation 38 for $\omega = \Delta\omega$. Equations 19 and 37 with $k_3 = k_5 = 0$ were used to calculate $f_{i, \lambda}$ and $f_{i, \lambda\lambda}$. In these equations, the derivatives $f_{i, \zeta}$ and $f_{i, \zeta\zeta}$ were approximated by equations 88 and 90.

At the stagnation point, $u_t = u_{,tt} = s_t = s_{,tt} = 0$. For inviscid flow the stagnation point temperature was precisely calculated from an isentropic equation and was constant.

5. COMPUTATIONS AND RESULTS

5.1 Introduction

In this investigation, digital computers were used to solve the difference equations presented in section 4. In the first computer codes, there were major problems with nodal distribution, wave fitting and numerical instabilities. Refinement of difference equations and computer codes was accomplished experimentally on digital computers. In order to keep the length of the report within a reasonable limit, only the more significant computations and results are presented. The two principal computer codes are INITIAL, based on initial value techniques of section 4.2, and MAIN, based on the techniques of sections 4.3 through 4.7. Results are presented for axisymmetrical, inviscid and viscous flows around hemispheres and hemisphere-cylinders. Because of stability problems and constraints on computational time, most development computations were restricted to hemispheres. Table 1 lists specifications of the systems that were solved in this investigation.

Table 1. Systems

System Number	Configuration*	Reynolds Number, Re_o	Mach Number, M_o
1	H - C	Inviscid	4
2	H	10^3	4
3	H - C	4×10^3	4
4	H	10^4	4
5	H	10^5	4
6	H	Inviscid	2
7	H	10^4	2

*Under "Configuration," H = hemisphere alone; H - C = hemisphere-cylinder combination.

For most of the systems of table 1, many computer runs were required before results were satisfactory. Systems 1 and 4 were used as test cases to develop the MAIN code and stabilizing terms. Aungier [1] solved system 1 by segmenting the field. As a check, his results were compared with those of this investigation. Steady or time dependent solutions of viscous systems with an afterbody, such as system 3, were not previously available in the open literature. Investigation of the effect of Reynolds number at $M_o = 4$ was the motivation for solving systems 2 and 4. Solutions of systems 2, 3, 4, 5 and 7 demonstrated that the codes were satisfactory for viscous systems. Solutions for systems 6 and 7 demonstrated that the codes are satisfactory for lower Mach numbers which have less inherent stability.

The specifications for computer runs are presented in table 2. Results of these runs are presented and discussed in succeeding sections. In table 2, IJ equals I just ahead of the junction of the hemisphere and cylinder, IL is at the downstream boundary, JE is at the edge of the boundary layer, JW is at the bow wave and KL is when computations were halted. In the following, most figures of a sub-subsection, such as 5.2.1, are presented at the end of that section.

5.2 Computer Codes

5.2.1 INITIAL. A simplified flow diagram of the INITIAL code is presented in figure 10. In it, ILP1 = IL+1 and JEP1 = JE+1. Both magnetic tape and punched cards were used to input data. The boundary layer tables of Cohen and Reshotko [19], bow wave parameters of Love [46] and body surface values of Clark [16] comprised several thousand entries which were recorded on magnetic tape. Punched card input was used to specify body shape, reference variables, boundary values and nodal parameters. After calculating initial values of ρ , m , n and S at each node, an output tape of their values was generated.

Table 2. Specifications of Computer Runs

Run	CF1	M ₀	Re ₀ x 10 ⁻³	IJ	IL	JW	KL	τ	α	β	Diff. T ² Sec.	ψ _i or ψ _j Eqn	C1	C2	C3	C4	C5	C6	C7	JE
1	H	4	10	14	13	16	1400	1.281	1.604	11.895	4.3.2	0								
2	H-C	4	10	14	24	16	1050	.956	1.604	11.895	4.3.2	0								
3	H	4	INV	14	13	11	975	2.940	1.604	.399	4.3.2	0								
4	H-C	4	INV	14	23	11	384	1.079	1.604	.399	4.3.2	0								
5	H-C	4	INV	14	20	11	800	2.820	1.604	.399	4.3.3	115			1.0	0				
6	H-C	4	INV	14	23	11	1000	3.660	1.604	.399	4.3.2	115			1.0	1.0				
7	H-C	4	INV	14	23	11	600	2.240	1.604	.399	4.3.2	110	1.0	1.0						
8	H-C	4	INV	14	23	11	1000	3.661	1.604	.399	4.3.2	110	3.0	3.0						
9	H	4	10	14	13	16	68	.067	1.604	11.895	4.3.3	115			1.0	1.0				
10	H	4	10	14	13	16	400	.368	1.604	11.895	4.3.2	115			1.0	1.0				
11	H	4	10	14	13	16	2000	1.832	1.604	11.895	4.3.2	116					1.0	1.0	4.0	8
12	H-C	4	10	14	24	16	2000	1.835	1.604	11.895	4.3.2	116					1.0	1.0	4.0	8
13	H-C	4	10	14	24	16	1400	1.255	1.604	11.895	4.3.2	110	1.0	1.0						
14	H-C	4	4	16	29	29	1600	2.466	.172	3.227	4.3.2	110	3.0	3.0						
15	H-C	4	4	16	29	29	800	1.268	.172	3.227	4.3.2	116					1.0	1.0	68.5	10
16	H	2	INV	14	13	11	1000	10.661	1.604	.405	4.3.2	115			1.5	1.5				
17	H	2	10	14	13	23	3000	3.420	1.604	21.961	4.3.2	116					1.5	1.5	4.0	8
18	H	4	1	14	13	21	1000	2.344	1.604	.132	4.3.2	116					1.0	1.0	10.3	12
19	H	4	4	16	13	29	2000	3.049	.172	3.227	4.3.2	116					1.0	1.0	68.5	10
20	H	4	100	14	13	23	3500	1.035	1.604	25.647	4.3.2	116					1.0	1.0	4.0	8
21	H-C	4	4	16	29	29	1600	2.477	.172	3.227	4.3.2	0								

1. CF = Configuration: H = hemisphere, H-C = hemisphere-cylinder. 2. Diff. T = Differencing Technique.

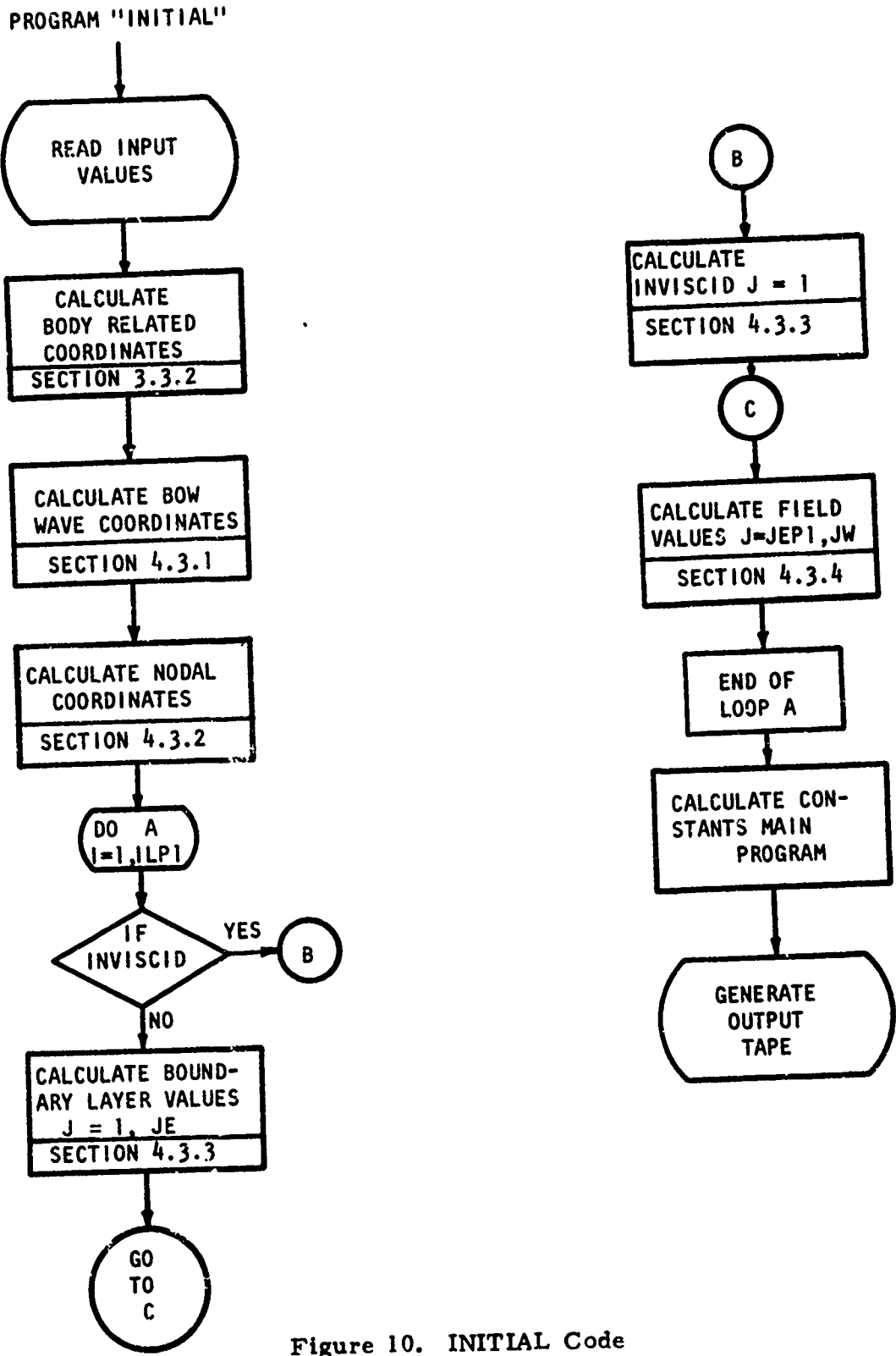


Figure 10. INITIAL Code

Execution time of program INITIAL was approximately 2 minutes on a GDC 3800 computer.

Initial bow coordinates were computed by the techniques of section 4.2.1. The computed bow wave was slightly upstream of the experimental one of Baer [4] as displayed in figure 11.

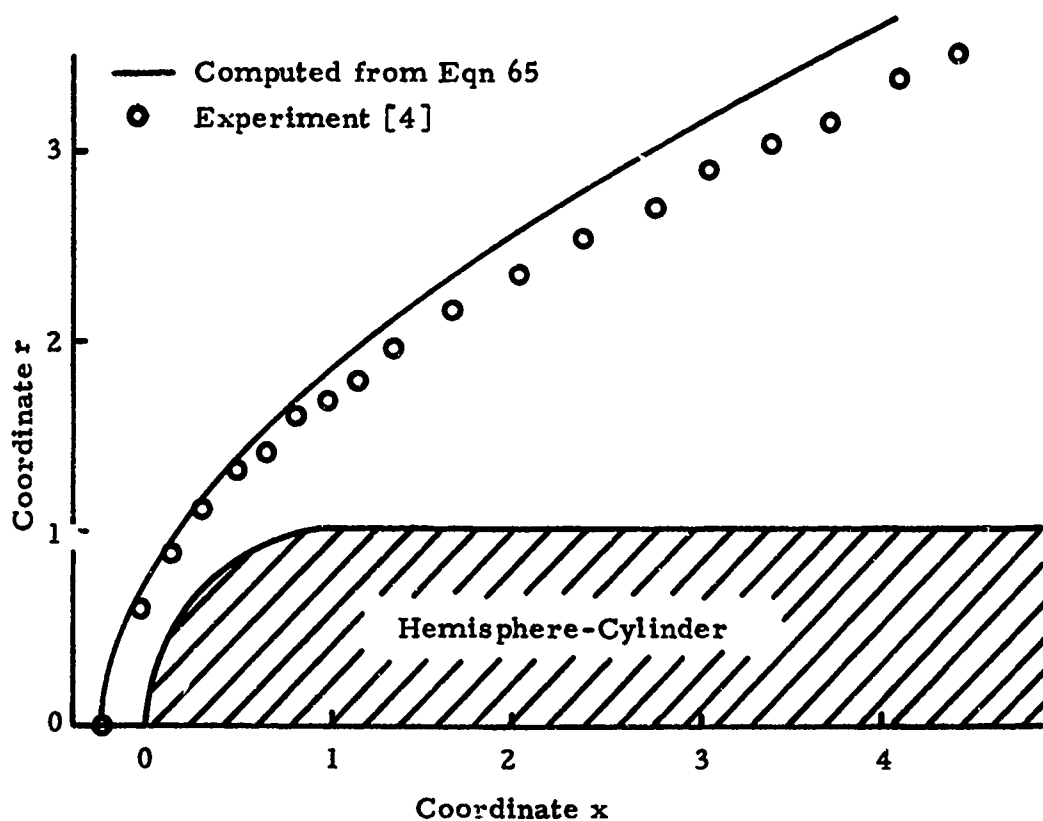


Figure 11. Computed and Experimental Bow Wave Coordinates at $M_0 = 4$

Since the MAIN code adjusted the location of the bow wave, the difference between computed and experimental bow wave coordinates was not important.

Initial values of pressure in the boundary layer were assumed independent of Reynolds number and ω . As expected, computed and

experimental initial body pressures of figure 12 are in good agreement, since the INITIAL code used experimental results of Clark [16] for a hemisphere. In the afterbody region, the initial pressure $p_b(\lambda)$ was equal to the initial pressure p_b at the junction of the hemisphere and cylinder. As shown in figure 13, this assumption resulted in a perturbation in the velocity thickness ω_e of the boundary layer near the junction. In the time dependent computations of the MAIN code, these perturbations in ω_e were quickly eliminated.

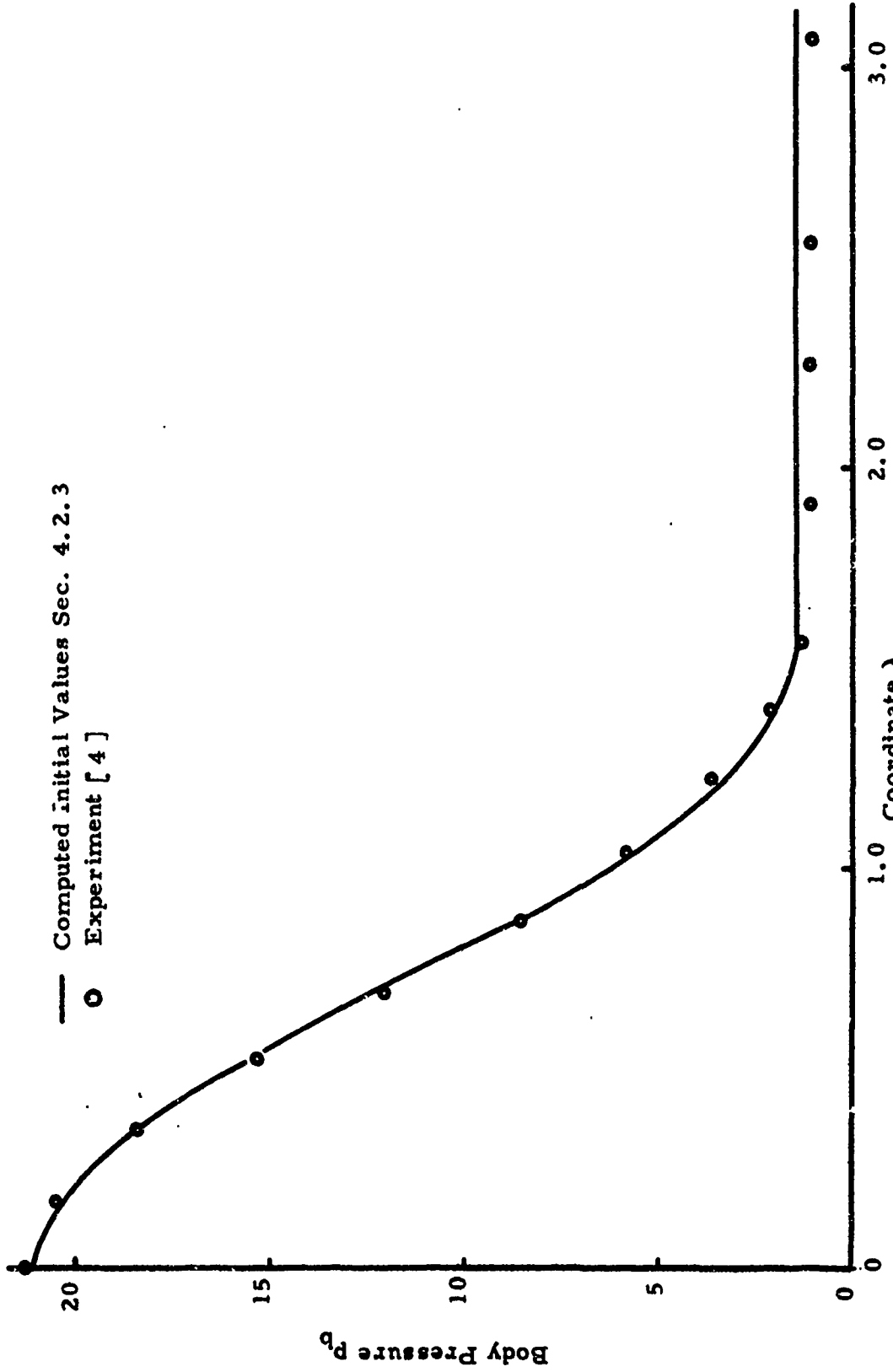


Figure 12. Initial Values of Body Pressure for $M_0 = 4$.

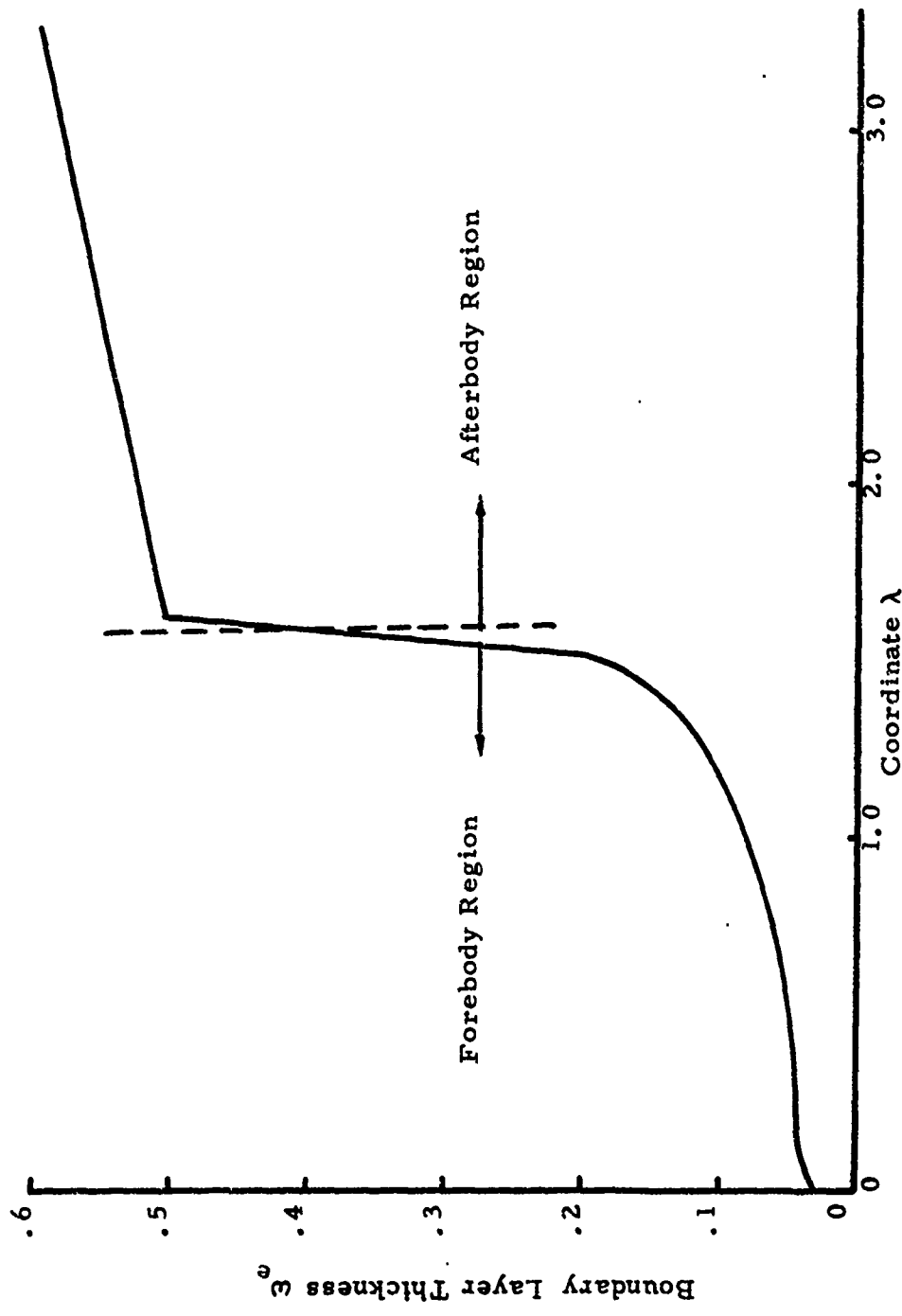


Figure 13. Initial Values of Velocity Thickness ω_e of Boundary Layer for $M_o = 4$ and $Re_o = 4000$.

5.2.2 MAIN. A simplified flow diagram of the MAIN code is presented in figure 14. A set of indicators was used to control input from the initial value tape, specify inviscid or viscous flow, specify the stabilizing term, set the output and run intervals and specify the size of the field. Integer values of I, J and K were used to identify nodes and time. The relationships between ζ , ν , τ and I, J, K are given by equations 66, 67 and 68. KIN and KL are starting and ending indices of times. If KIN = 1, initial values were obtained from INITIAL. If KIN > 1, initial values were obtained from an output tape of a previous run. Computations were halted at KL, and results were printed and recorded on tape.

In operation 1 of figure 14, equation 109 was used to compute Δt_{ℓ} at all nodes. $\Delta \tau$ equaled the minimum of Δt_{ℓ} for one cycle of the A loop. In operation 2, bow wave coordinates were updated according to section 4.6.2. Operation 3 computed values at the body surface, and operation 4 computed values along the stagnation streamline. In operation 5, values at all other nodes were calculated using the equations of sections 4.3 and 4.5. Extrapolation of values at the downstream boundary was accomplished in operation 6.

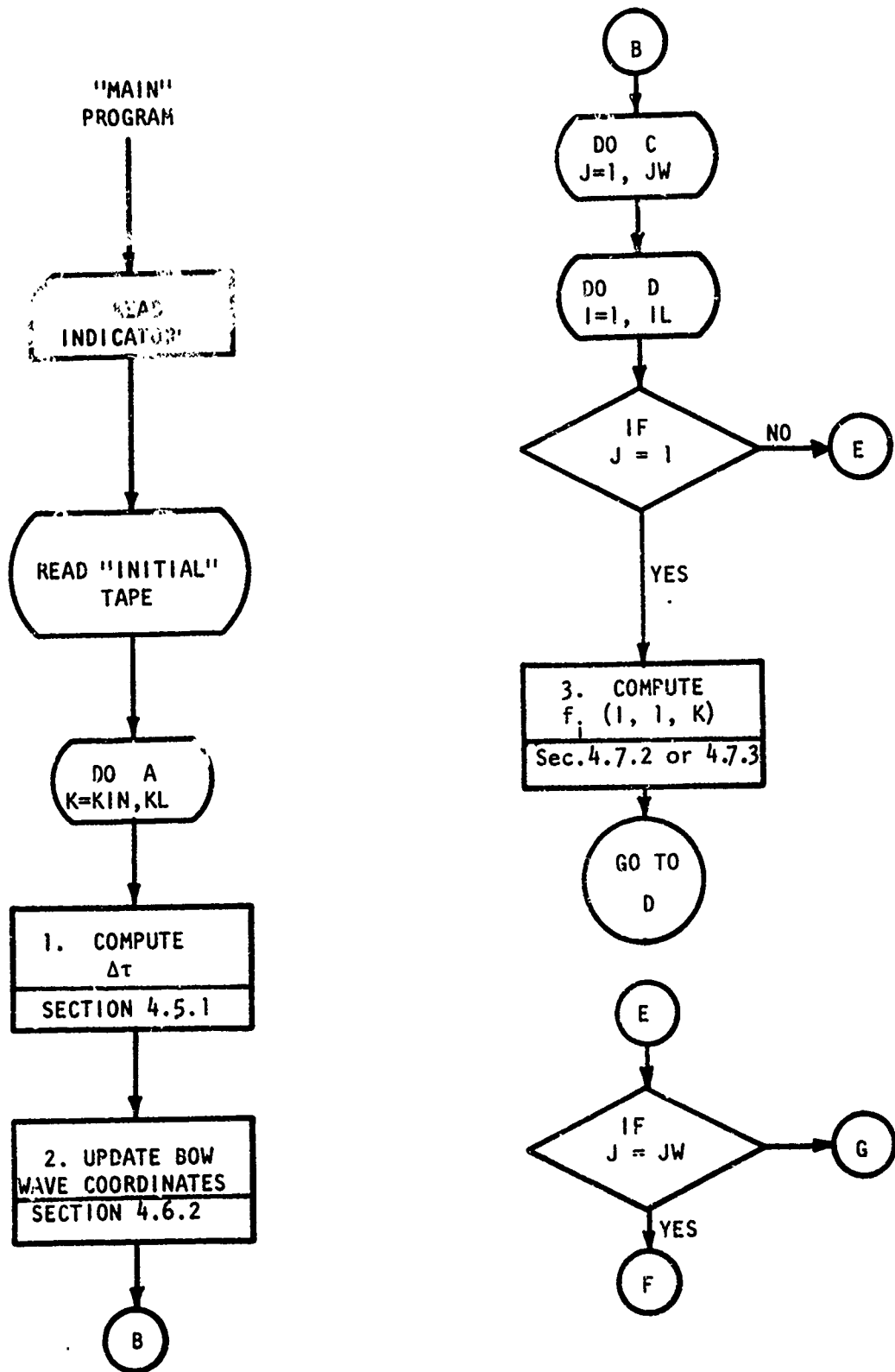


Figure 14a. MAIN Code

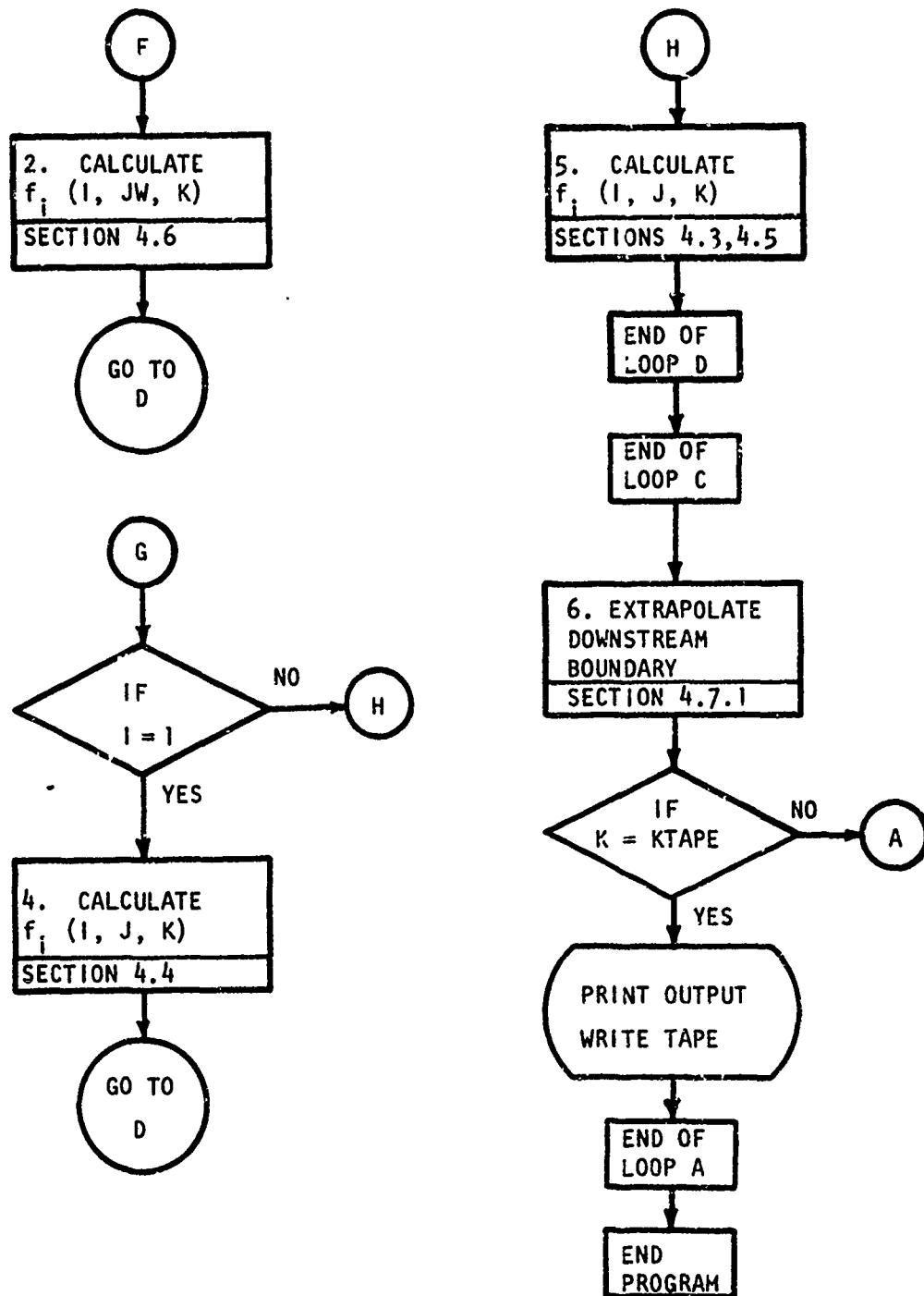


Figure 14b. MAIN Code

5.2.3 Computational Times. Field values were computed at a rate of 56.7 nodes/second on a CDC 3800 computer. Values of $f_i(I, JW, K)$ at the downstream side of the bow wave were computed at a rate of 17.8 nodes/second. For a CDC 3800 computer,

$$t_c = (K)(IL)[c(JW - 1) + .0563] \quad (147)$$

where: t_c = execution time in seconds $\pm 5\%$

c = .0154 for inviscid flow and = .0177 for viscous flow

$K \geq 100$ cycles

The percentage of total CDC 3800 computer time required for wave fitting is shown in figure 15.

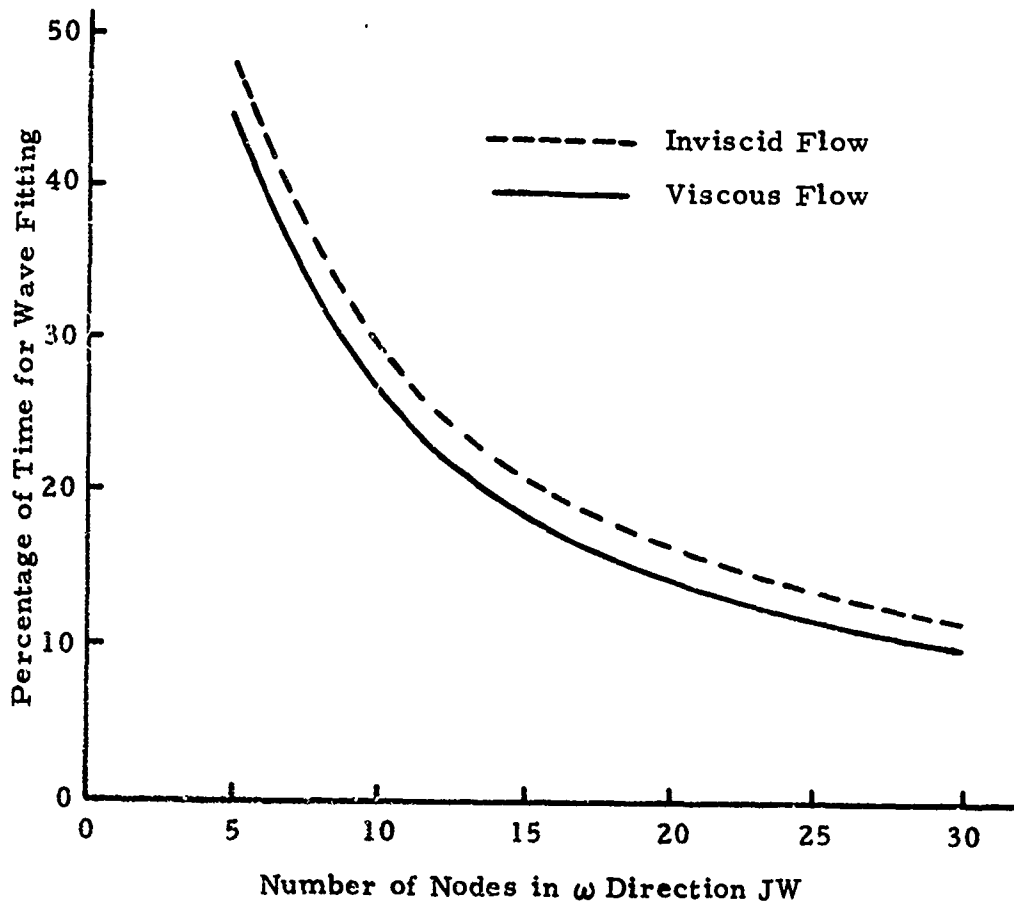


Figure 15. Percentage of Computer Time for Wave Fitting

In this investigation, $JW = 11$ for inviscid flows and $16 \leq JW \leq 29$ for viscous flows. Assuming that wave fitting could be accomplished as quickly as field computations, from 10 to 48 percent of the total computational time could be saved. Numerical experiments were made in an attempt to speed up the wave fitting computations. The attempt first involved increasing 10^{-5} to 10^{-3} in expression 132. The second attempt was to use equation 129 to compute η' . Neither of those attempts was successful because of lack of convergence near the bow wave.

5.3 Stabilization of Computations

5.3.1 Introduction. The first computation of viscous, compressible flow around a hemisphere-cylinder without stabilizing terms displayed numerical instabilities. A major problem of this investigation was to achieve numerical stability without destroying accuracy. Many attempts were made to avoid the use of a stabilizing term, including one dimensional wave fitting investigations, stationary coordinate frames, modification of coordinates of nodes and variation of differencing techniques. Results of unstabilized computations, the development of satisfactory stabilizing terms and accurate solutions of several systems are presented in this section.

5.3.2 Unstabilized Computations. Specifications of runs 1 through 4 for viscous and inviscid flows with $\psi_i = 0$ are given in table 2. The location and extent of instabilities are displayed in figures 16 through 19 at the end of this section on pages 87 to 90. For viscous flow in run 1, spatial

oscillations in the u-velocities at $I = 3$ of figure 16 began near the center of the field and spread into the region next to the body. As displayed in figure 17, there was an instability in u-velocities in run 2 at $I = 19$. There were similar instabilities in other variables. These instabilities were maximum at $I = 19$. Oscillations were small near the body surface and were maximum near the center of the field. Results of runs 3 and 4 for inviscid flow are shown in figures 18 and 19. Since the instabilities occurred for inviscid flow, they were attributed to the inviscid part of the field equations. Since the instabilities were similar for viscous and inviscid flows, it was concluded that viscous terms had little effect on the instabilities.

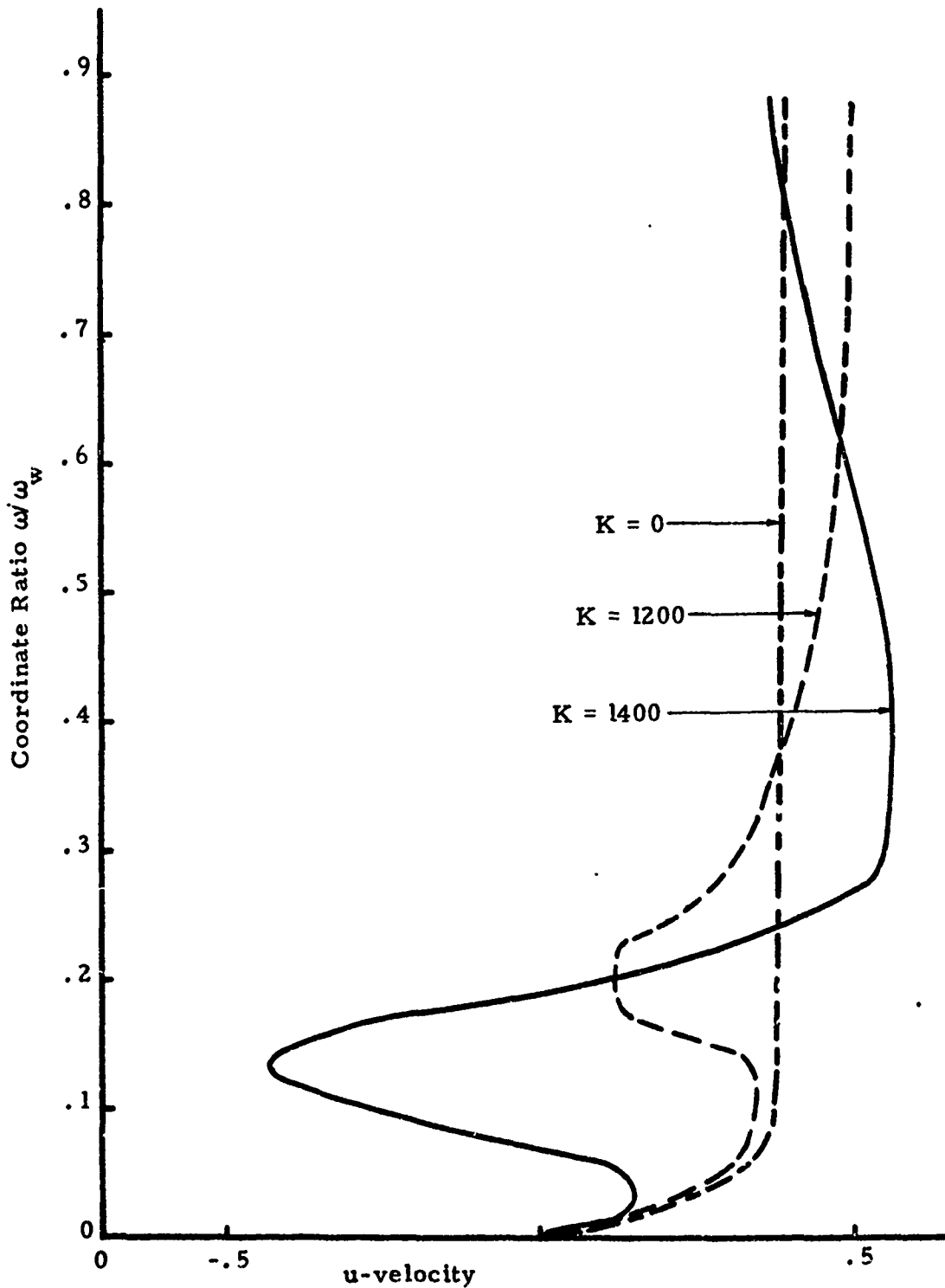


Figure 16. Instabilities in Forebody Region at $I = 3$. Run 1. Viscous Flow Around a Hemisphere with $\psi_i = 0$.

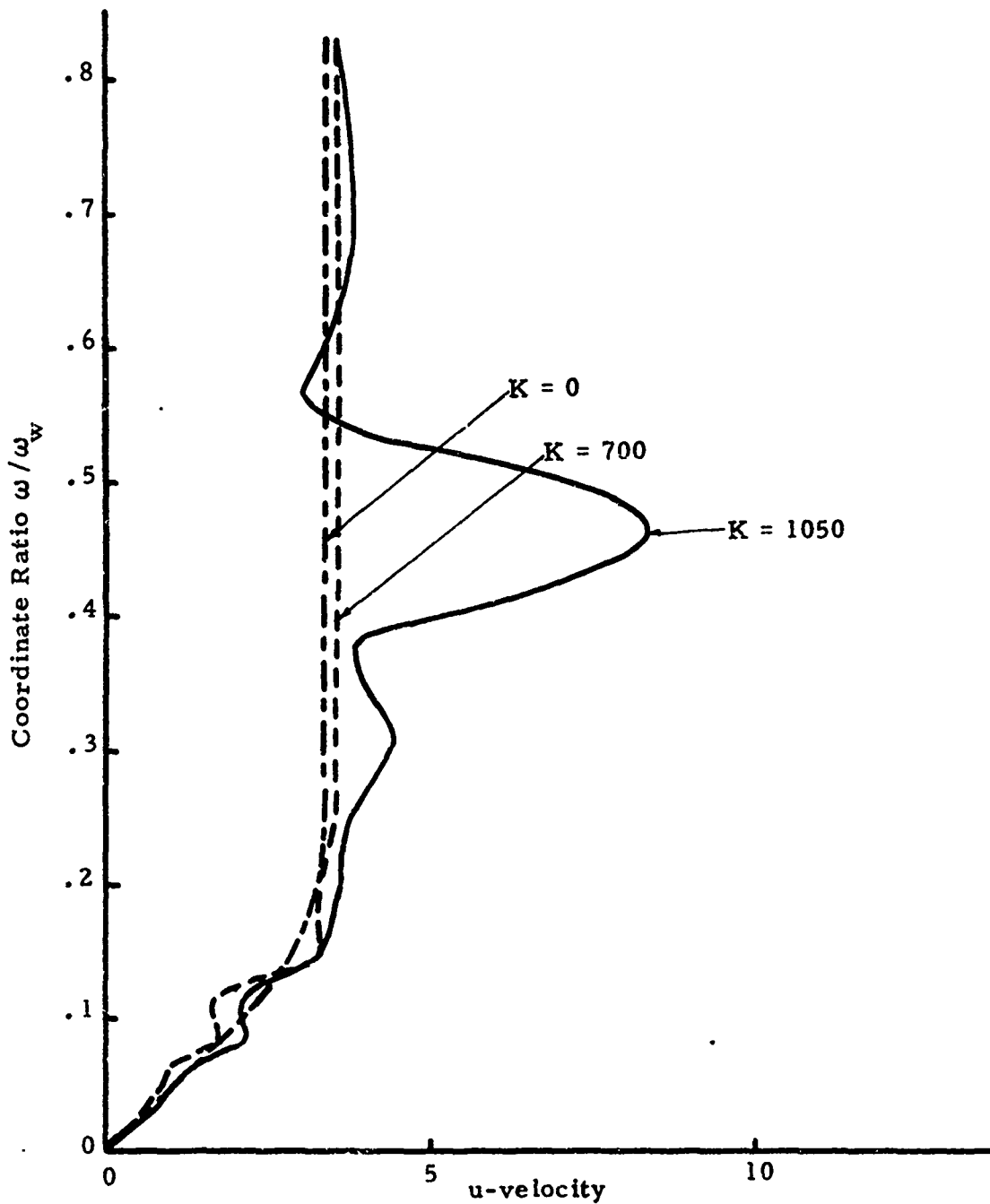


Figure 17. Instabilities in Afterbody Region at $I = i9$. Run 2. Viscous Flow Around a Hemisphere-Cylinder with $\psi_1 = 0$.

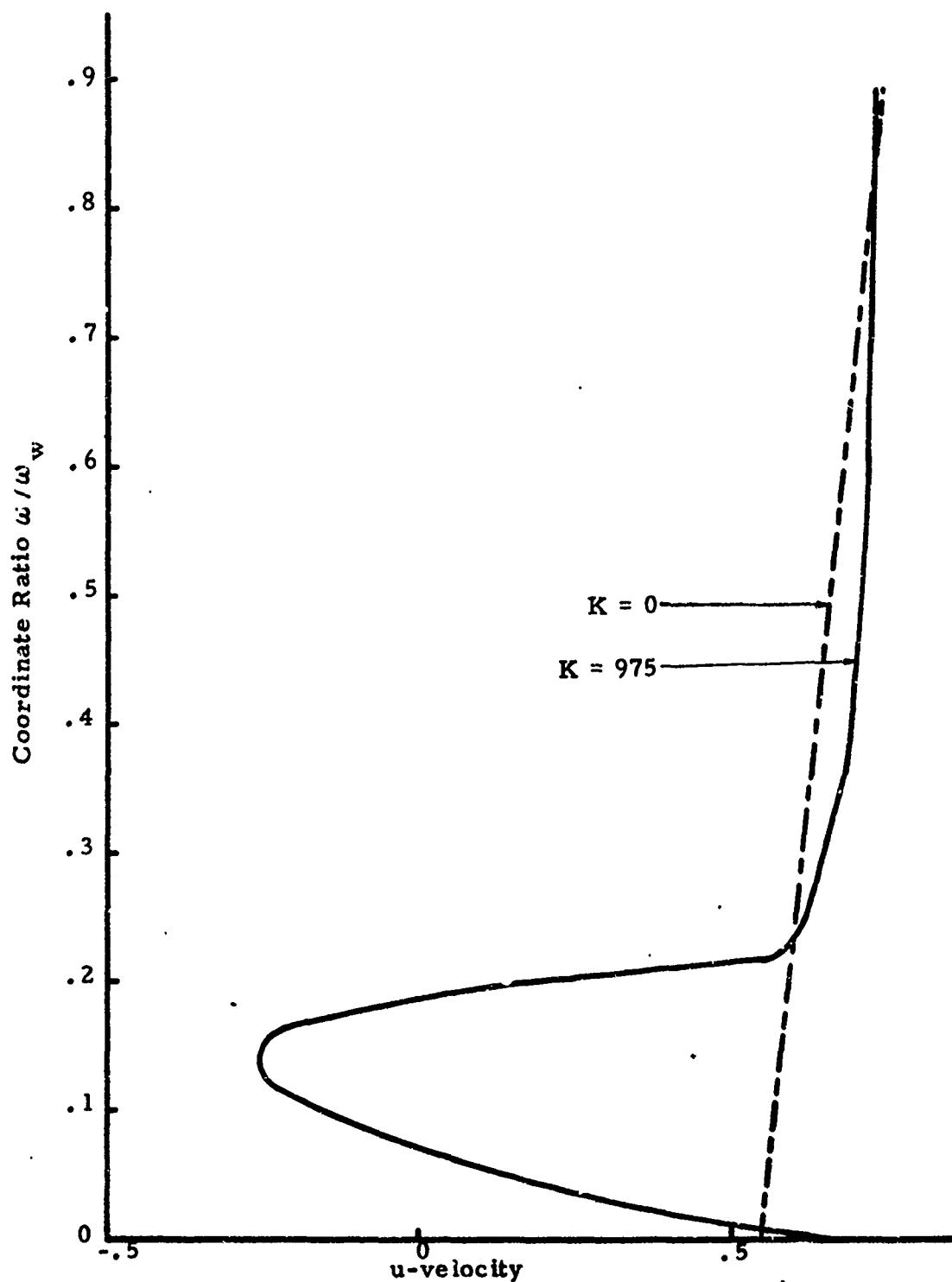


Figure 18. Instability in Forebody Region at $I = 3$.
 Run 3. Inviscid Flow Around a Hemisphere with $\psi_1 = 0$.

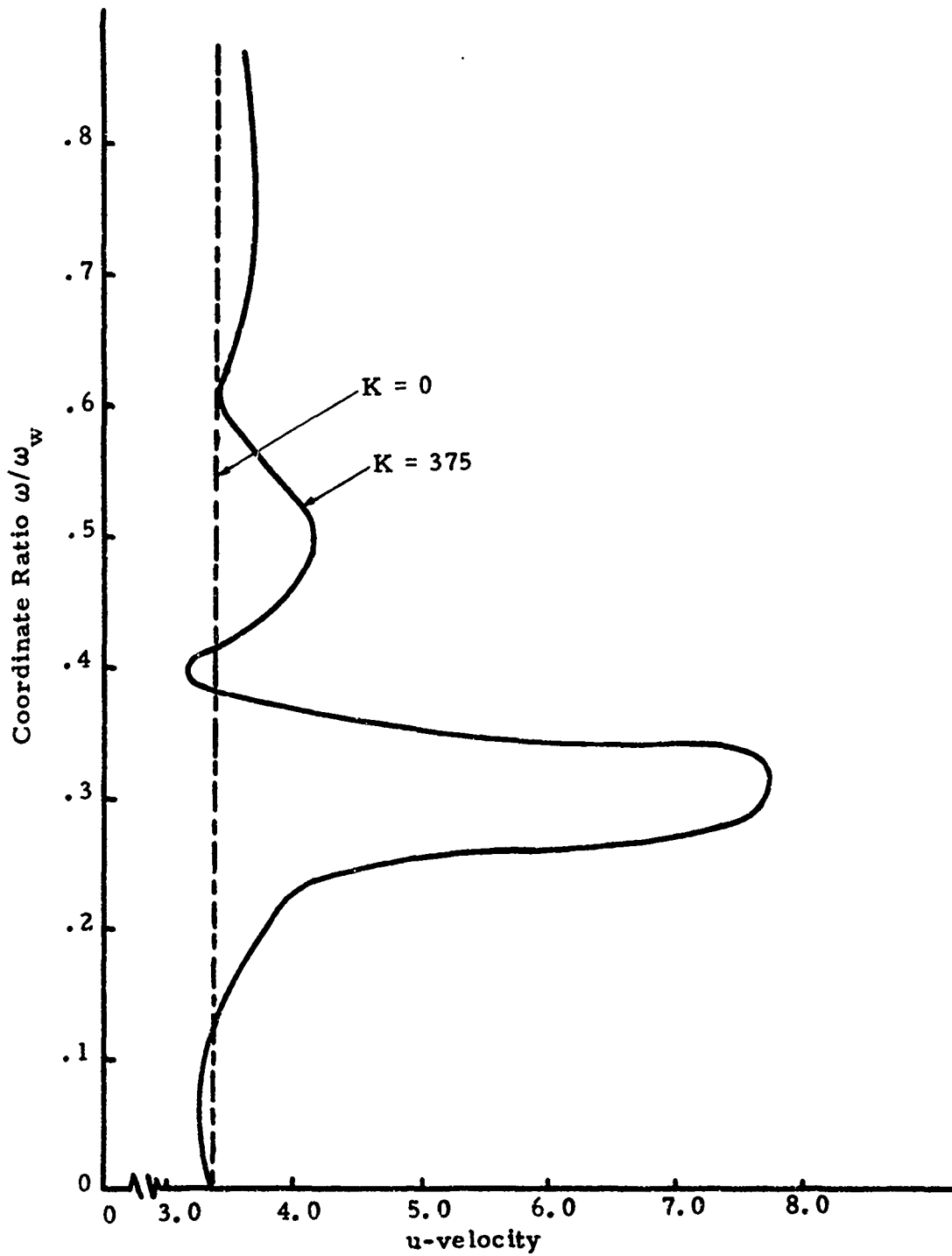


Figure 19. Instability in Afterbody Region at $I = 19$.
 Run 4. Inviscid Flow Around a Hemisphere-Cylinder with $\psi_i = 0$.

5.3.3 Development of Stabilizing Terms. A development program was initiated to determine the cause of the instabilities and to find techniques for stabilizing solutions. Inviscid flow solutions converged approximately four times faster than the corresponding viscous ones. Therefore, inviscid systems were used in this phase. The first step was to determine if instabilities were caused by errors in equations or computer coding. To detect errors in equations of section 4.3.2 and their coding, results of computations using them were checked with those of a simpler two-step technique of the form

$$f_i(\zeta, \nu, \tau + \frac{\Delta\tau}{2}) = f_i(\zeta, \nu, \tau) + \frac{\Delta\tau}{2} f_{i,\tau}(\zeta, \nu, \tau) \quad (148)$$

$$f_i(\zeta, \nu, \tau + \Delta\tau) = f_i(\zeta, \nu, \tau) + \Delta\tau f_{i,\tau}(\zeta, \nu, \tau + \frac{\Delta\tau}{2}) \quad (149)$$

Using these equations with the specifications of runs 3 and 4 of table 2, the instabilities were similar to those of figures 18 and 19, except they grew more rapidly. It was concluded that the equations of section 4.3.2 were correct and properly coded.

The differencing technique of section 4.3.3 with a stabilizing term was used in run 5 of table 2 to determine if wave fitting and downstream boundary equations introduced perturbations. The solution was stable at $K = 800$. Computed body pressures of figure 20, page 96, are in agreement with the measurements of [4]. The differences of computed and measured bow wave coordinates in figure 21 were not considered detrimental to other parts of the field and were partially attributed to

the averaging of body curvature $\kappa(\lambda)$ in equation 96. It was concluded that the bow wave and downstream boundary equations were satisfactory. The results of runs 5 and 6 with the differencing techniques of sections 4.3.3 and 4.3.2 and stabilizing terms were within 1 percent of each other except near the junction of the hemisphere and cylinder. The results of run 6 were smoother and in better agreement with the measurements of [4].

Equation 110 was used to stabilize the solutions in runs 7 and 8. In run 7, $C_1 = C_2 = 1$, and in run 8, $C_1 = C_2 = 3$. In figure 22, body surface pressures of those runs display an incorrect hump near the junction. Body surface pressures of run 6 in figure 22 are in better agreement with the measurements of [4] than are those of runs 7 and 8. As shown in figure 23 near the junction of the hemisphere-cylinder, the v -velocities of run 8 deviate from those of runs 6 and 7. From figures 22 and 23 for inviscid flows, the stabilizing term of equation 115 yielded more accurate results than those of equation 110.

The development of stabilizing terms for viscous flows was more difficult than for inviscid flows because conditions in the boundary layer are sensitive to stabilizing terms. In run 9, with the differencing technique of section 4.3.3 and the stabilizing term of equation 115, results were unstable near the stagnation point at $KL = 68$. Run 10, with the differencing technique of section 4.3.2 and stabilizing term of equation 115, was stable but was unsatisfactory because the stabilizing term ψ_1 was much larger than the viscous term ϕ_1 in the boundary layer. This

meant the boundary layer results were inaccurate. A few runs were tried with a new stabilizing term

$$\psi_i = (C_8 u^2_{f,\lambda\lambda} + C_9 v^2_{f,\omega\omega}) \frac{\Delta t^2}{2} \quad (150)$$

where $C_8 = C_9 = 1, 2$ or 3 . Although ψ_i was small compared to φ_i in the boundary layer, severe oscillations occurred outside the boundary layer and equation 150 was abandoned.

Run 11, for viscous flow around a hemisphere, utilized the stabilizing term of equation 116 for which $\psi_i(\lambda, 0, t) = 0$ at the body surface. As shown in figures 24, 25 and 26, in the boundary layer, the stabilizing term ψ_i is small compared to the viscous term φ_i . Small oscillations in φ_3 were not reproduced in figure 25. The steady bow wave coordinates and body pressures agreed with the measurements of [4]. The results of run 11 are given in section 5.5.2. In runs 11, and 17 through 20, the stabilizing term of equation 116 was satisfactory for hemispheres at $M_o = 2$ and 4 and $Re_o = 10^3$ to 10^5 . For each set of Mach and Reynolds numbers, numerical experiments were used to determine values of C_5, C_6, C_7, J_e and nodal parameters.

For viscous flow around a hemisphere-cylinder, the stability problem was more difficult than for a hemisphere. Figure 27 displays pressures versus ω/ω_w in the afterbody region at $I = 19$ for runs 2, 12 and 13. Run 2 was unstabilized and was discussed in section 5.3.2. Runs 12 and 13 used the differencing technique of section 4.3.2 and stabilizing terms of equations 116 and 110 respectively. Pressures in run 12 at

KL = 2000 are unstable and are approaching those of run 1 without stabilization. In run 13, small oscillations are present; however, these oscillations decreased as K increased. Values of other variables were smooth in run 13. As illustrated in figure 28 for run 13, ψ_i was larger than ϕ_i in the boundary layer, so that results were inaccurate. Moreover, in figure 23 for inviscid flow, the results of equation 110 were less accurate than those of equation 115. From the analysis of runs 1 through 13:

1. For inviscid flow, the differencing technique of section 4.3.2 and stabilizing term of equation 115 was accurate.
2. For viscous flow and the differencing technique of section 4.3.2, the stabilizing term of equation 116 yielded accurate results in the boundary layer.
3. Other numerical techniques and coding used in conjunction with items 1 and 2 were satisfactory.
4. Solutions involving equation 110 with $C_1 = C_2 = 3$ converged rapidly and eliminated perturbations but were inaccurate in the boundary layer.
5. Nodal spacing was critical for stability and accuracy.

By incorporating these ideas into the specifications of runs 14 and 15, a satisfactory solution was obtained for viscous flow around a hemisphere-cylinder. The small Reynolds number of 4000 was selected to reduce the number of cycles required for convergence. Experimentation revealed that stability was enhanced by increasing the number of nodes. The number of nodes was 384 in runs 12 and 13 and was 841 in

runs 14 and 15. In run 14 with the stabilizing term of equation 110 with $C_1 = C_2 = 3$, the perturbations of initial values were not apparent in the results at $K = 1600$. Using the output tape of run 14 for initial values in run 15, the results converged within 800 cycles. As illustrated by figure 29, the effect of the stabilizing term was small, even in the boundary layer. Results of run 15 are presented in section 5.5.3.

In applying equation 11c to other viscous systems, acceptable values of C_5 , C_6 , C_7 and J_e may be determined by numerical experiments in which relative magnitudes of φ_i and ψ_i are compared. Additional numerical experiments may be desirable to optimize the number of nodes and nodal spacing.

— Run 5, Section 4.3.3, Equation 115, $\mu = 0$

● Experiment [4], $Re_0 = 1.28 \times 10^6$

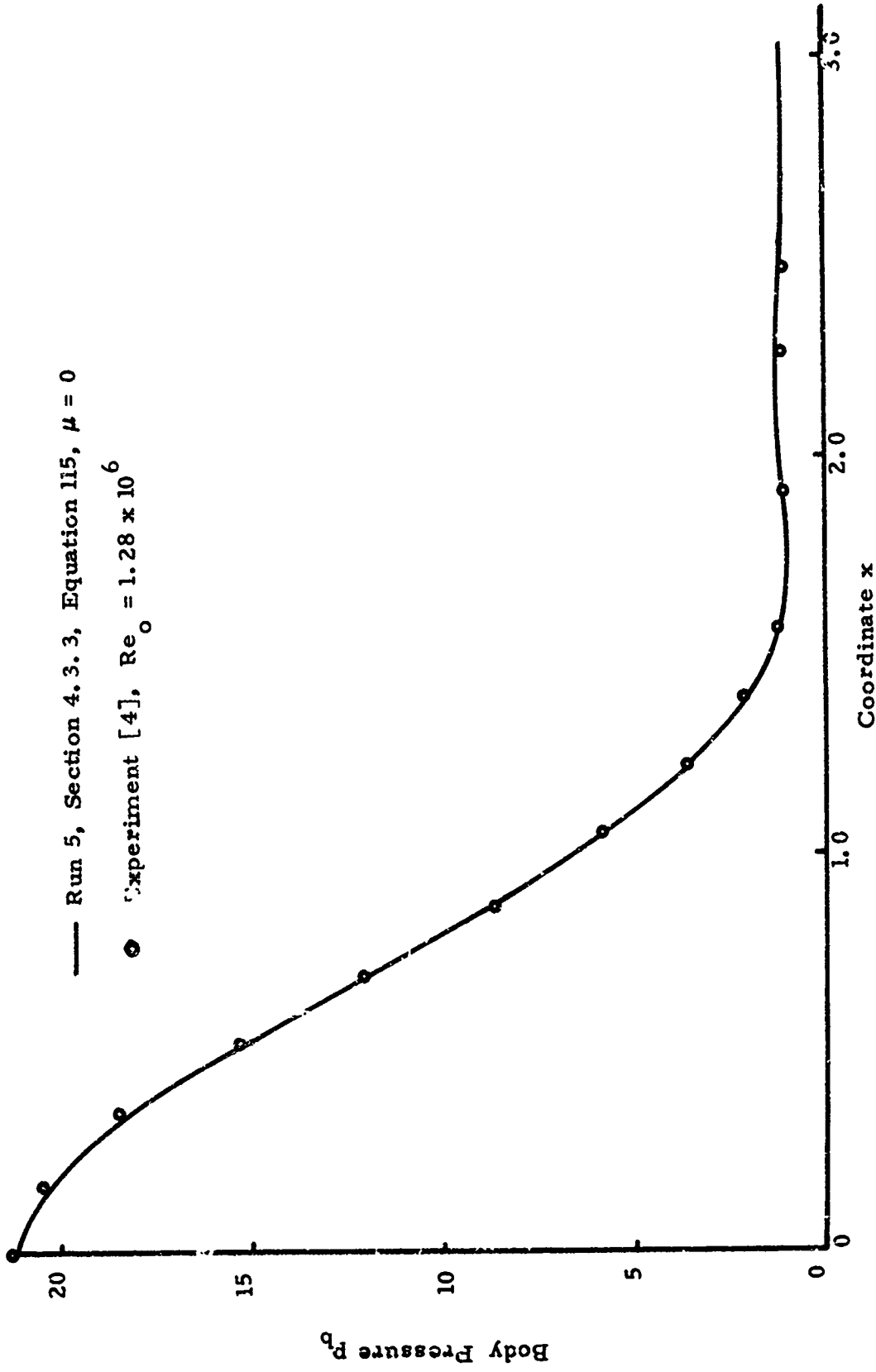


Figure 20. Computed and Experimental Body Surface Pressures around Hemisphere-Cylinder. $M_0 = 4$.

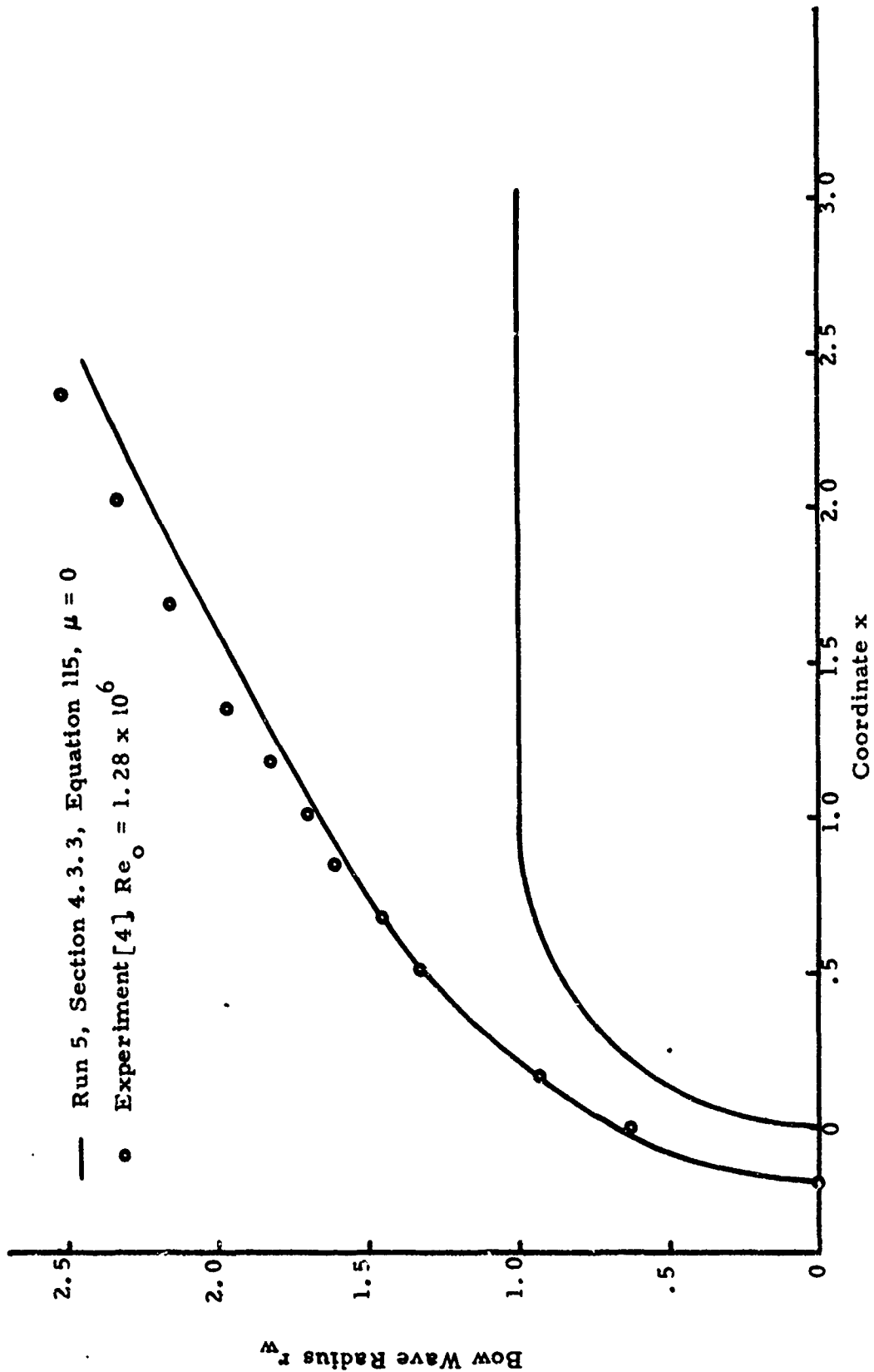


Figure 21. Computed and Experimental Bow Wave Coordinates around Hemisphere-Cylinder. $M_0 = 4$.

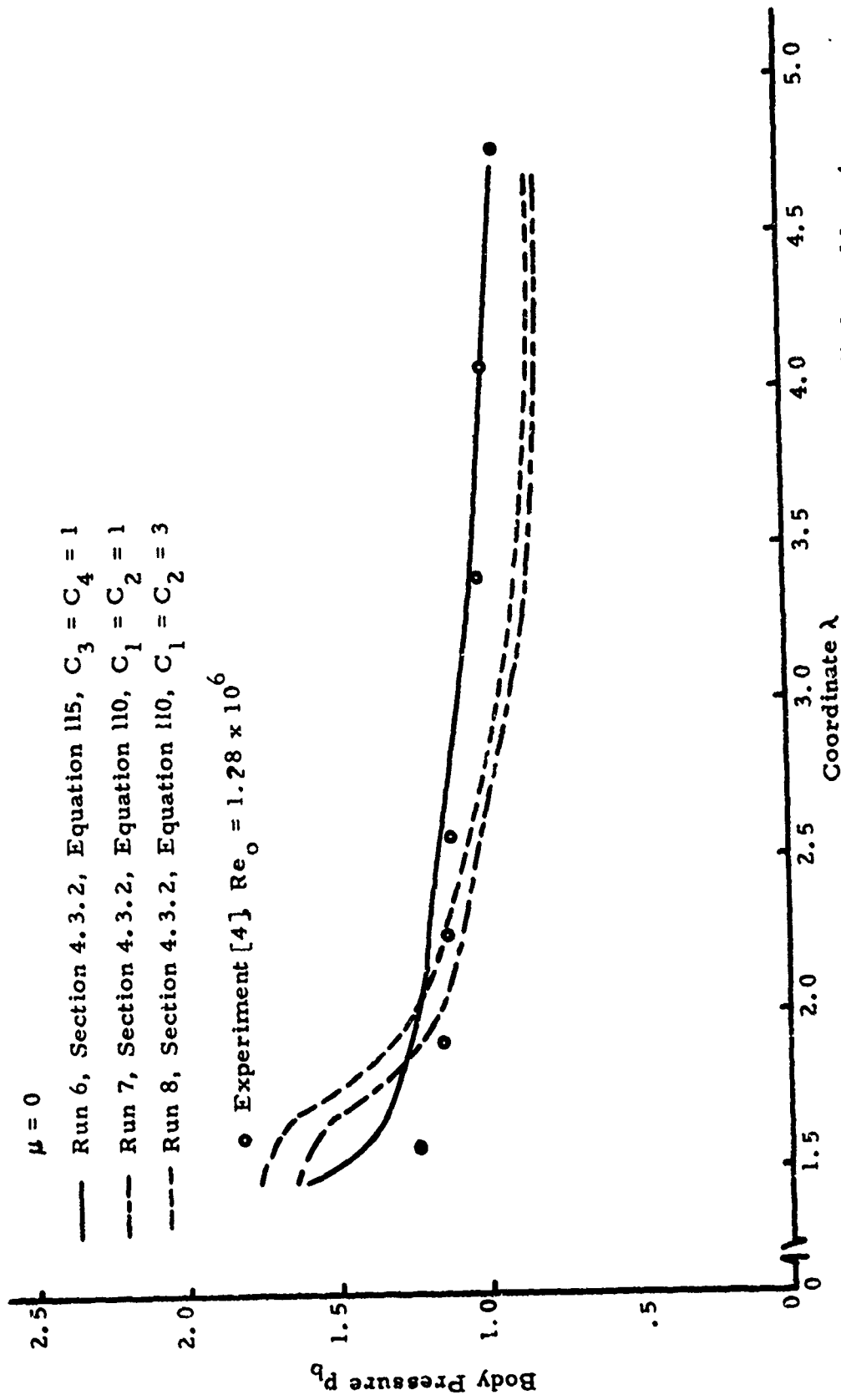


Figure 22. Body Surface Pressures Near Junction of Hemisphere-Cylinder. $M_0 = 4$.

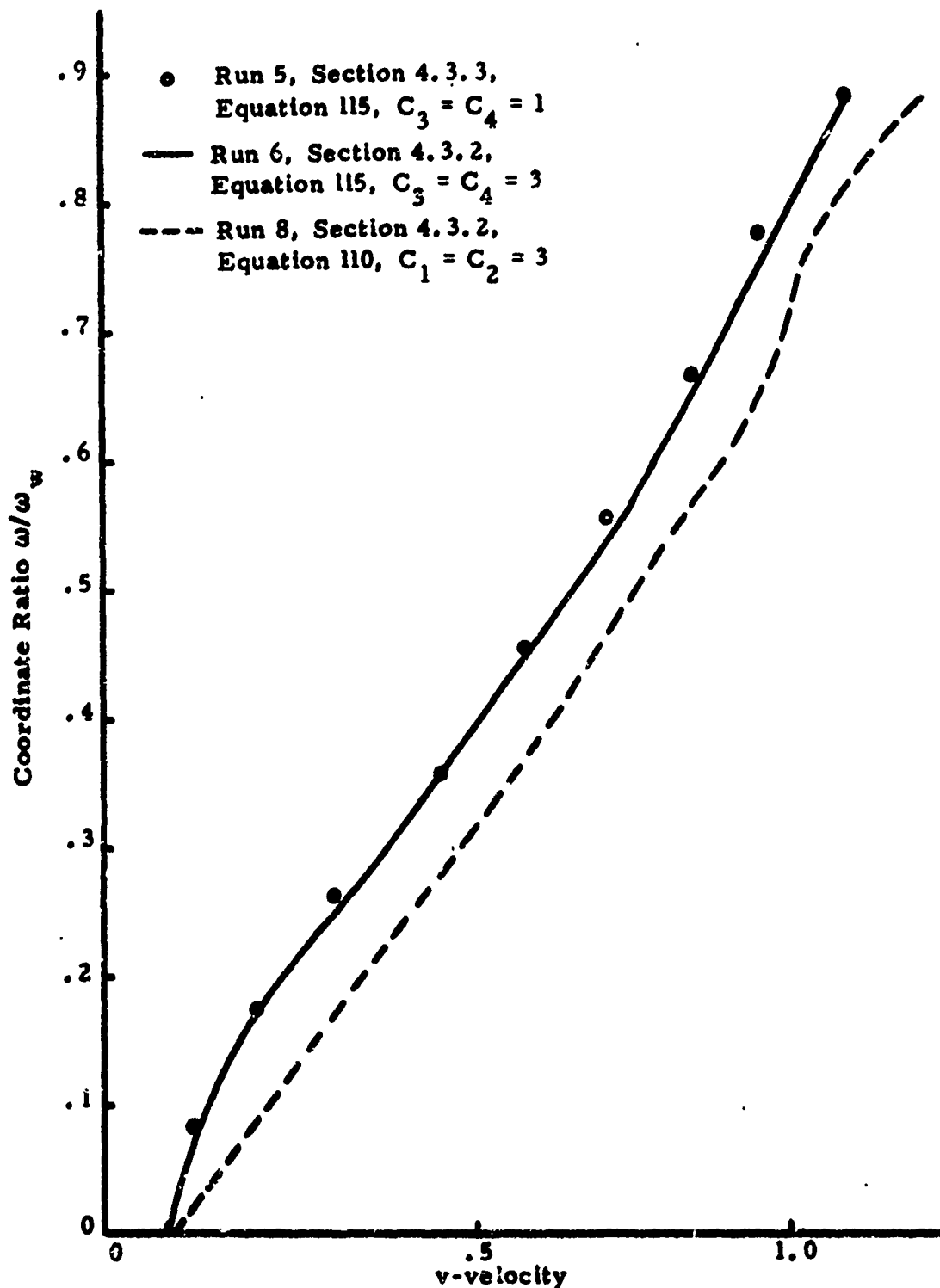


Figure 23. Computed v-velocities. Near Junction at $l = 16$. Inviscid Flow around Hemisphere-Cylinder. $M_0 = 4$.

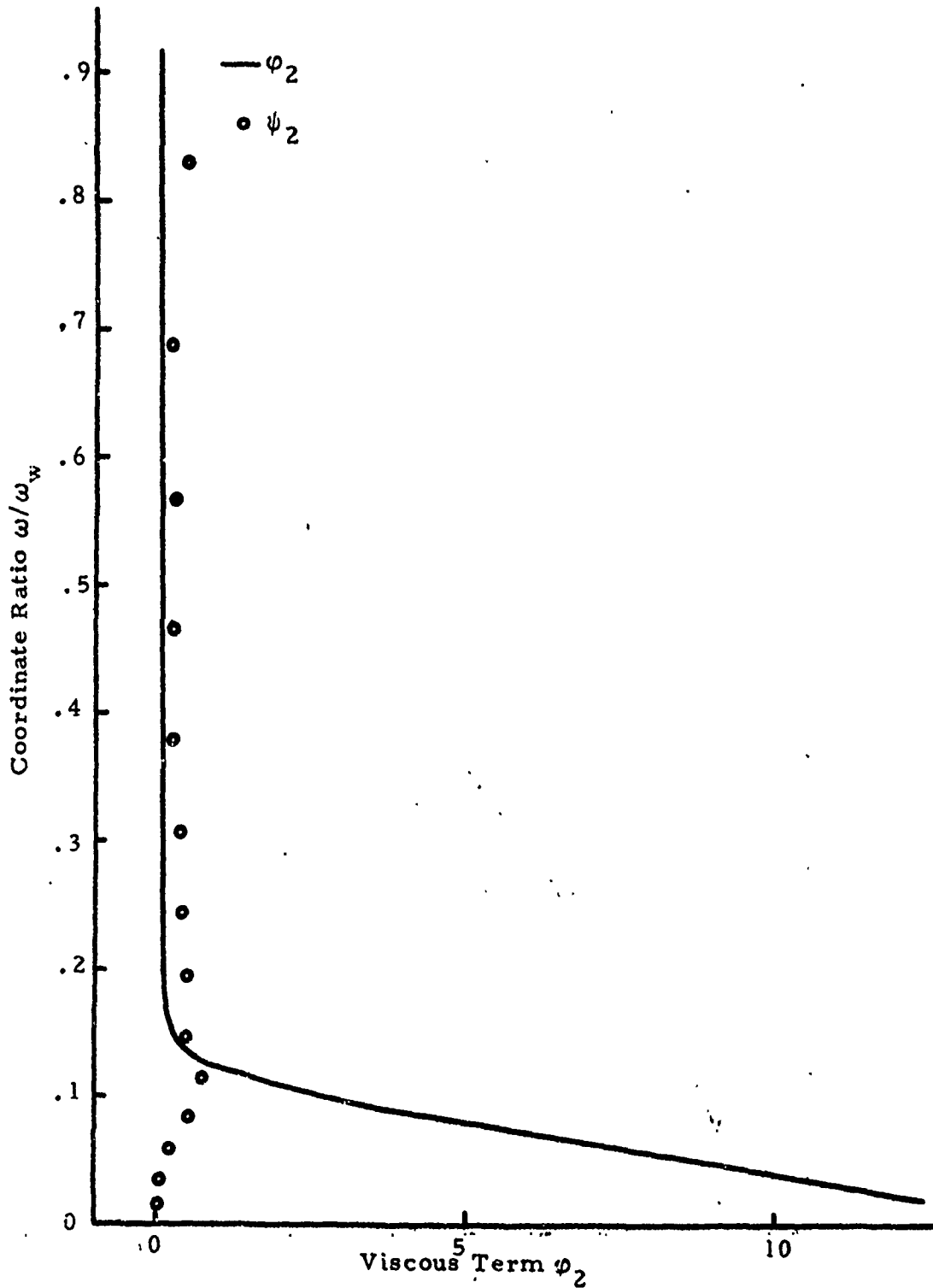


Figure 24. Viscous Term ϕ_2 and Stabilizing Term ψ_2 at $I = 8$ and $K = 2000$. Run 11. Hemisphere at $M_o = 4$ and $Re_o = 10^4$; Computed by Section 4.3.2 with Equation 116.

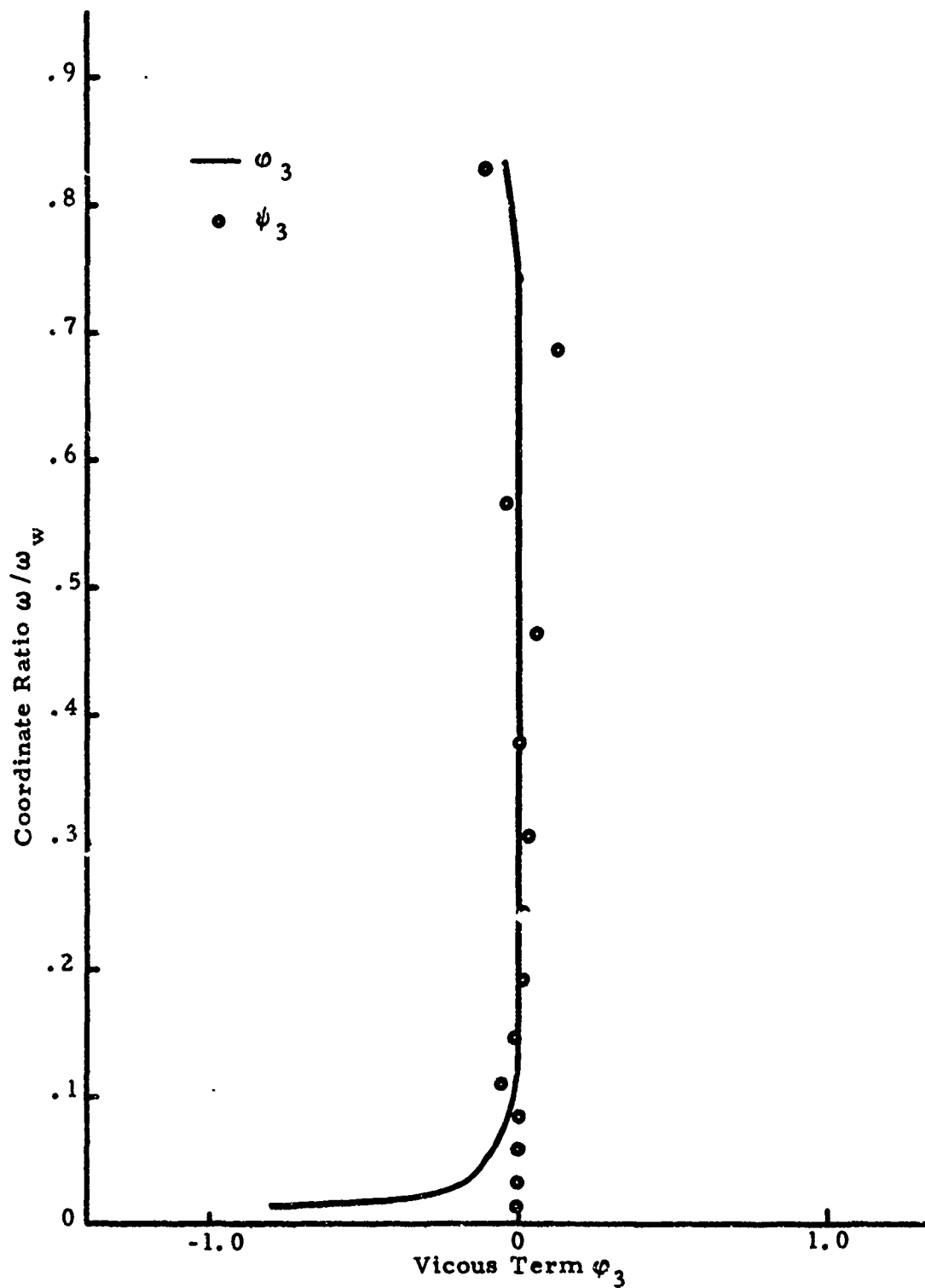


Figure 25. Viscous Term ϕ_3 and Stabilizing Term ψ_3 at $I = 8$ and $K = 2000$. Run 11. Hemisphere at $M_o = 4$ and $Re_o = 10^4$. Computed by Section 4.3.2 with Equation 116.

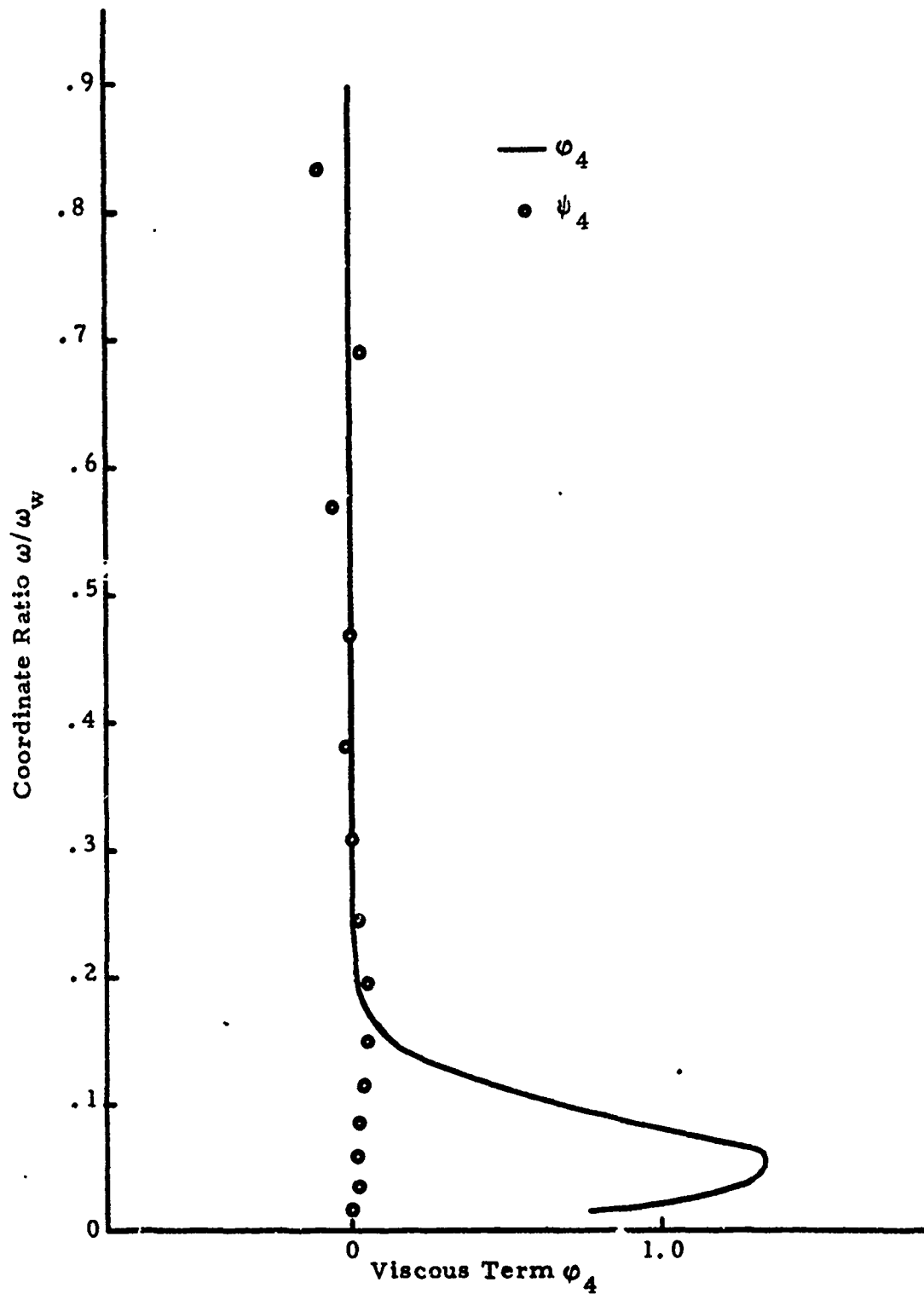


Figure 26. Viscous Term ϕ_4 and Stabilizing Term ψ_4 at $I = 8$ and $K = 2000$. Run 11. Hemisphere at $M_o = 4$ and $Re_o = 10^4$. Computed by Section 4.3.2 with Equation 116.

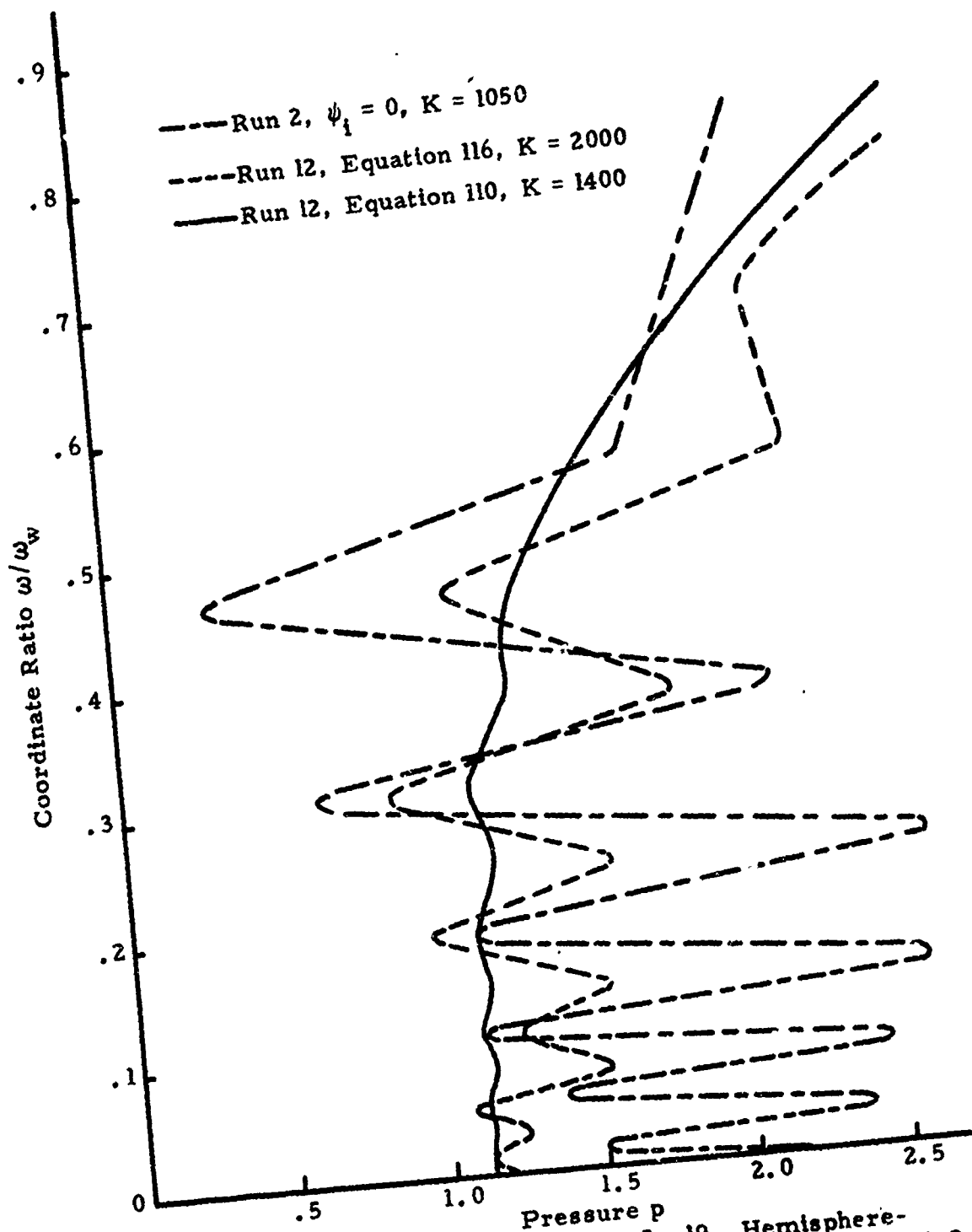


Figure 27. Pressure Oscillations at $I = 19$. Hemisphere-Cylinder at $M_o = 4$ and $Re_o = 10^4$. Computed by Section 4.3.2.

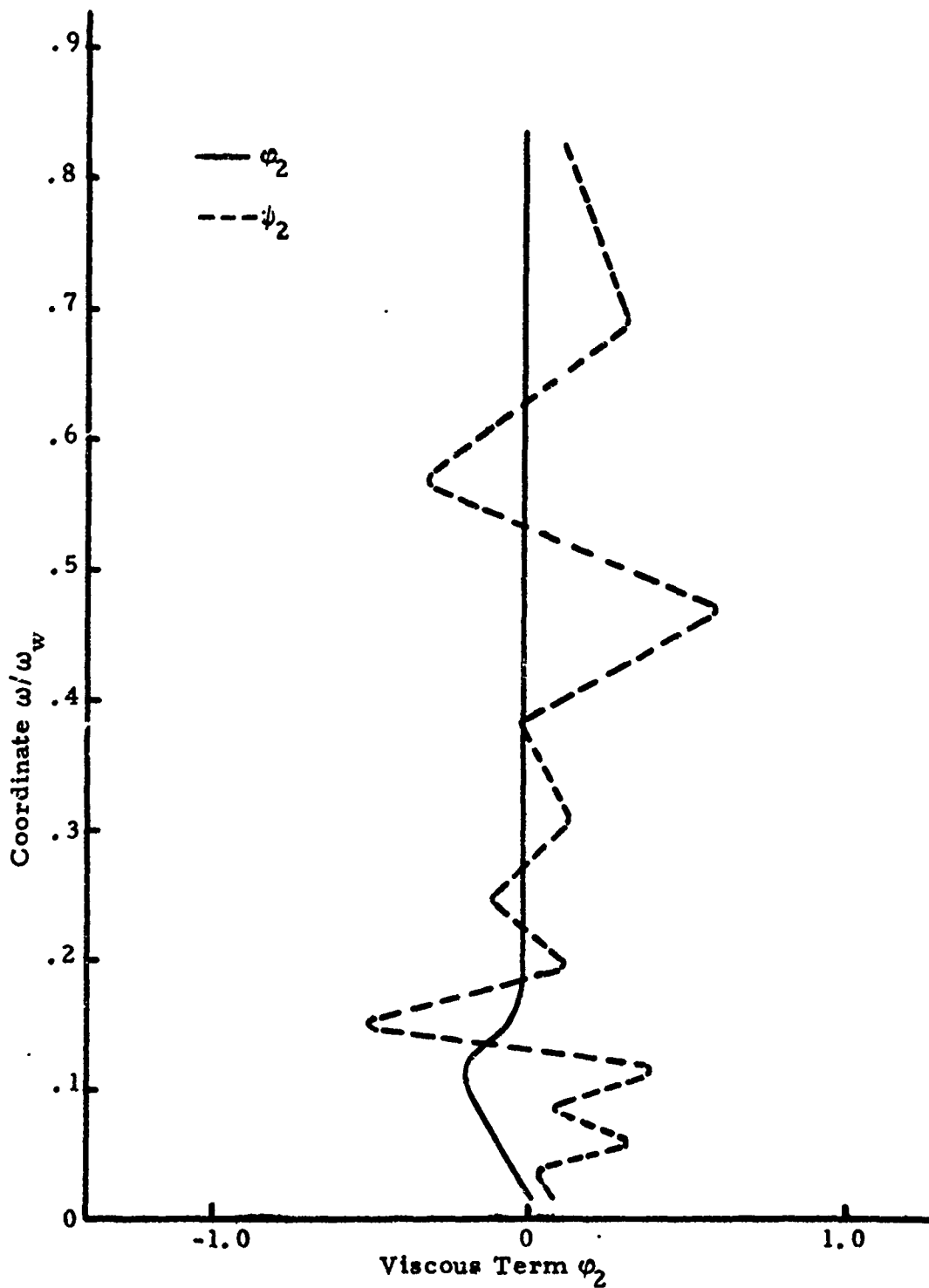


Figure 28. Viscous Term ϕ_2 and Stabilizing Term ψ_2 at $I = 19$ and $K = 1400$. Run 13. Hemisphere-Cylinder at $M_o = 4$ and $Re_o = 10^4$. Computed by Section 4.3.2 with Equation 110.

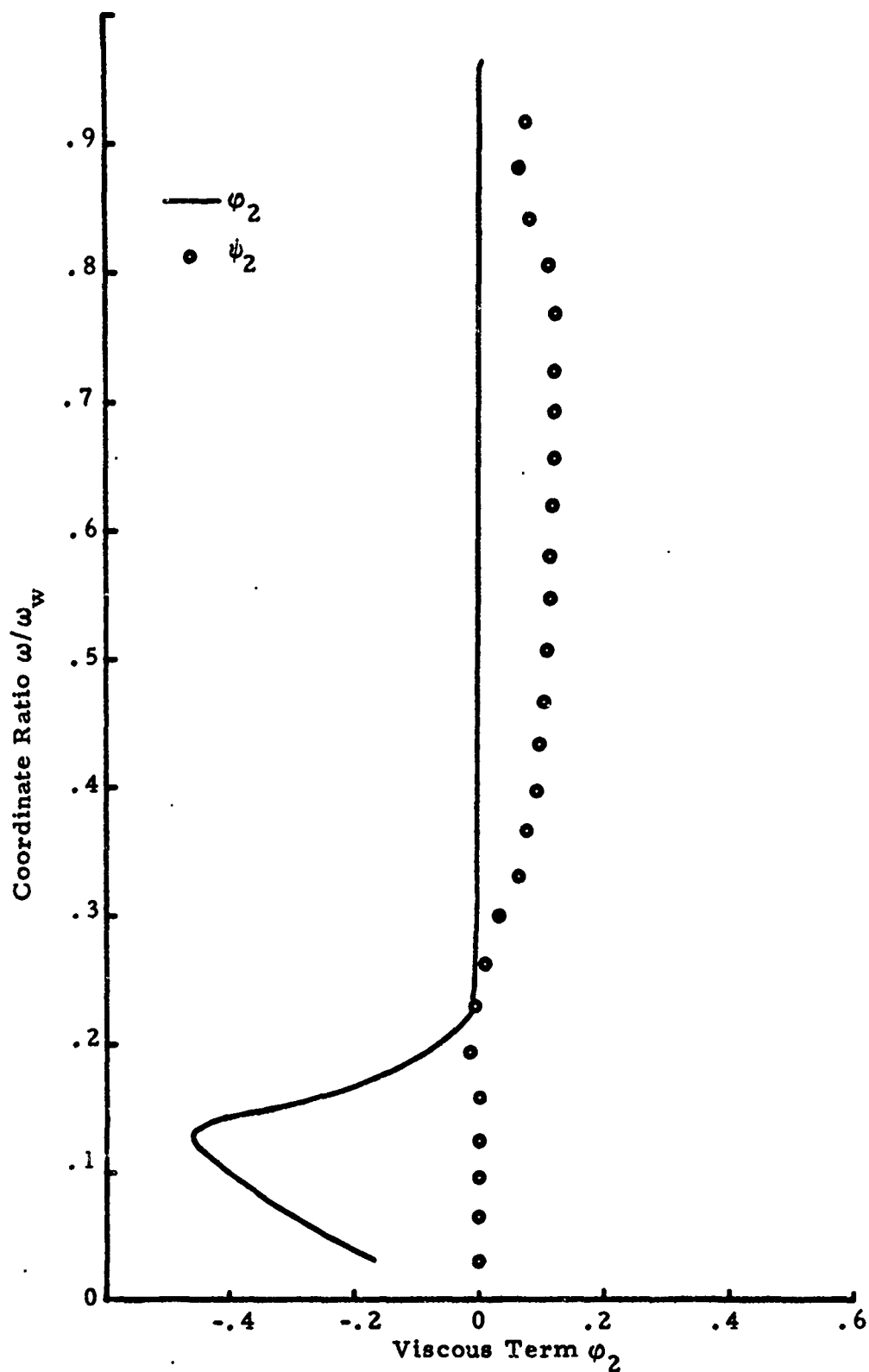


Figure 29. Viscous Term ϕ_2 and Stabilizing Term ψ_2 at $I = 24$ and $K = 800$. Run 15. Hemisphere-Cylinder at $M_0 = 4$ and $Re_0 = 4000$. Computed by Section 4.3.2 with Equation 116.

5.4 Accuracy

5.4.1 Comparisons with Measurements. The accuracy of results could not be determined analytically and was estimated by comparisons with computed and measured results of others. Measurements of bow wave coordinates and body surface pressures are available in [4] at $M_o = 2$ and 4 and $Re_c = 4.93 \times 10^5$ and 1.28×10^6 respectively. Steady solutions of viscous flows for such high Reynolds numbers would require excessive computing time and were not attempted. It was assumed that computed inviscid results of runs 6 and 16 should agree with these measurements. Measured and computed values were not at the same points and differences of results were estimated from graphs. Computed and measured results are shown in figures 20 and 21 on pages 96 and 97 for $M_o = 4$ and in figures 30 and 31 on pages 108 and 109 for $M_o = 2$.

Computed and measured [75] u/u_e -velocities in the boundary layer at several locations are displayed in figures 32 through 34. The agreement verifies the accuracy of the numerical techniques for the boundary layer. The central angle θ_c of computed and measured results is slightly different because of nodal requirements.

Tabulated average and maximum differences are presented in Table 3. In these comparisons, maximum differences as high as 13.7 percent were noted at selected points where either measurements or calculations were difficult to obtain. However, the average difference of measured and computed results was 5.4 percent or less. Considering the probable error of the measurements, agreement of results is very good.

Table 3. Percentage Differences of Computations and Measurements

Variable	Max. % Diff.	Avg. % Diff.	Location Max. Diff.	M_o	Re_o	Run	Experi- ment	Figure
p_b	11.7	1.9	$\lambda=1.57$	4	INV	6	[4]	22
p_b	1.0	.4	$\lambda=1.02$	2	INV	16	[4]	31
ω_w	9.9	4.5	$\lambda=1.91$	4	INV	6	[4]	23
ω_w	6.2	4.8	$\lambda=1.02$	2	INV	16	[4]	30
d_w	4.9		$\lambda=0$	4	INV	6	[4]	23
d_w	5.3		$\lambda=0$	2	INV	16	[4]	30
u/u_e	4.4	2.1	$\omega=.0144$	4	10^4	17	[75]	32
u/u_e	13.7	5.4	$\omega=.006$	4	10^4	17	[75]	33
u/u_e	5.7	2.5	$\omega=.016$	4	10^4	17	[75]	34

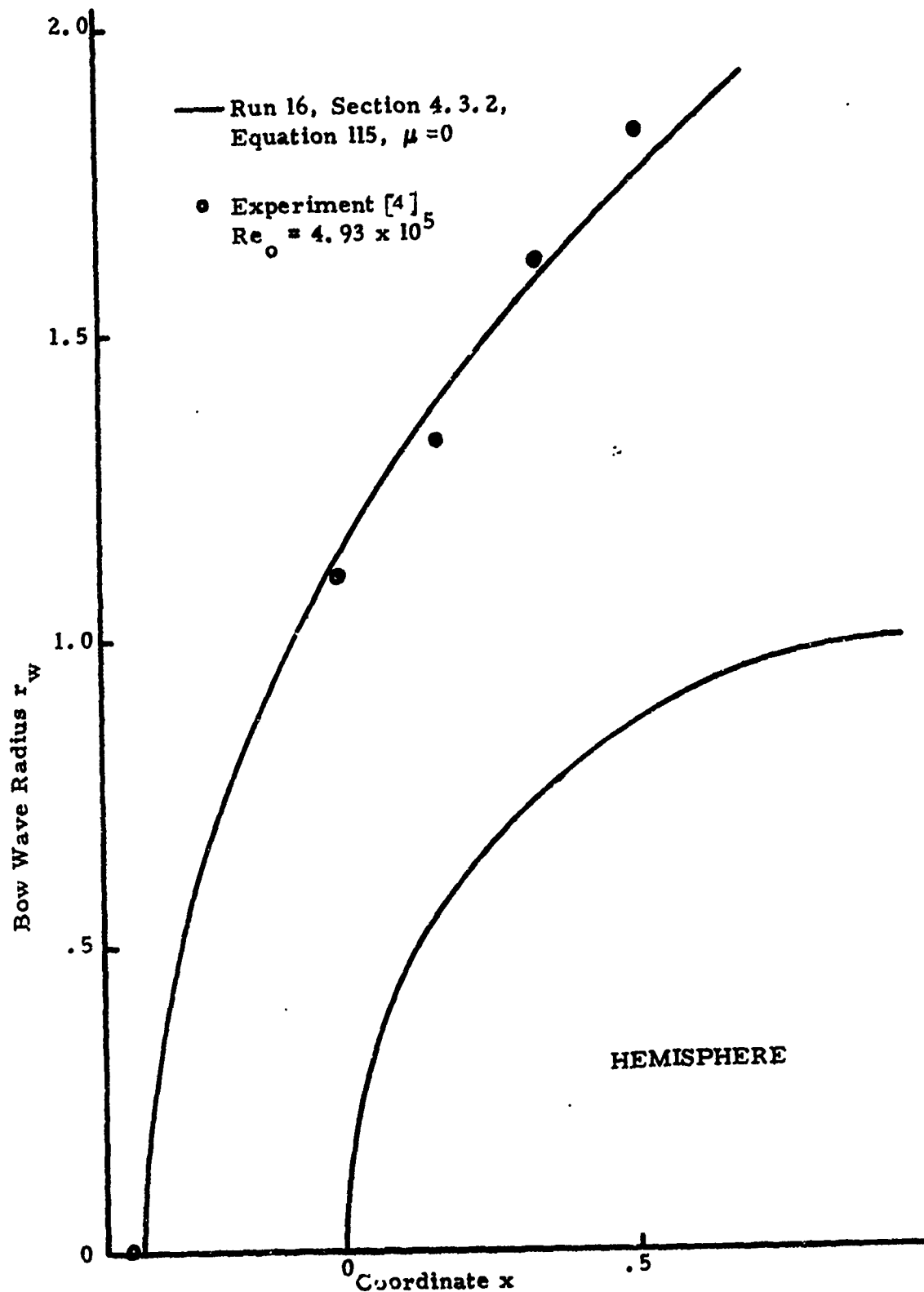


Figure 30. Computed and Experimental Bow Wave Coordinates around Hemisphere. $M_o = 2$.

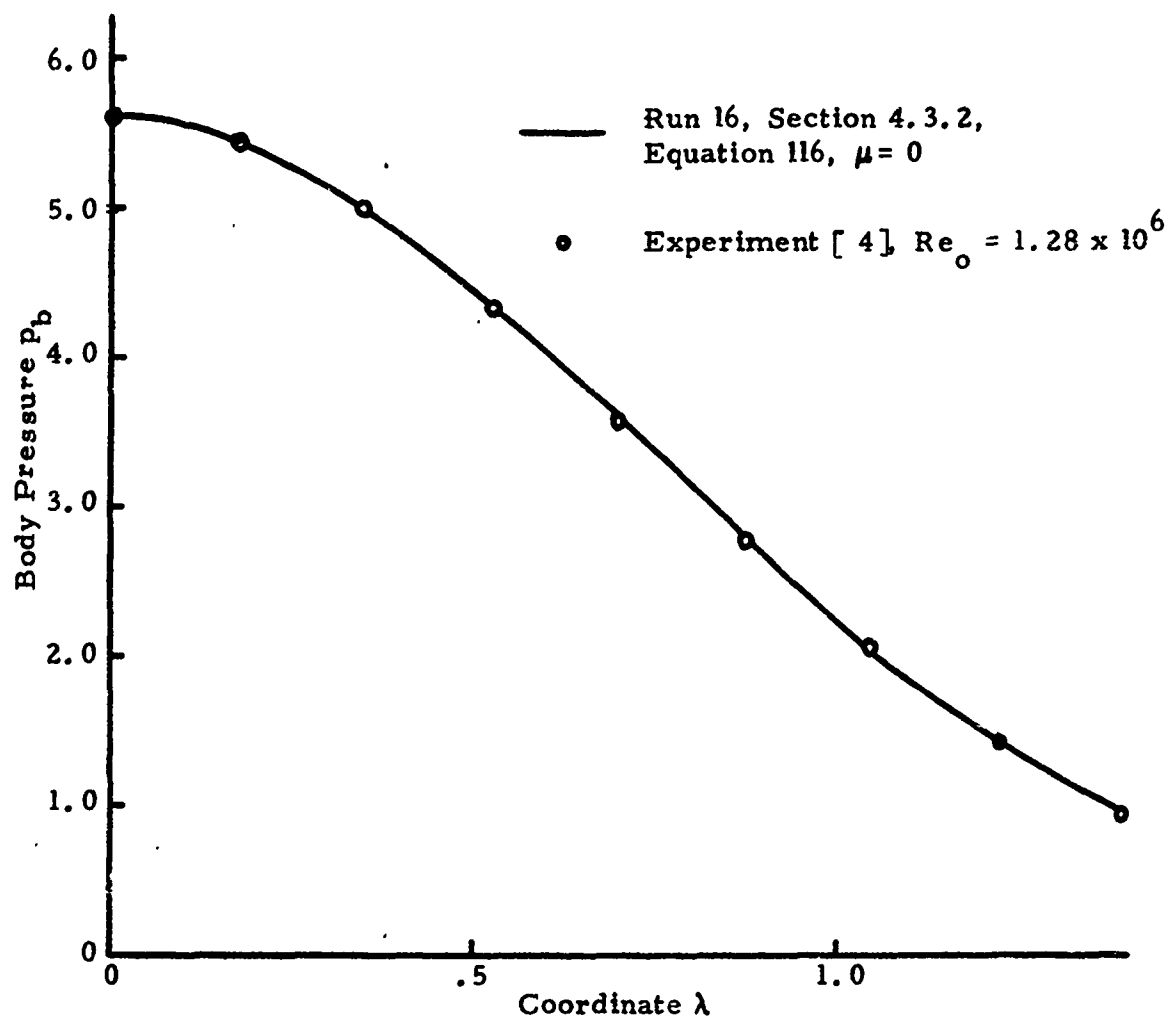


Figure 31. Computed and Experimental Body Surface Pressures around Hemisphere. $M_0 = 2$.

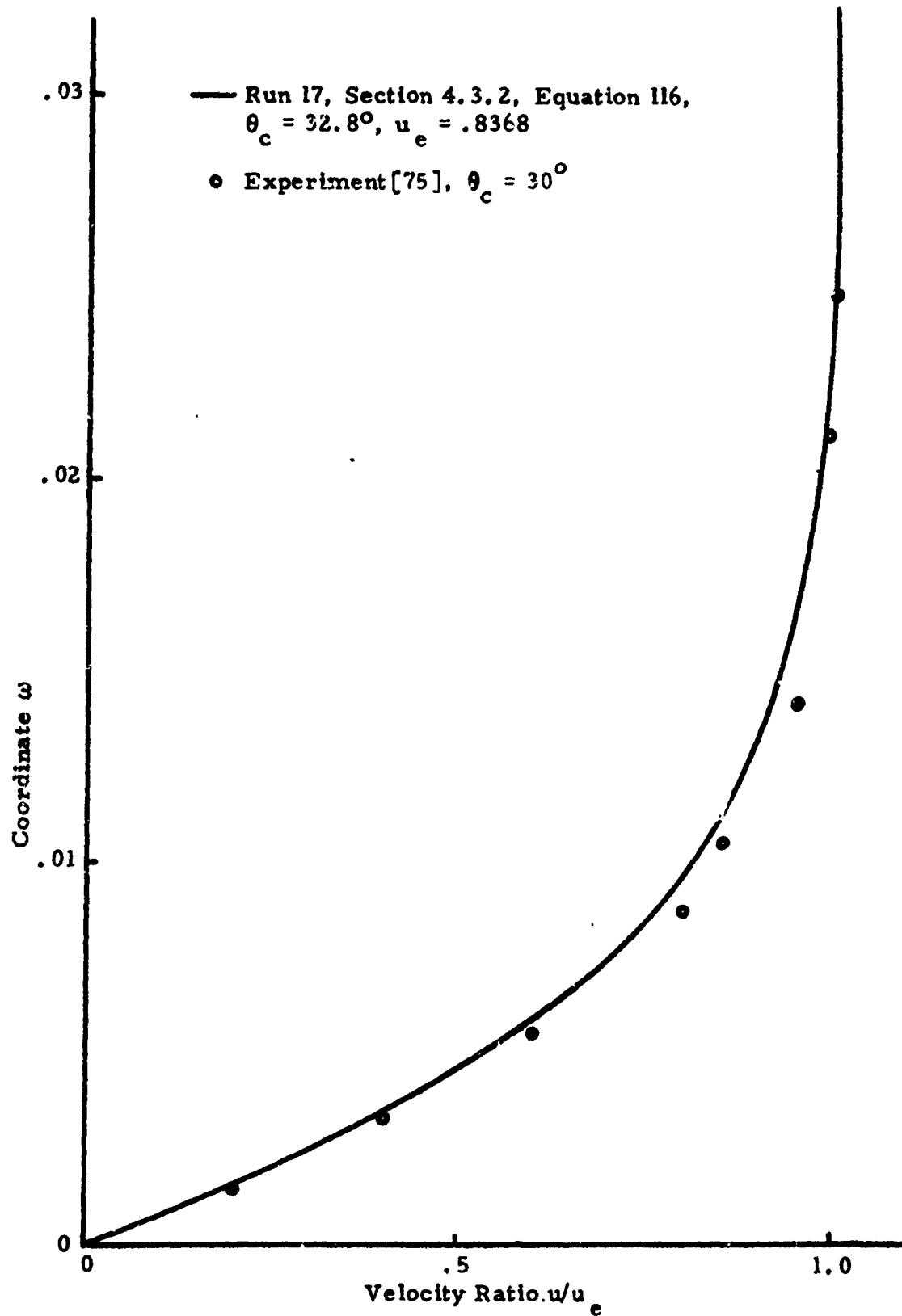


Figure 32. Boundary Layer Velocity Ratios around Hemisphere at $M_o = 2$ and $Re_o = 10^4$.

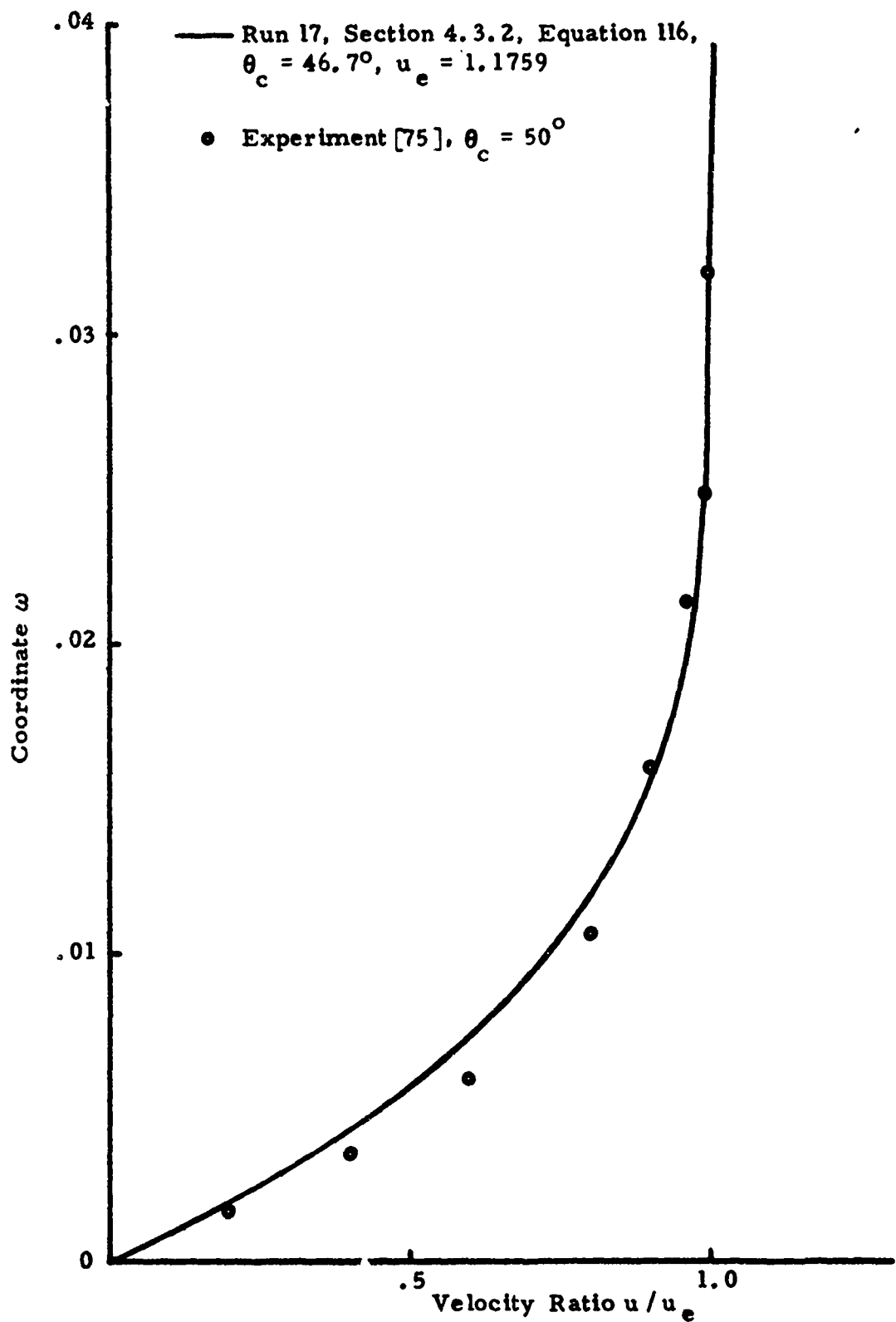


Figure 33. Boundary Layer Velocity Ratios around Hemisphere at $M_o = 2$ and $Re_o = 10^4$.

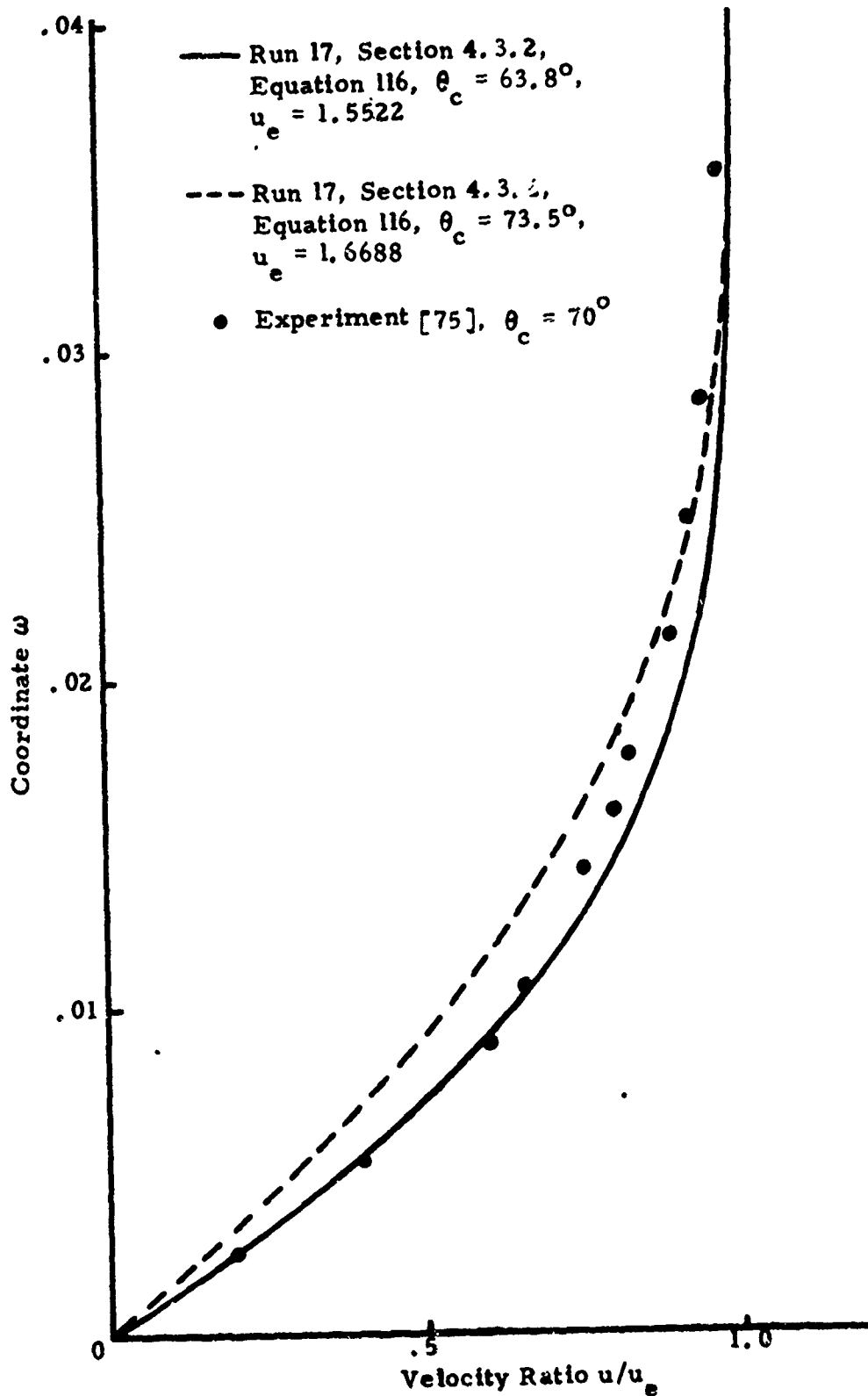


Figure 34. Boundary Layer Velocity Ratios around Hemisphere at $M_\infty = 2$ and $Re_\infty = 10^4$.

5.4.2 Comparison with Computed Results of Others. Prior to this investigation, computed results were not available for viscous flow around a hemisphere or hemisphere-cylinder. Therefore, comparisons of computed results were restricted to inviscid flow systems. Comparisons were made with numerical results of Aungier [1] and analytical results of Belotserkovskii [5] at $M_{\infty} = 2$ and 4. The latter analytical results were obtained by a method of integral relations that is discussed in section 2.5. A summary of differences in results is presented in table 4. Entropy along the body surface was constant for run 6 and reference 1. The difference of those entropies was 0.2 percent. Body surface entropy values were not presented in [1] for $M_{\infty} = 2$. For inviscid flow, body surface entropies were calculated theoretically. Comparisons with those values are also included in table 4. As indicated by tables 3 and 4, the results of runs 6, 16 and 17 were in agreement with those of [1], [4], [5] and [75]. These solutions demonstrated that the computer code developed in this investigation is satisfactory for inviscid and viscous compressible flows around axisymmetrical bodies.

Table 4. Percentage Differences of Computed Results of this Investigation and Others.

Variable	Max. % Diff.	Avg. % Diff.	Location Max. Diff.	M_o	Run	Reference or Theory
p_b	≈ 0	≈ 0		2	16	[1]
p_b	≈ 0	≈ 0		4	6	[1]
ω_w	4.8	3.2	$\lambda=1.28$	2	16	[1]
ω_w	3.1	1.8	$\lambda= .84$	4	6	[1]
d_w	3.4		$\lambda=0$	2	16	[1]
d_w	2.2		$\lambda=0$	4	6	[1]
d_w	0.8		$\lambda=0$	4	6	[5]
s_b	0.2	0.2	$\lambda=0$	4	6	[1]
s_b	1.4			2	16	Theory
s_b	0.4			4	6	Theory

5.5 Results

5.5.1 Introduction. This section includes solutions of inviscid and viscous flows around hemispheres and hemisphere-cylinders. Prior to this investigation, time dependent solutions of viscous compressible flow about hemispheres and hemisphere-cylinders were not available in the open literature.

5.5.2 Results for a Hemisphere. Specifications of runs 6, 11, 18, 19 and 20 for hemispheres are presented in table 2. Each run was preceded by numerical experiments to determine satisfactory parameters for the stabilizing terms of equations 115 and 116. As in

section 5.3.3, comparisons were made of stabilizing and viscous terms. Runs 6 and 11 at $M_o = 4$ with inviscid and viscous flows were a part of the development phase. Their results are described in section 5.3.3. Run 20 for $M_o = 4$ and $Re_o = 10^5$ was difficult because of the thin boundary layer. Since the total number of nodes was large and $\Delta\tau$ was small, the computing time for run 20 was greater than in other runs. Results were nearly steady at $K = 3500$.

For $M_o = 4$, the standoff distance shown in figure 35, page 117, decreases as Reynolds number increases. In figure 36, there is a decrease in body surface pressure for an increase in Reynolds number. In that figure, inviscid flow and $Re_o = 10^5$ are represented by a single line for $\lambda < .8$. The boundary layer displacement thicknesses of figure 37 were computed from

$$\delta^* = \int_0^{\omega_e} \left(1 - \frac{m}{m_e}\right) d\omega \quad (151)$$

where: $m = \rho u$

e refers to the edge of the boundary layer.

The limit ω_e was determined from a graph, such as figure 38, of u-velocity versus ω at the point where the boundary layer effects seemed negligible. For $Re_o = 10^4$ and 10^5 , there are oscillations in δ^* near the stagnation point where the boundary layer is thin because of small oscillations in u-velocity near the edge of the boundary layer. For the relatively thick boundary layers of $Re_o = 10^3$ and 4×10^3 , these

oscillations had a minor effect on δ^* . In figures 38 through 40, u-velocities, pressures and temperatures are presented. The decrease in boundary layer thickness with increasing Reynolds numbers is apparent.

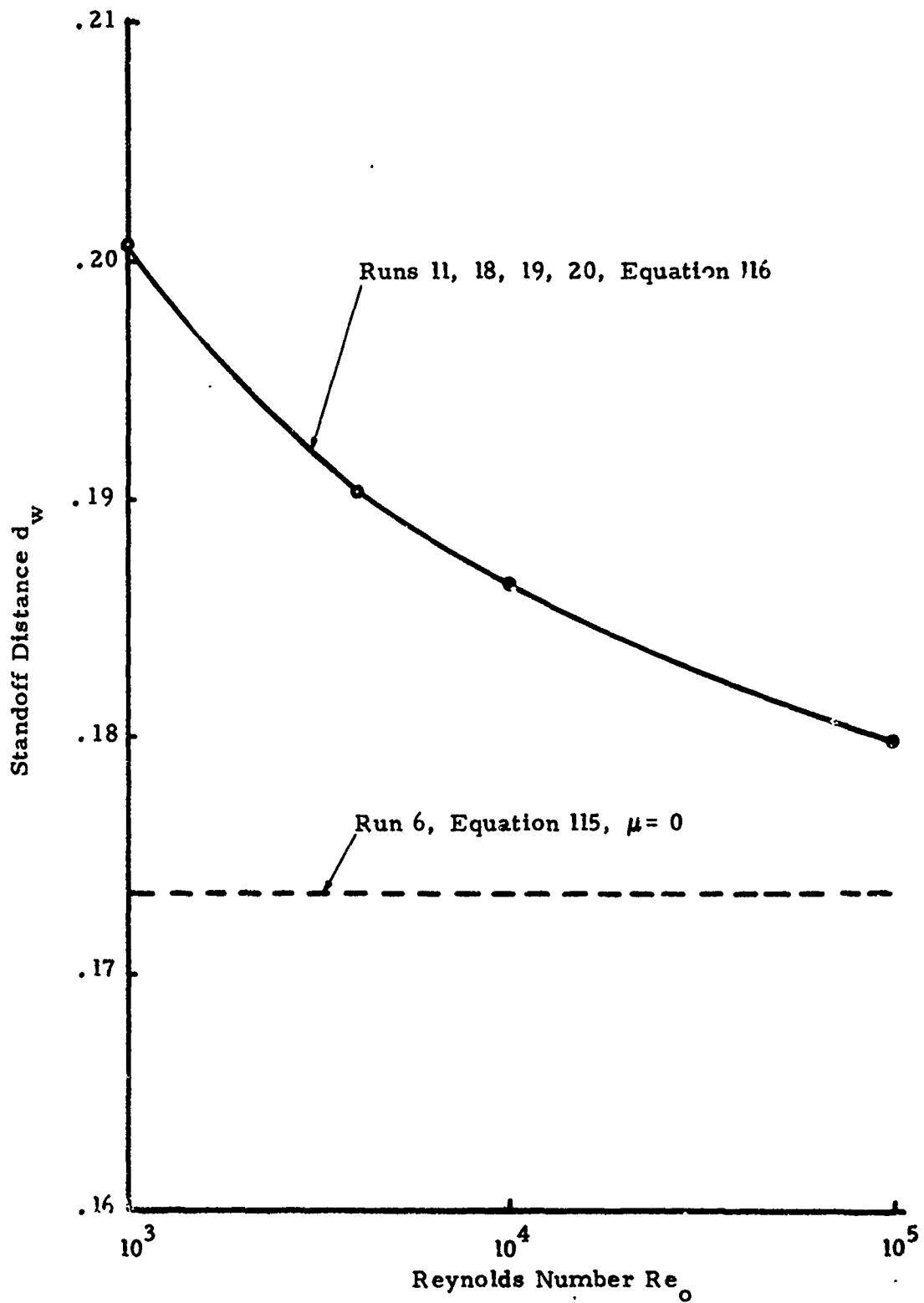


Figure 35. Standoff Distance for Flow around a Hemisphere at $M_o = 4$. Computed by Section 4.3.2.

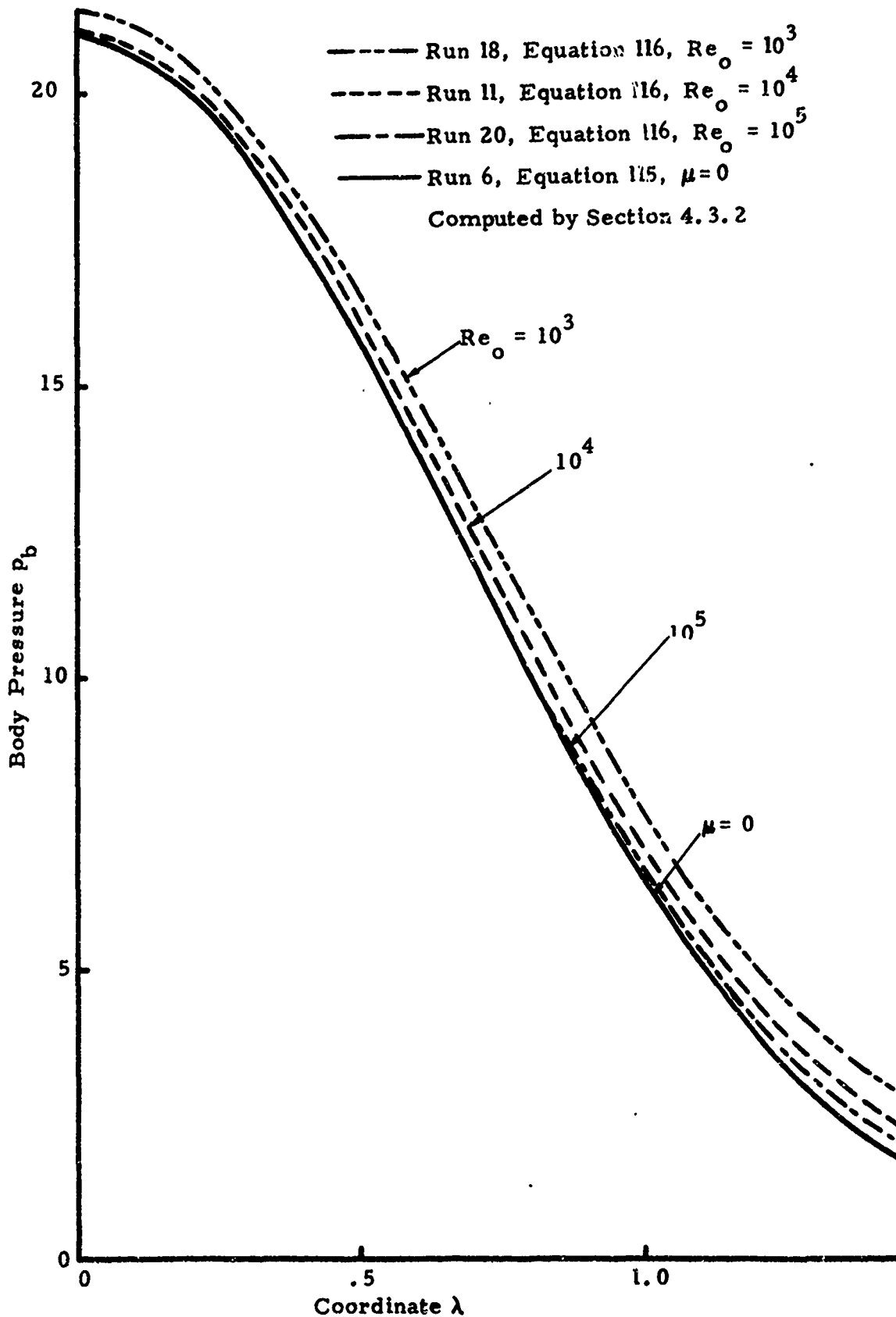


Figure 36. Body Surface Pressures of Hemisphere at $M_o = 4$.

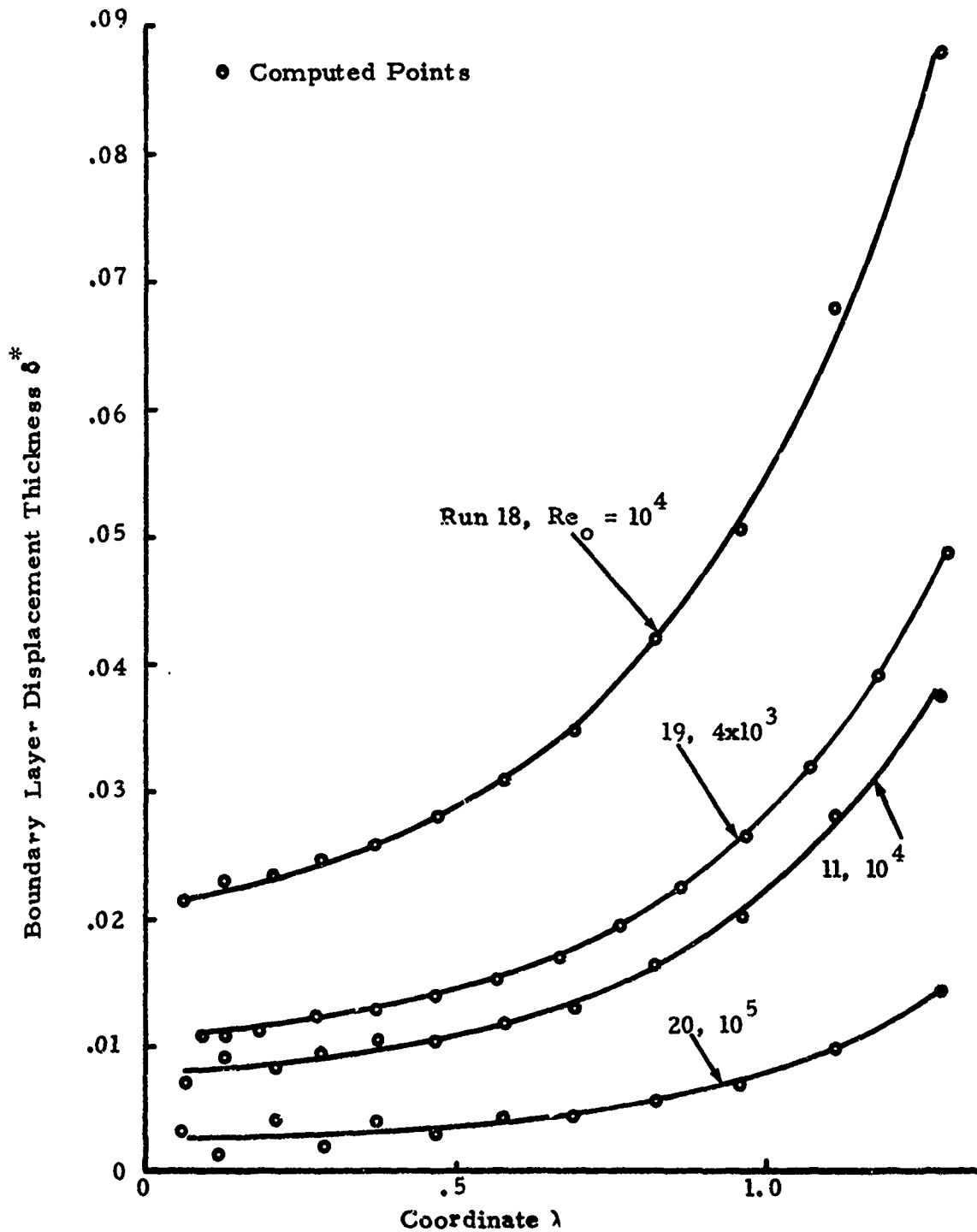


Figure 37. Boundary Layer Displacement Thicknesses for Hemisphere at $M_0 = 4$. Computed by Section 4.3.2 and Equation 116.

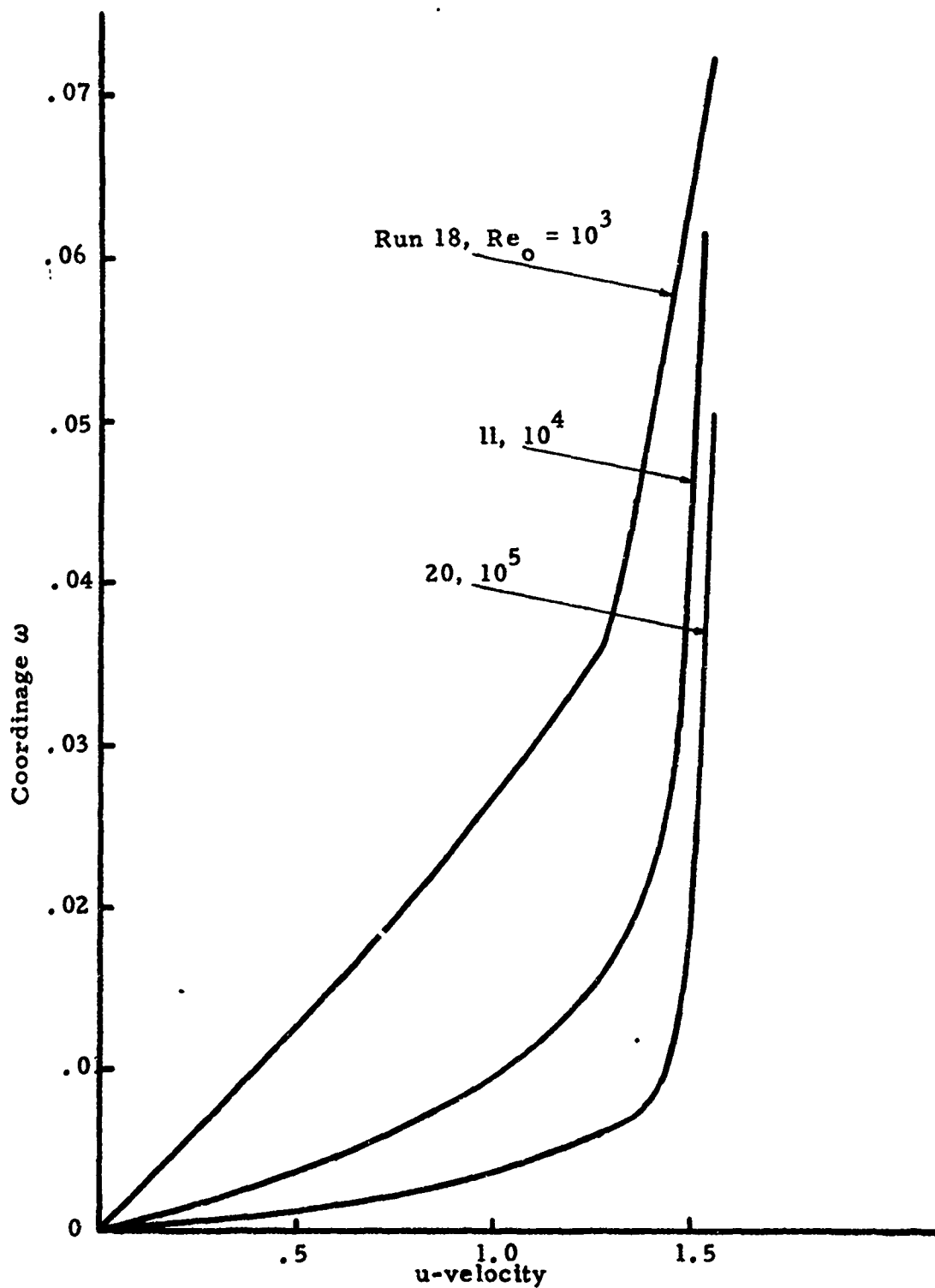


Figure 38. u-velocities for Hemisphere at $M_o = 4$ and $\theta_c = 32.8$. Computed by Section 4.3.2 and Equation 116.

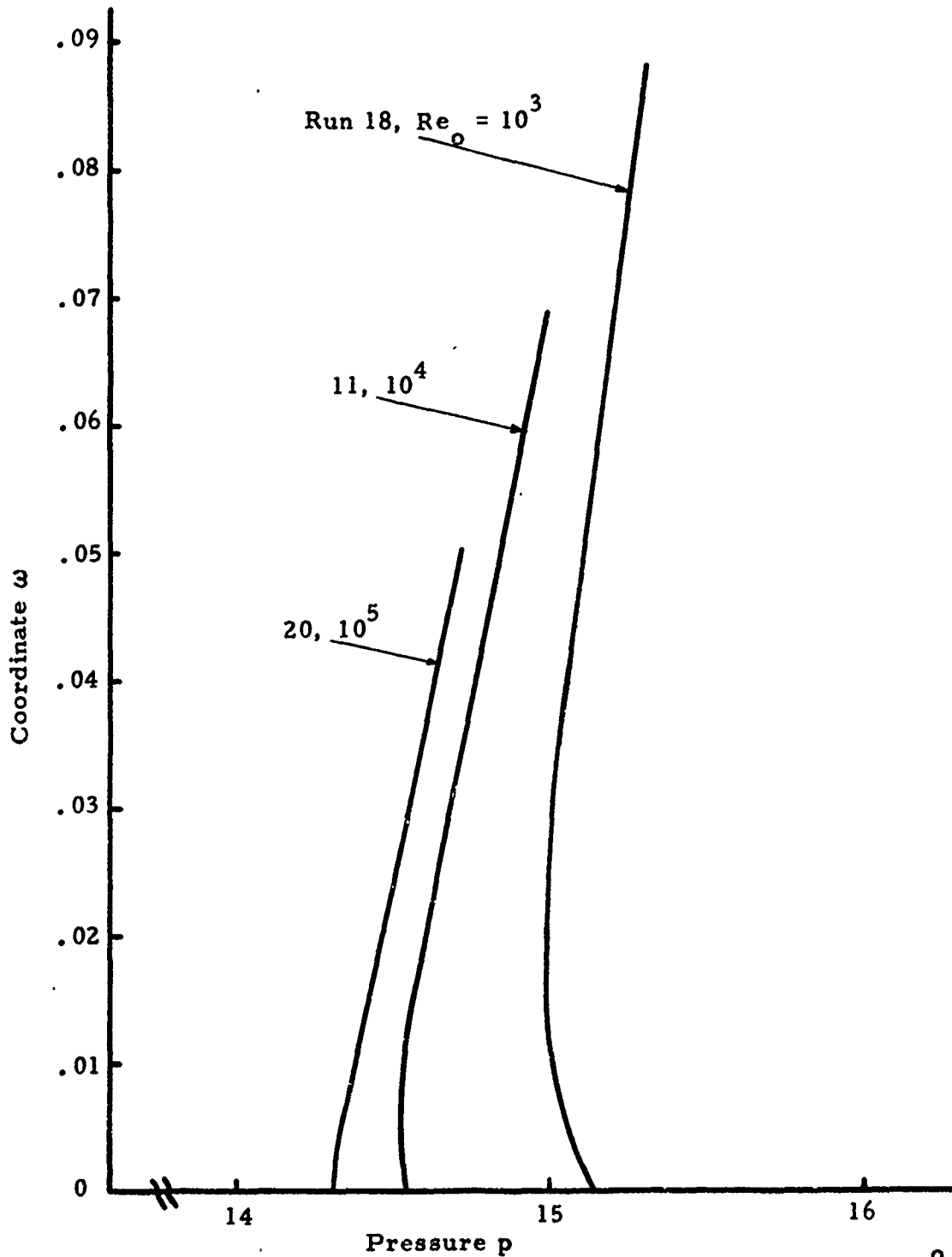


Figure 39. Pressures for Hemisphere at $M_0 = 4$ and $\theta_c = 32.8^\circ$
 Computed by Section 4.3.2 and Equation 116.

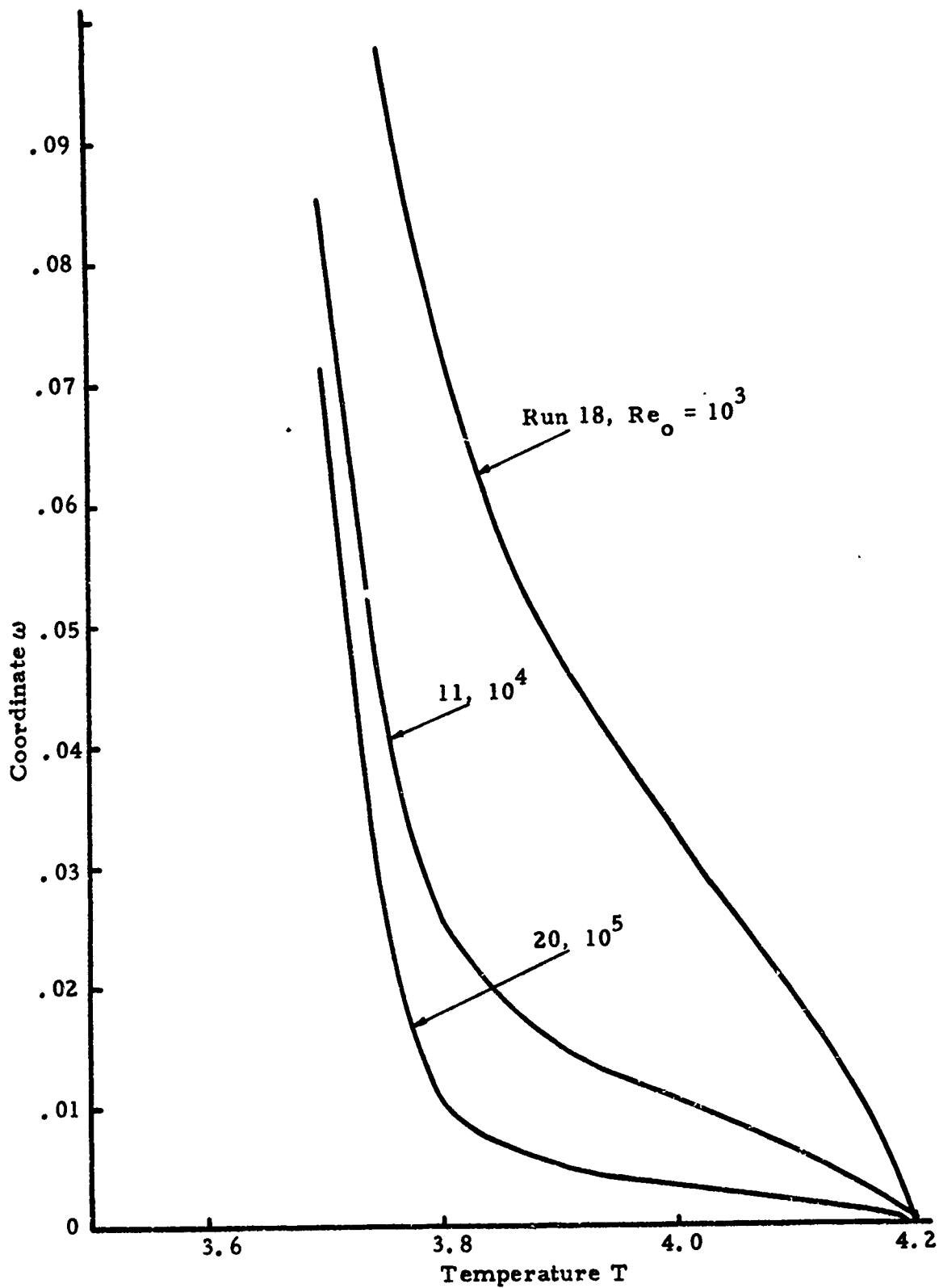


Figure 40. Temperatures for Hemisphere at $M_o = 4$ and $\theta_c = 32.8^\circ$. Computed by Section 4.3.2 and Equation 116.

5.5.3 Results for a Hemisphere-Cylinder. Based on the numerical results of section 5.3.3, the specifications of runs 14 and 15 of table 2 were selected for a solution of viscous compressible flow around a hemisphere-cylinder. In run 14 for $K \leq 1600$, the stabilizing term of equation 110 was used to remove initial perturbations. By $KL = 1600$, a favorable pressure gradient had been established in the afterbody region, and the bow wave had moved close to its steady location. The results of run 14 at $KL = 1600$ were used as input to run 15 in which the stabilizing term was that of equation 116. In run 15 at $KL = 800$, the solution was steady and seemed accurate in the boundary layer and other parts of the field. Results of run 15 for $KL = 800$ are presented in figures 41 through 56 at the end of this section on pages 127 to 142. Contours of Mach number, temperature, pressure and entropy are presented in figures 41 through 44. The contours are consistent with each other. Near the downstream boundary and bow wave, there are oscillations in the results. The contours for Mach number and temperature in figures 41 and 42 are similar. Boundary layer growth along the body is apparent. Mach number contours outside of the boundary layer in the forebody region are similar to those of inviscid flow in [52]. In figure 43, as expected, there is an expansion fan near the junction of the hemisphere and cylinder. Entropy contours of figure 44 were smooth and resembled streamlines outside of the boundary layer. Along the isothermal body surface $T_b = 4.2$ and entropy increases because pressure decreases.

Boundary layer displacement and momentum thicknesses of figure 45 seem reasonable. There is a substantial increase of boundary layer thickness along the afterbody. Figures 46 through 49 present u-velocities, v-velocities and temperatures versus ω at several I indices. The coordinate ω was chosen instead of ω/ω_w to display growth of the boundary layer. Variations in u-velocities and temperatures are smooth. At I = 16 near the junction in figure 46, there is a small decrease in u-velocity near the edge of the boundary layer. Near the forebody, variations in v-velocities of figure 47 are smooth. As shown in figure 48, they oscillate in the afterbody region where they are small and sensitive to perturbations. Although undesirable, those oscillations were not considered detrimental to the accuracy of other variables. In figure 49, temperature gradients $\left. \frac{\partial T}{\partial \omega} \right)_b < 0$ and their absolute values increase with increasing I indices. Since body temperature is greater than adiabatic stagnation temperature, heat transfer is from the body and $\left. \frac{\partial T}{\partial \omega} \right)_b$ should be negative.

Specifications of runs 15 and 19 in table 2 for a hemisphere-cylinder and hemisphere were identical. As indicated by table 5, results of both runs in the forebody region are about the same.

Table 5. Percentage Differences of Computed Results of Hemisphere and Hemisphere-Cylinder. Runs 15 and 19, $M_o = 4$, $Re_o = 4000$.

Variable	Max. % Difference	Avg. % Difference	Location of Maximum Difference
M_o	3.3	.6	$\lambda = 0$
p	1.3	.1	$\lambda = 1.28$
T	3.0	.3	$\lambda = 1.28$
ω_w	1.2	.4	$\lambda = 1.28$
d_w	.4		$\lambda = 0$

A conclusion was that satisfactory results for the forebody region of the hemisphere-cylinder may be obtained by considering the hemisphere alone. The conclusion may be true for other shapes and conditions, but additional results are needed to strengthen this conclusion.

In run 21, the stabilizing term was zero and results of run 15 at $KL = 800$ were used for initial values. In run 21, results were steady at $KL = 1600$. Typical results of runs 15 and 21 for the forebody region are shown in figures 50 through 52. The maximum difference is 9 percent. Average differences of all variables is less than 2 percent. The variation in pressure versus K index in the afterbody region for various stabilizing terms is shown in figure 53 at $I = 19$ and $J = 26$ where differences of runs 15 and 21 were a maximum. The large differences at that point were due to the spatial oscillations in the results of run 21. u-velocities, v-velocities and pressure for run 15 and 21 at $I = 19$ are

shown in figures 54 through 56. Oscillations of the steady results of run 21 are a maximum near the bow wave and are insignificant in the boundary layer. Where there are no significant oscillations of results, the differences between runs 15 and 21 are less than 3 percent. The oscillations of run 21 without stabilizing terms were about the smooth values of run 15. The agreement of the results of runs 15 and 21 indicates that the accuracy of the results of run 15 were not seriously affected by the addition of stabilizing terms.

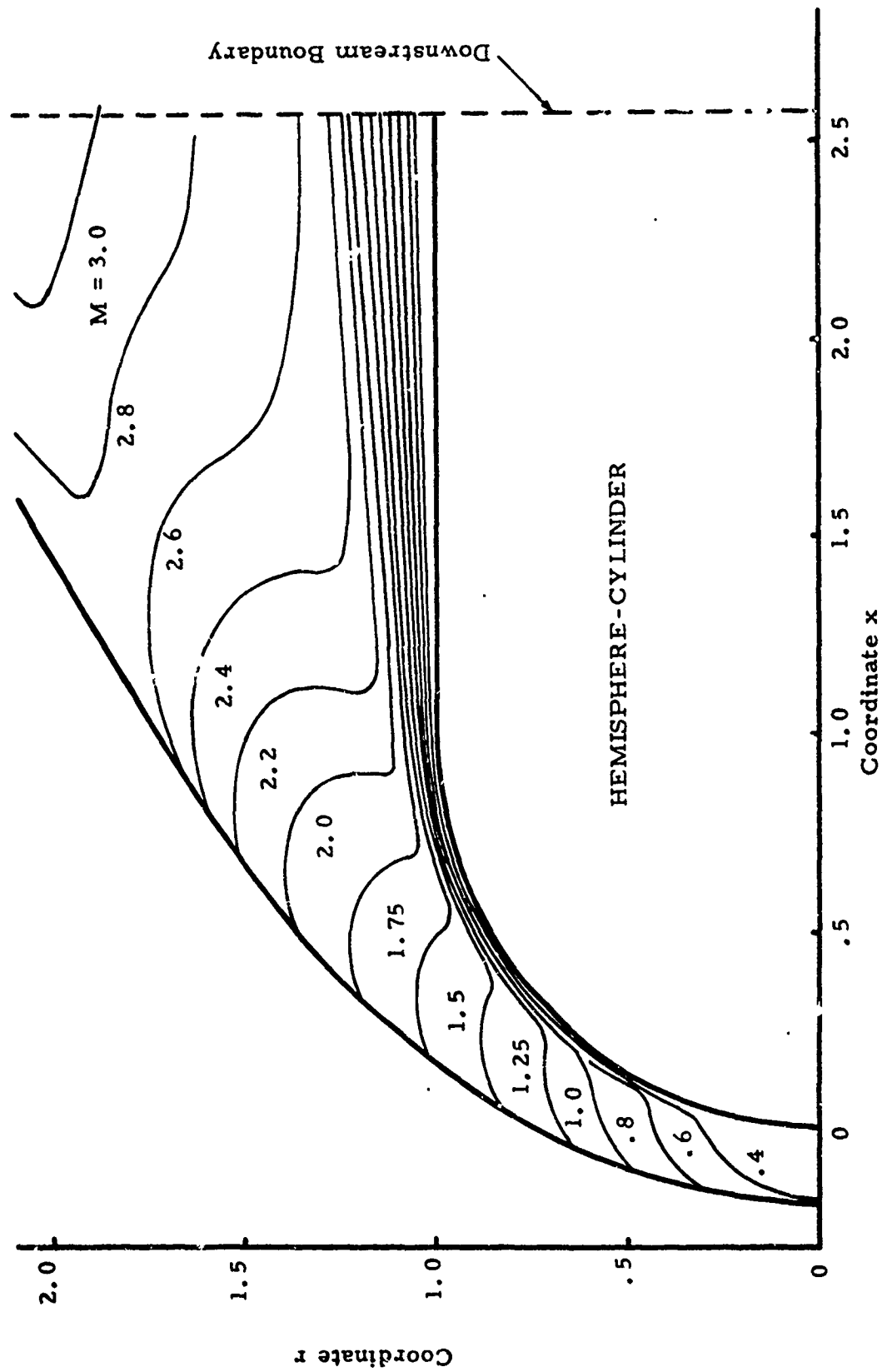


Figure 41. Mach Number Contours for Hemisphere-Cylinder at $M_0 = 4$ and $Re_0 = 4000$.
 Run 15. Computed by Section 4.3.2 and Equation 116.

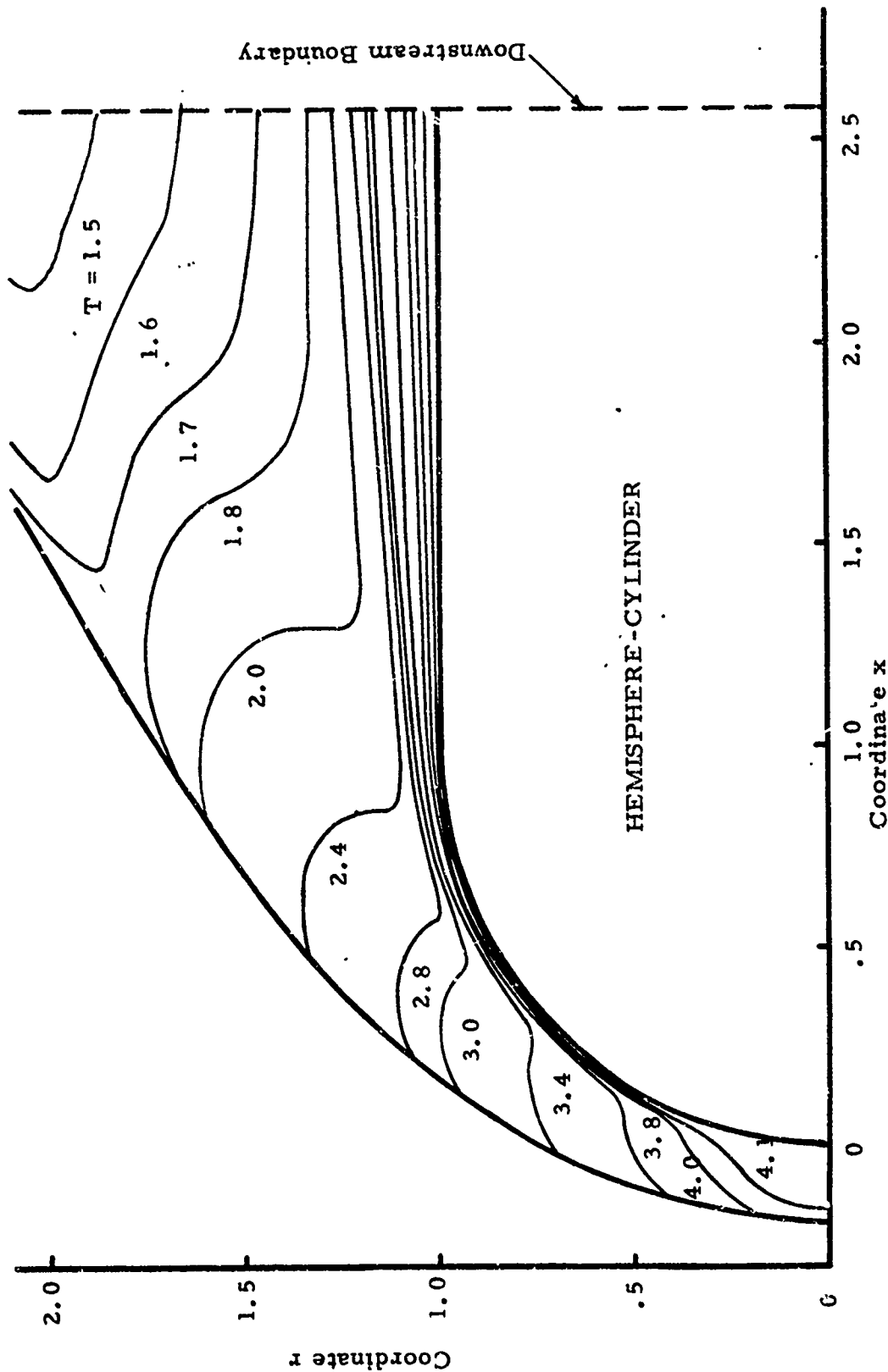


Figure 42. Temperature Contours for Hemisphere-Cylinder at $M_o = 4$ and $Re_o = 4000$.
 Run 15. Computed by Section 4.3.2 and Equation II6.

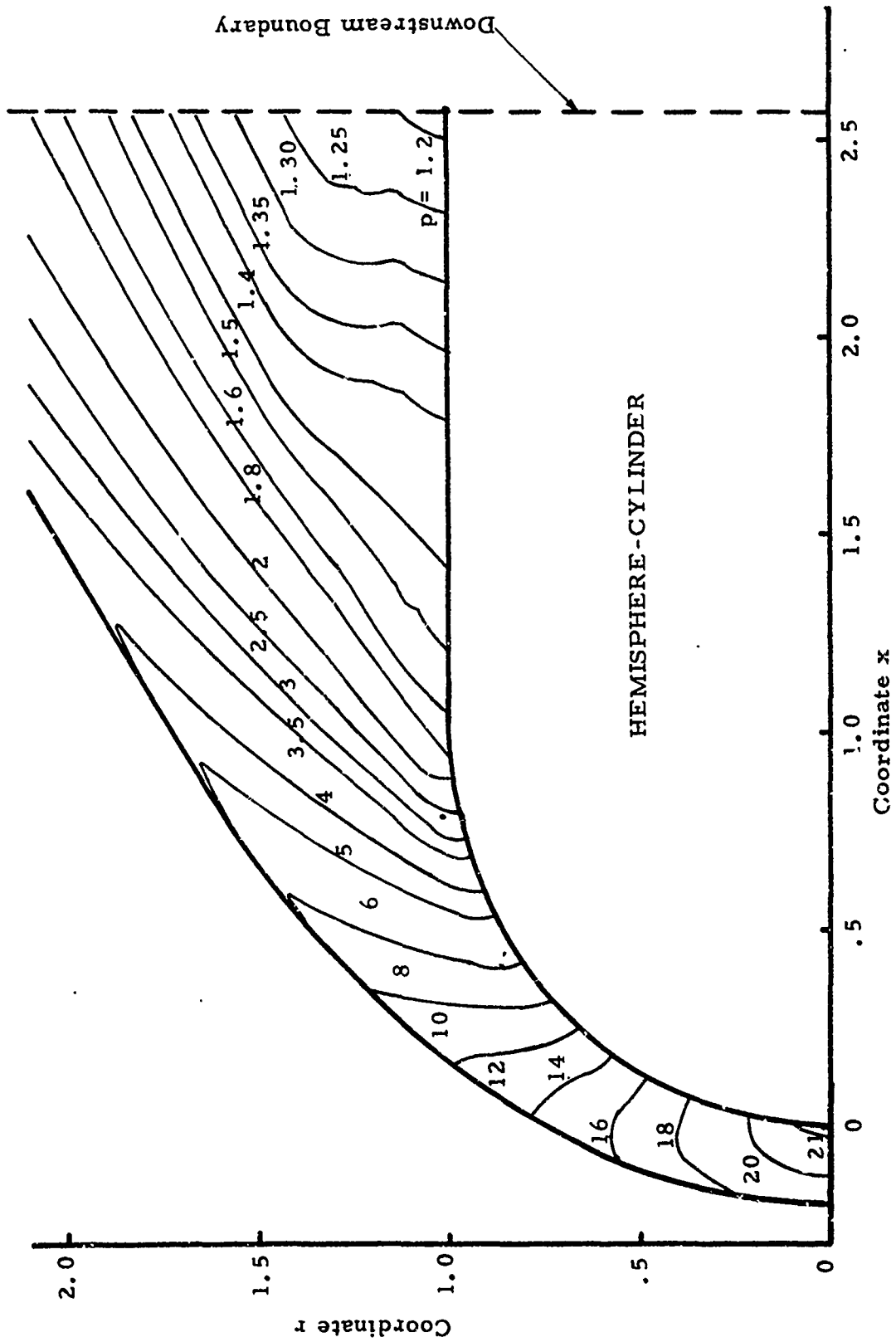
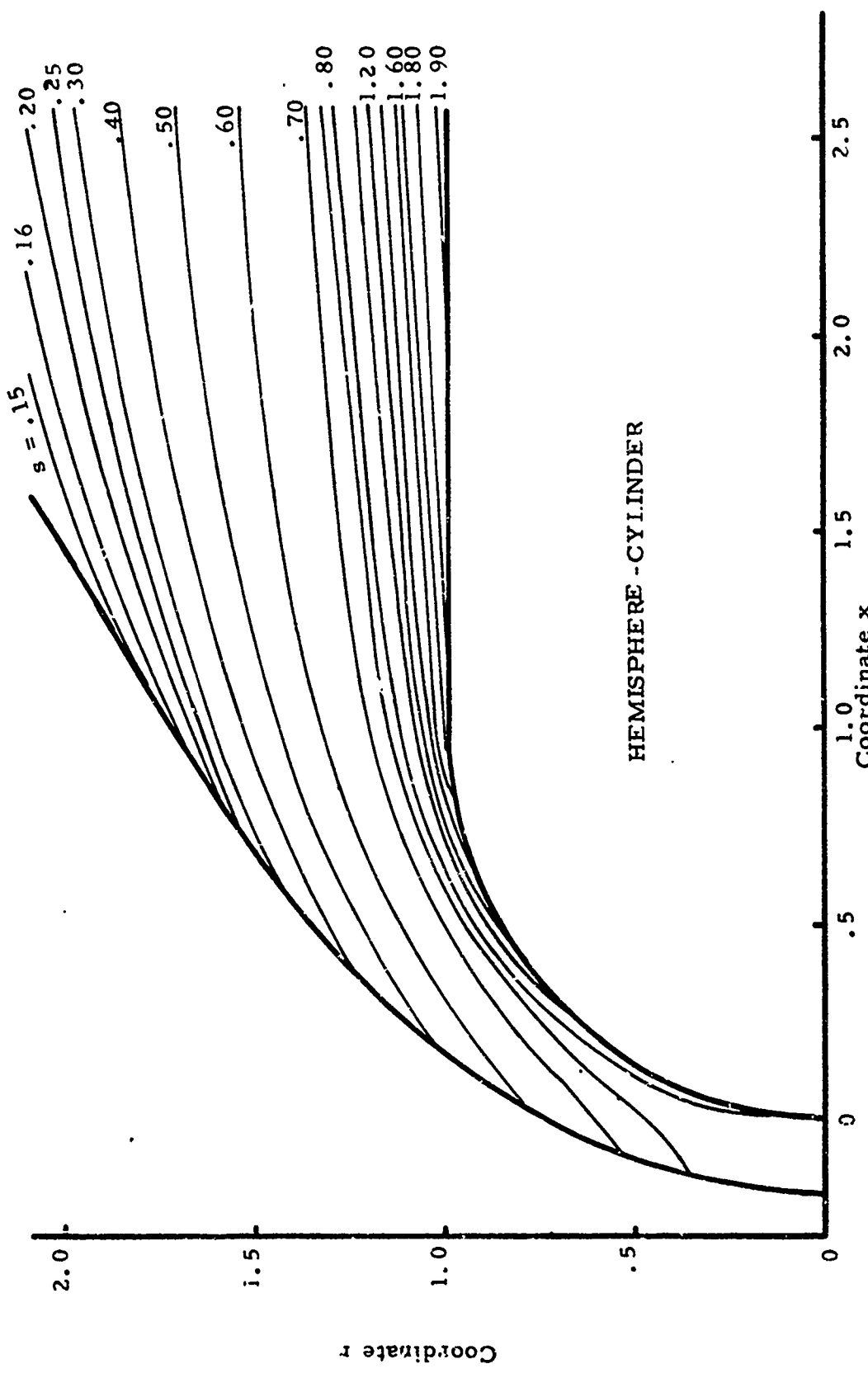


Figure 43. Pressure Contours for Hemisphere-Cylinder at $M_0 = 4$ and $Re_0 = 4000$.
 Run 15. Section 4.3.2 and Equation 116.



HEMISPHERE - CYLINDER

Figure 44. Entropy Contours for Hemisphere-Cylinder at $M_0 = 4$ and $Re_0 = 4000$. Run 15. Computed by Section 4.3.2 and Equation 116.

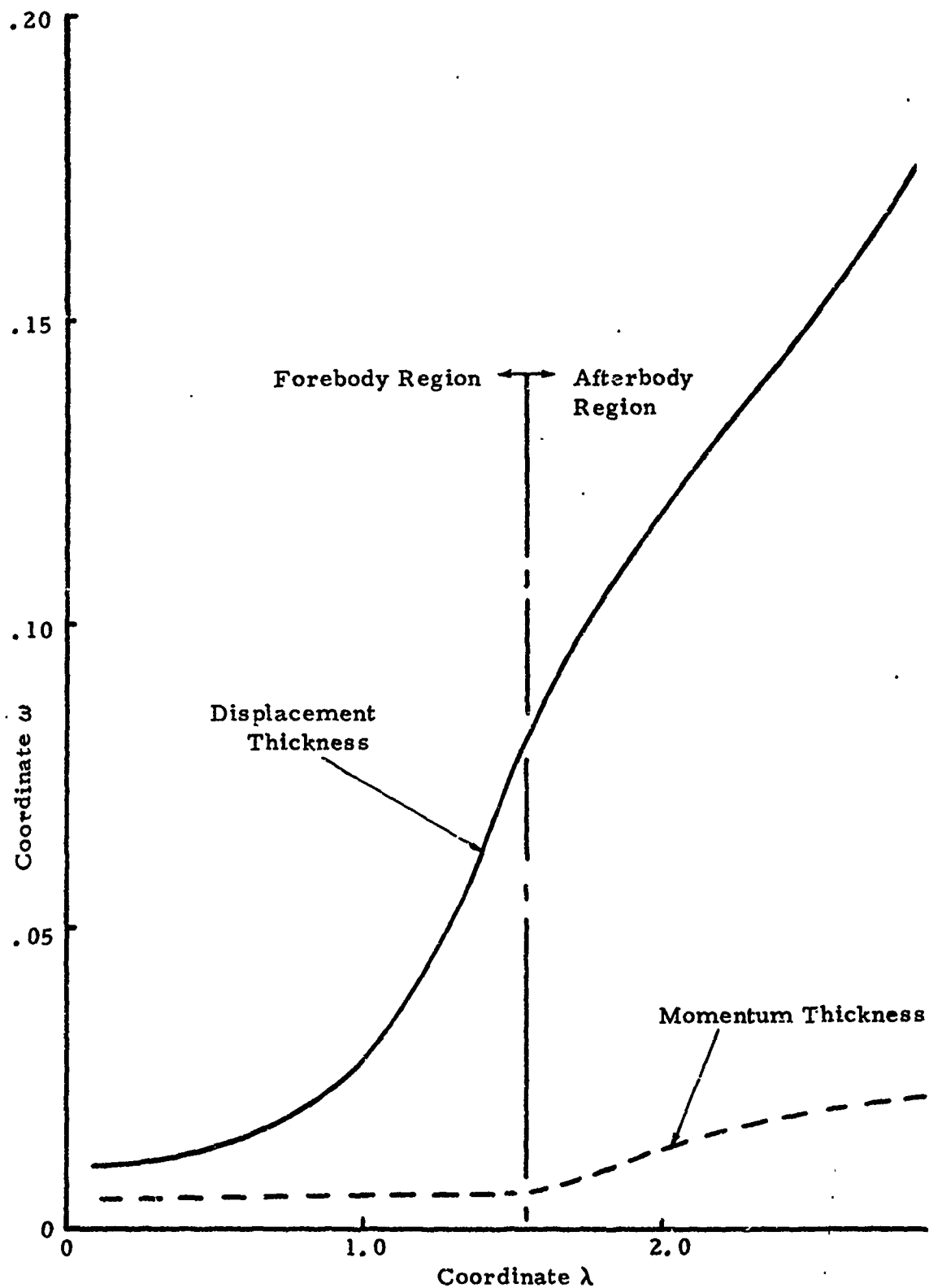


Figure 45. Boundary Layer Displacement and Momentum Thickness for Hemisphere-Cylinder at $M_0 = 4$ and $Re_0 = 4000$. Run '5. Computed by Section 4.3.2 and Equation 116.

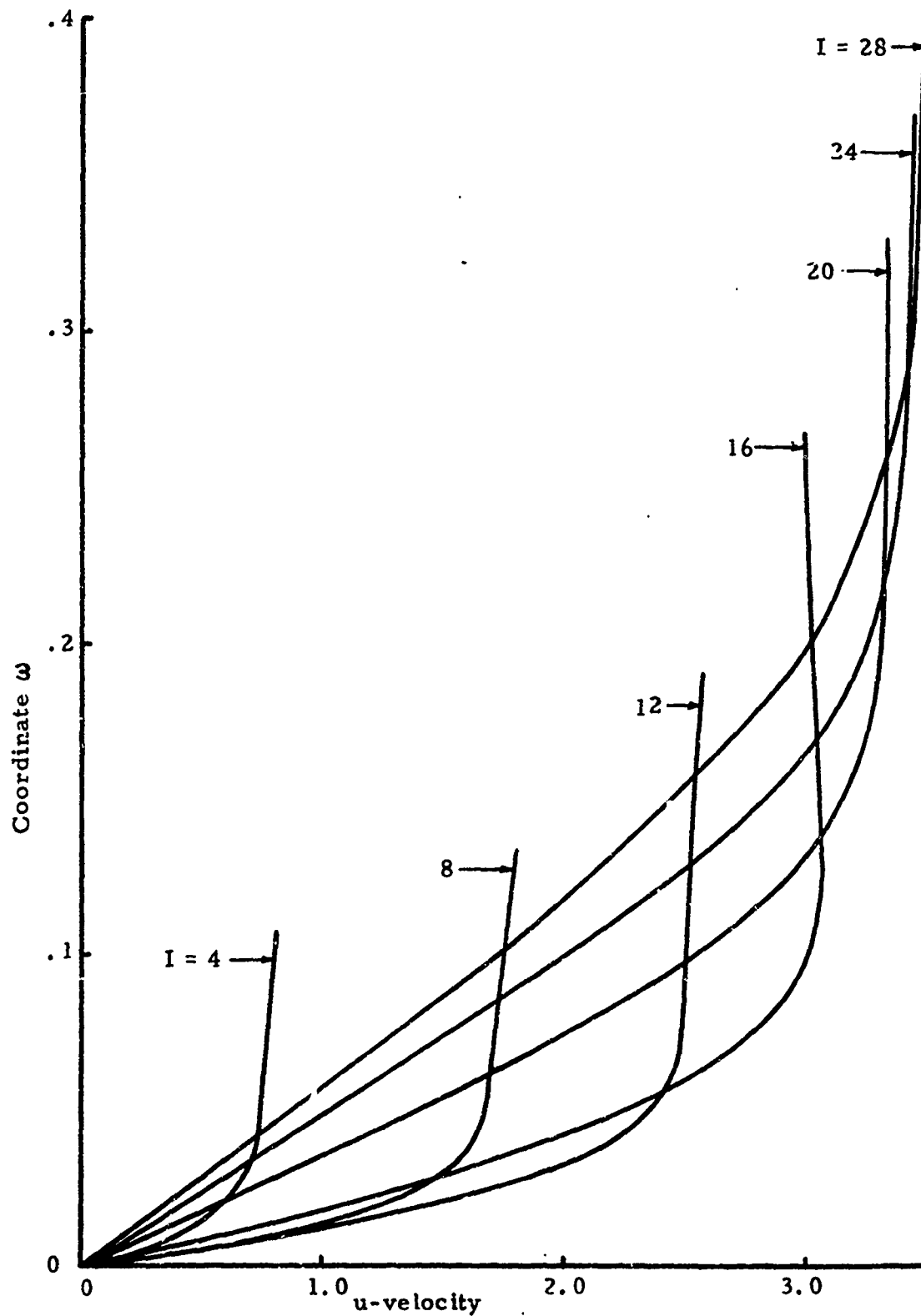


Figure 46. u -velocities for Hemisphere-Cylinder at $M_0 = 4$ and $Re_0 = 4000$. Run 15. Computed by Section 4.3.2 and Equation 116.

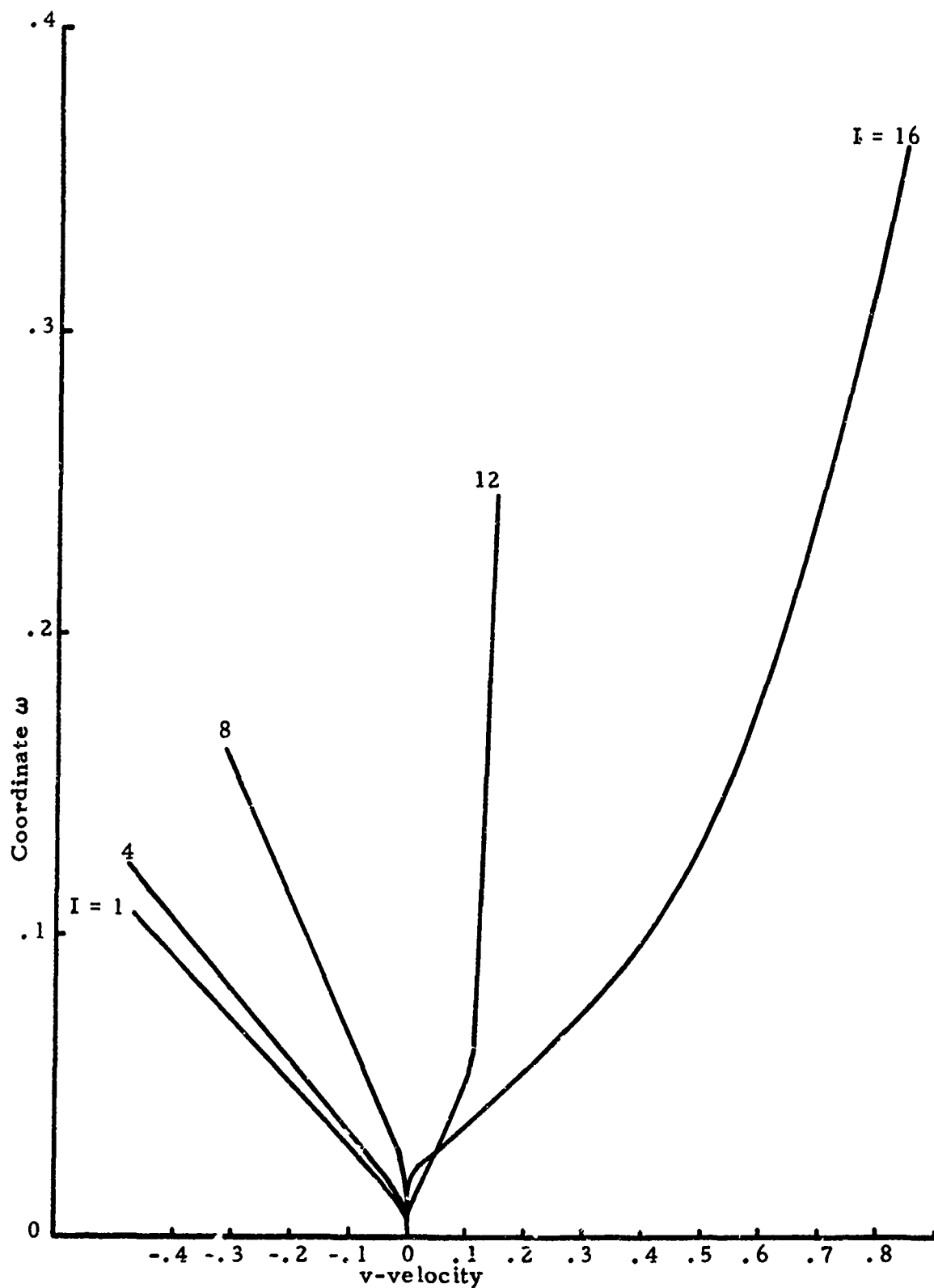


Figure 47. v -velocities in Forebody Region of Hemisphere-Cylinder at $M_o = 4$ and $Re_o = 4000$. Run 15. Computed by Section 4.3.2 and Equation 116.

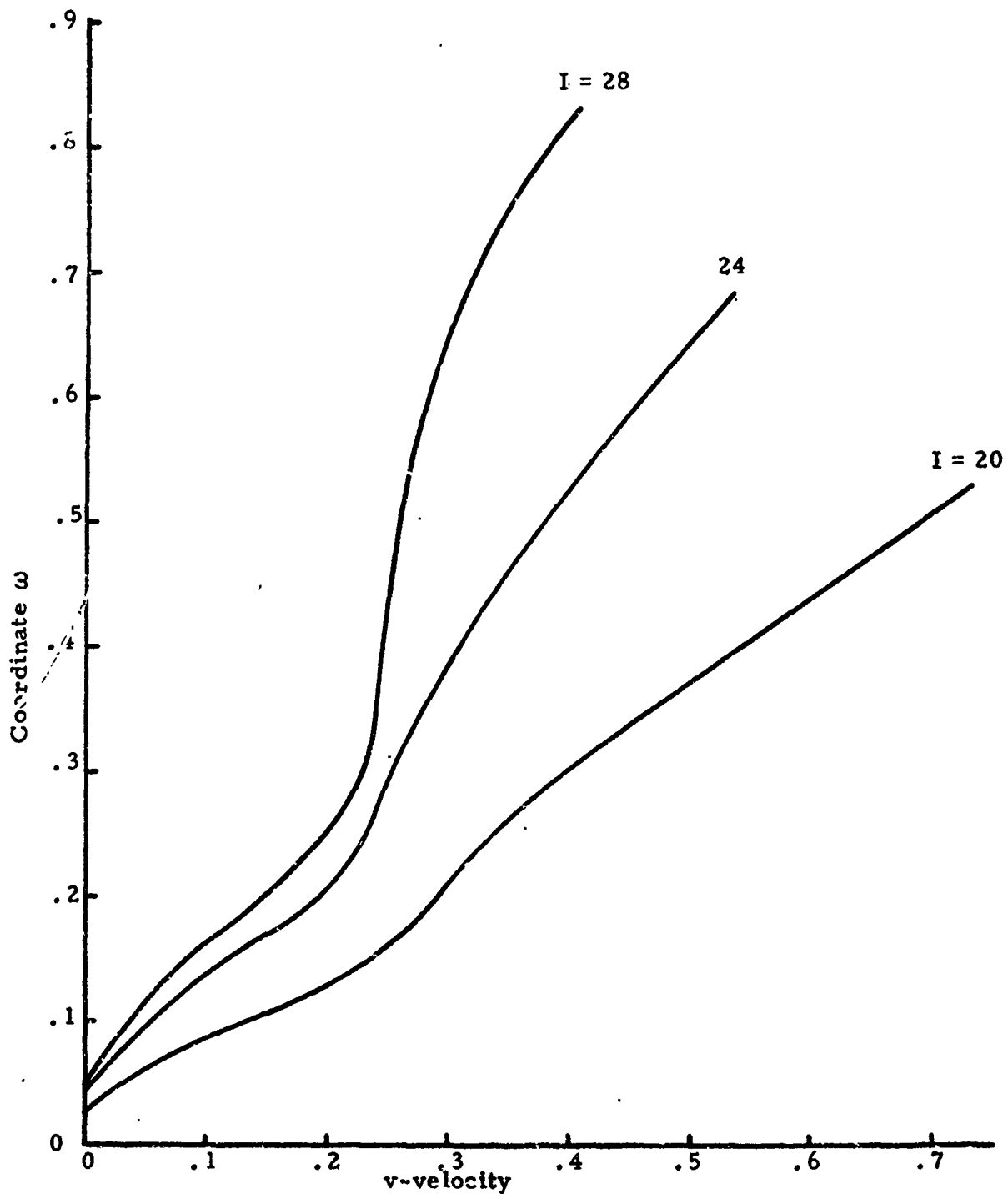


Figure 48. v-velocities in Afterbody Region of Hemisphere-Cylinder at $M_0 = 4$ and $Re_0 = 4000$. Run 15. Computed by Section 4.3.2 and Equation 116.

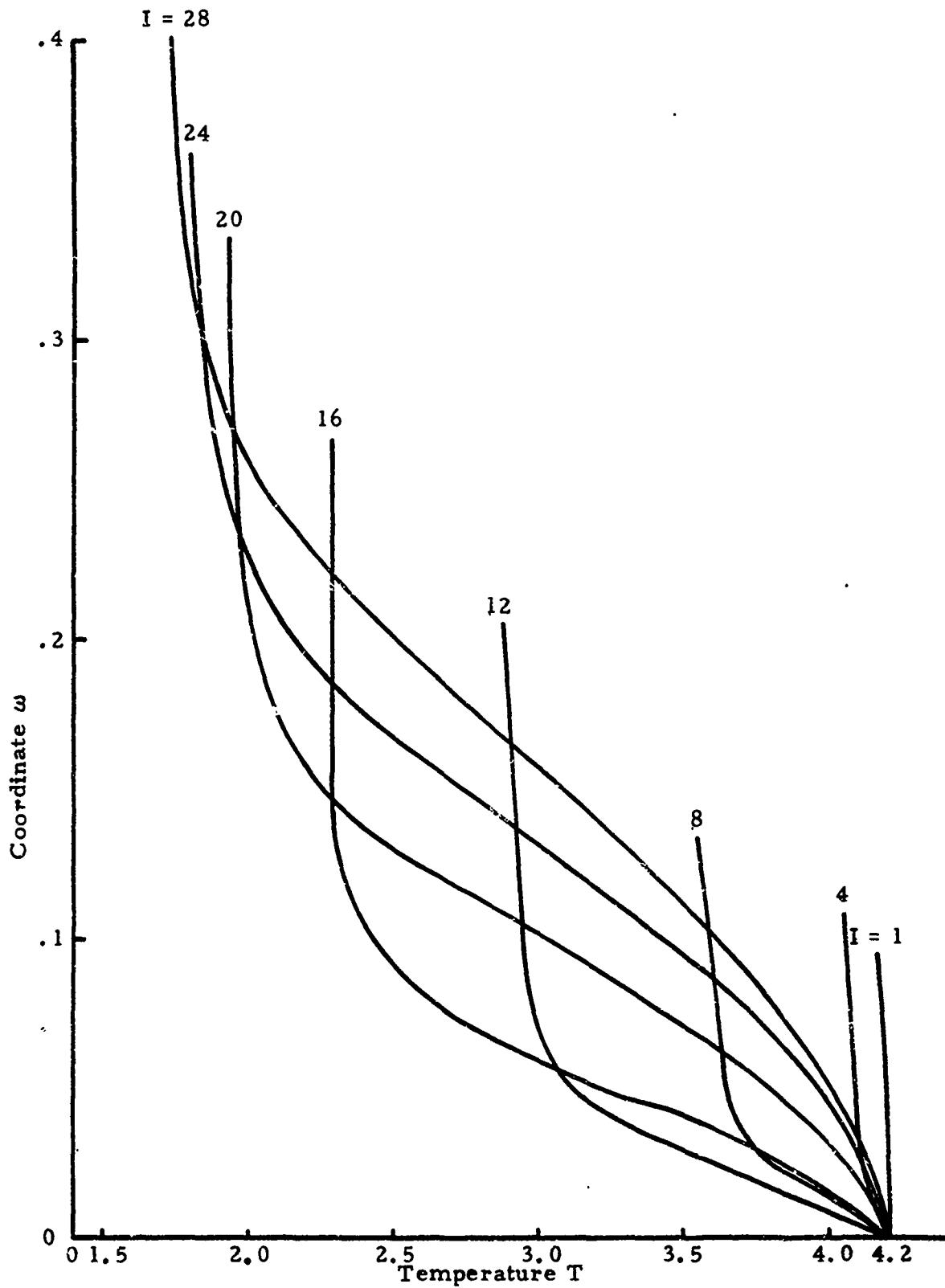


Figure 49. Temperature for Hemisphere-Cylinder at $M_0 = 4$ and $Re_0 = 4000$. Run 15. Computed by Section 4.3.2 and Equation 116.

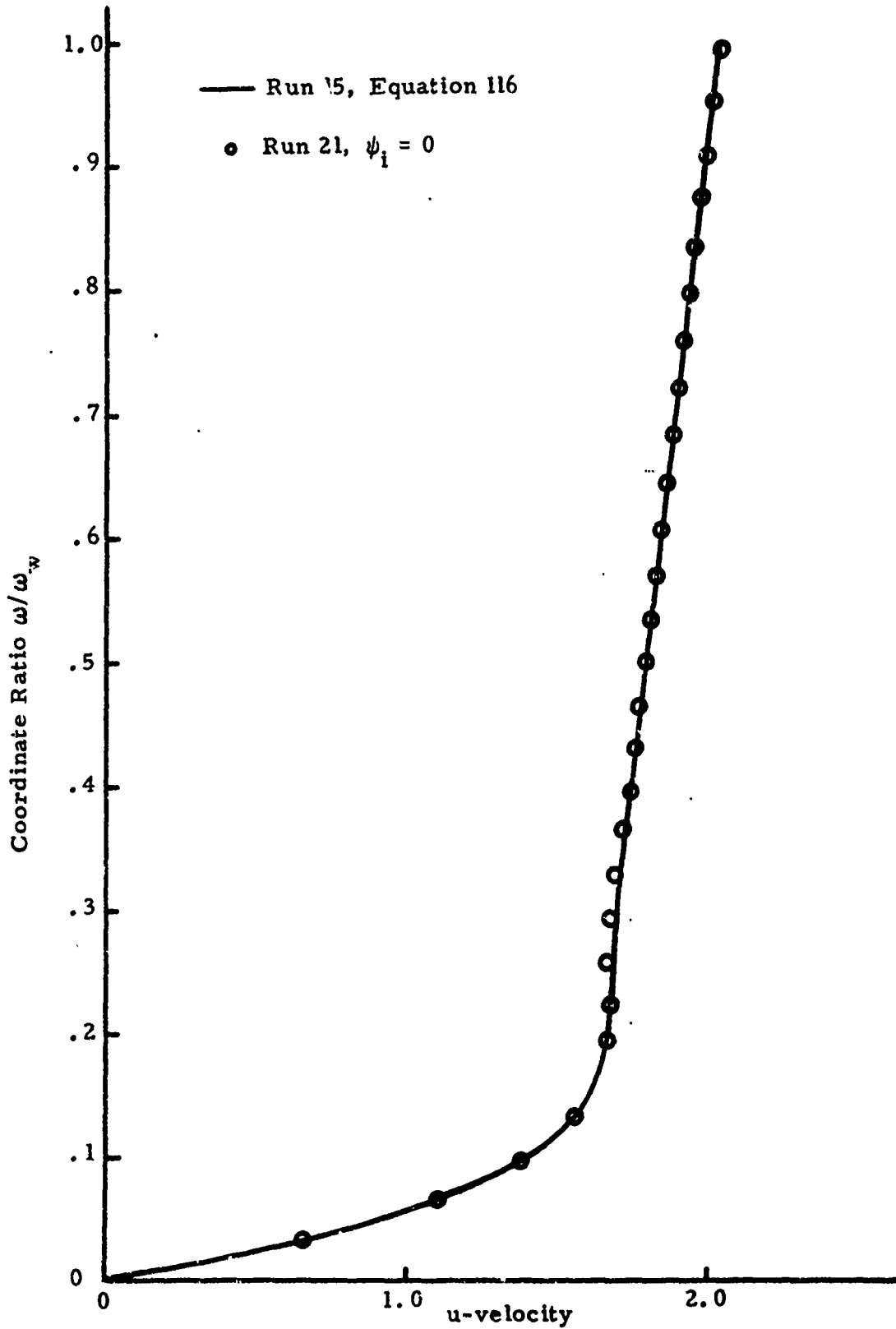


Figure 50. u -velocities in Forebody Region of Hemisphere-Cylinder at $I = 8$ with and without Stabilizing Terms. Computed by Section 4.3.2. $M_o = 4$ and $Re_o = 4000$.

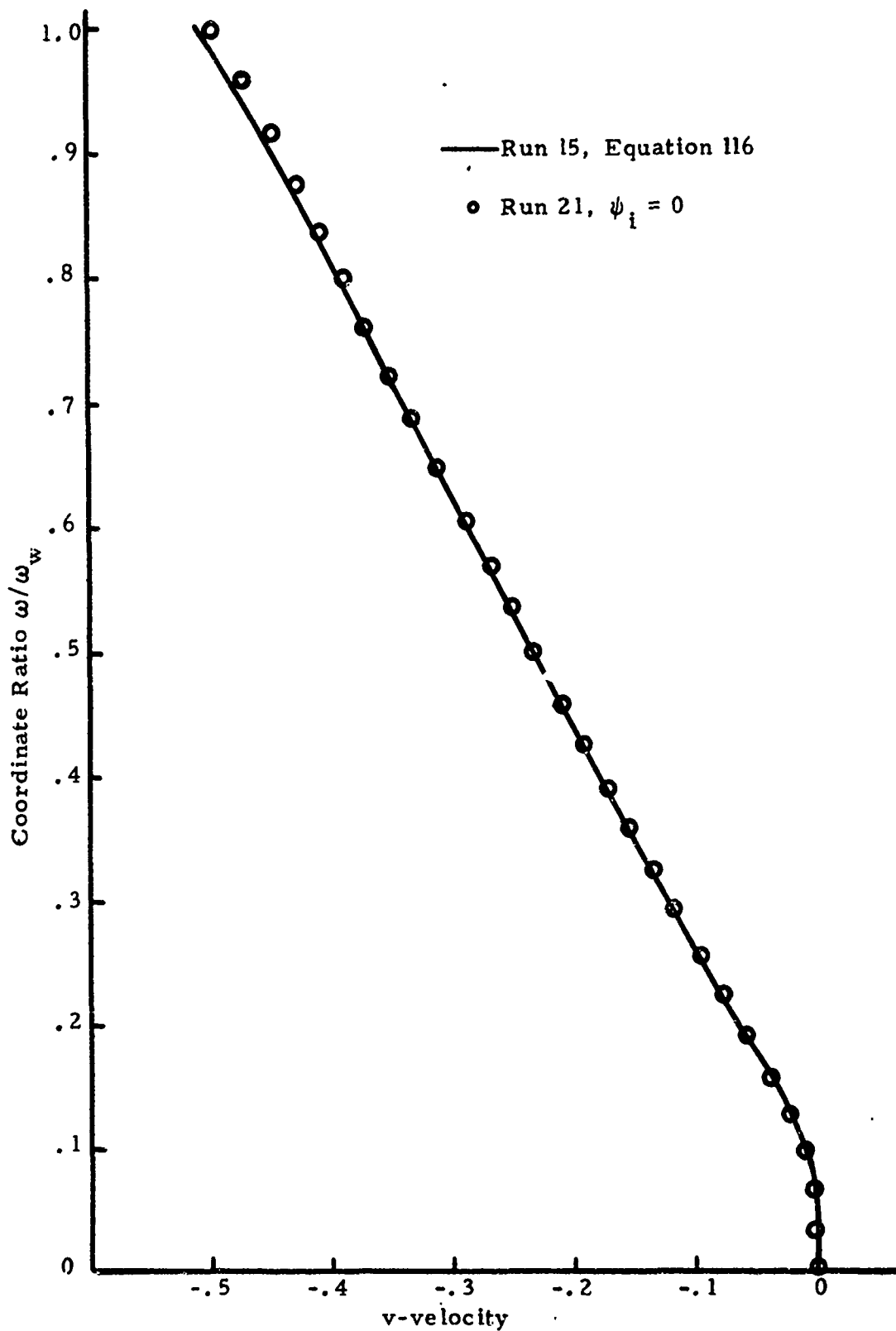


Figure 51. v -velocities in Forebody Region of Hemisphere-Cylinder at $I = 8$ with and without Stabilizing Terms. Computed by Section 4.3.2. $M_o = 4$ and $Re_o = 4000$.

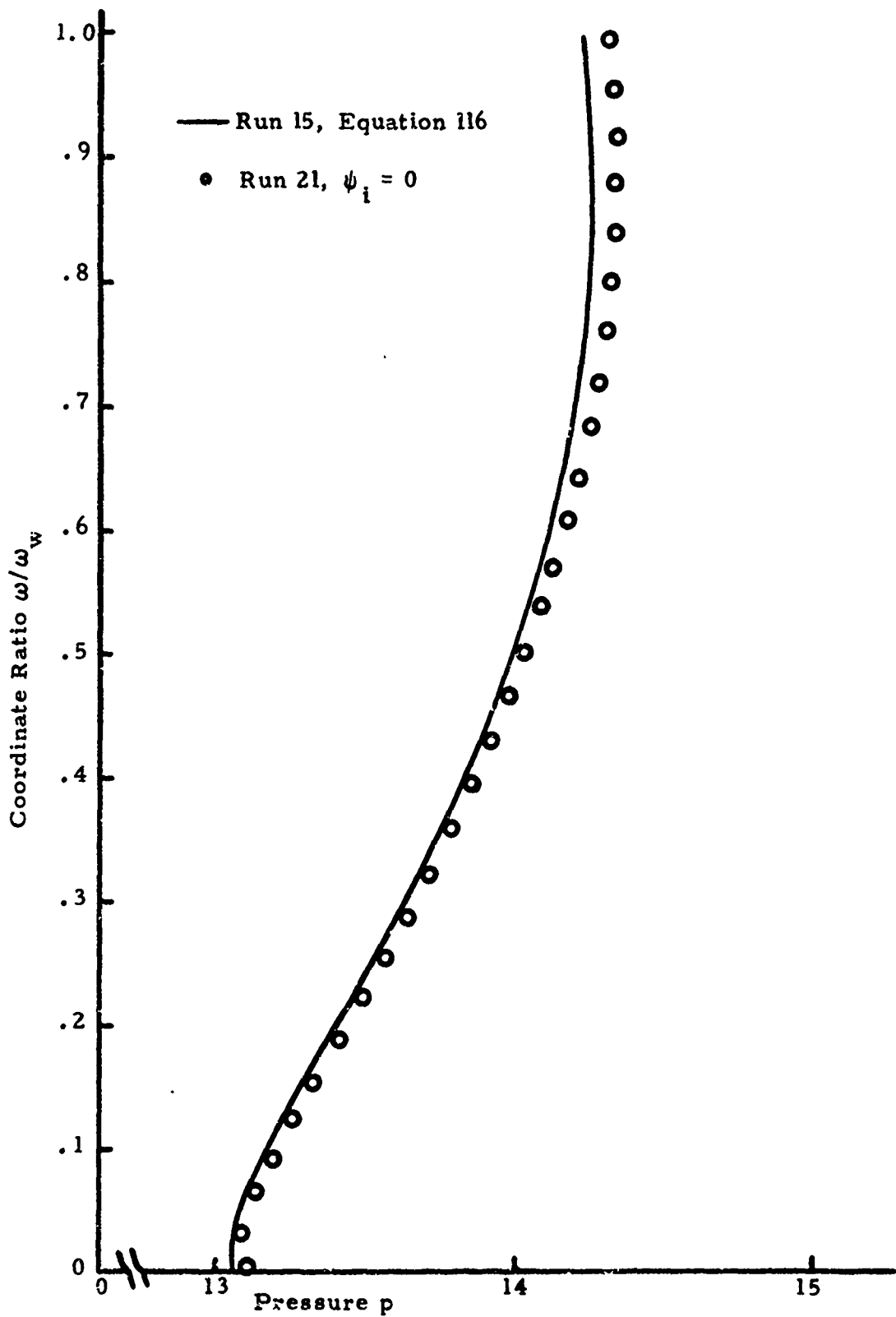


Figure 52. Pressures in Forebody Region of Hemisphere-Cylinder at $I = 8$ with and without Stabilizing Terms. Computed by Section 4.3.2. $M_o = 4$ and $Re_o = 4000$.

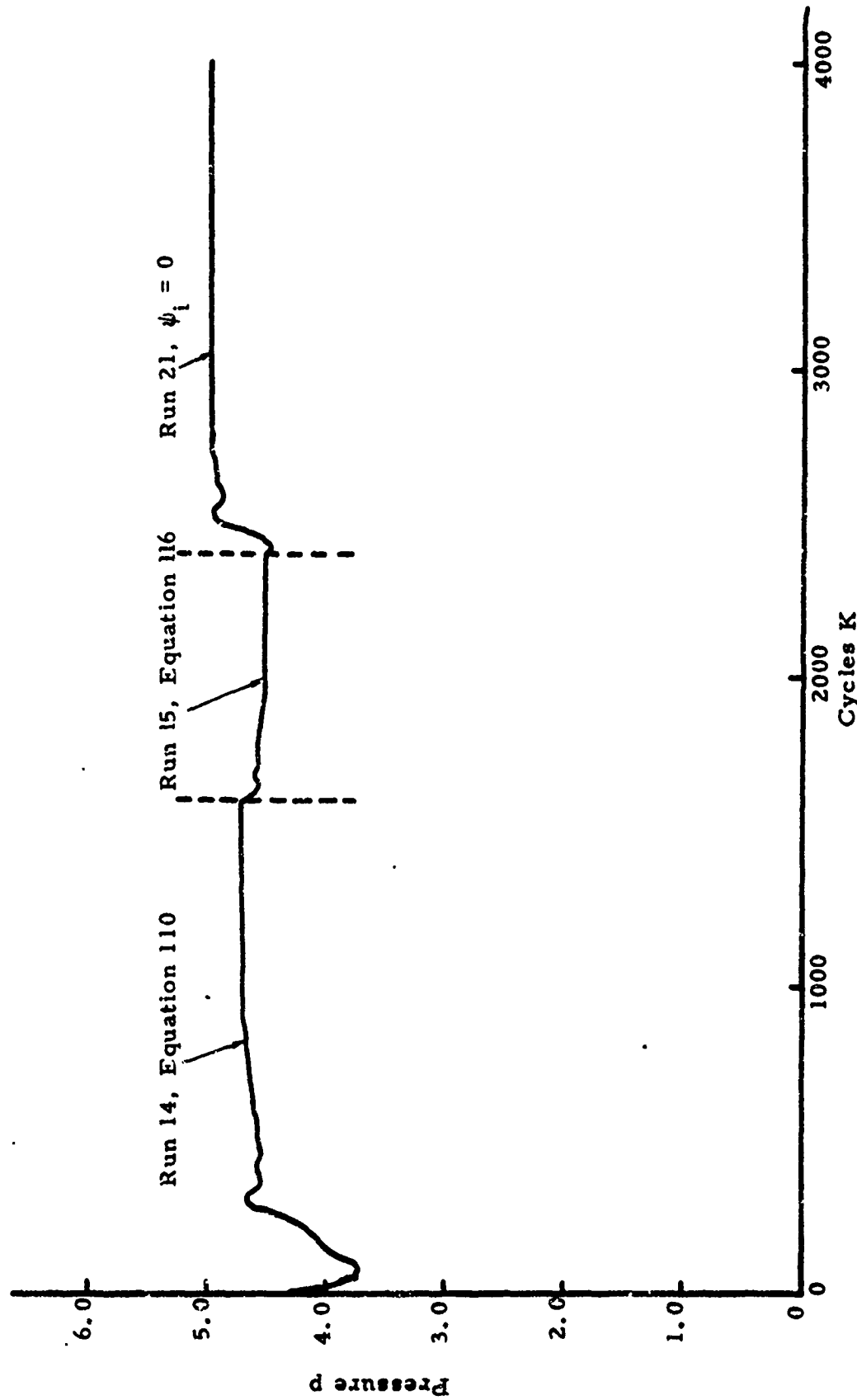


Figure 53. Pressure Versus K Index at $I = 19$, $J = 26$. Computed by Section 4.3.2.
 $M_o = 4$ and $Re_o = 4000$.

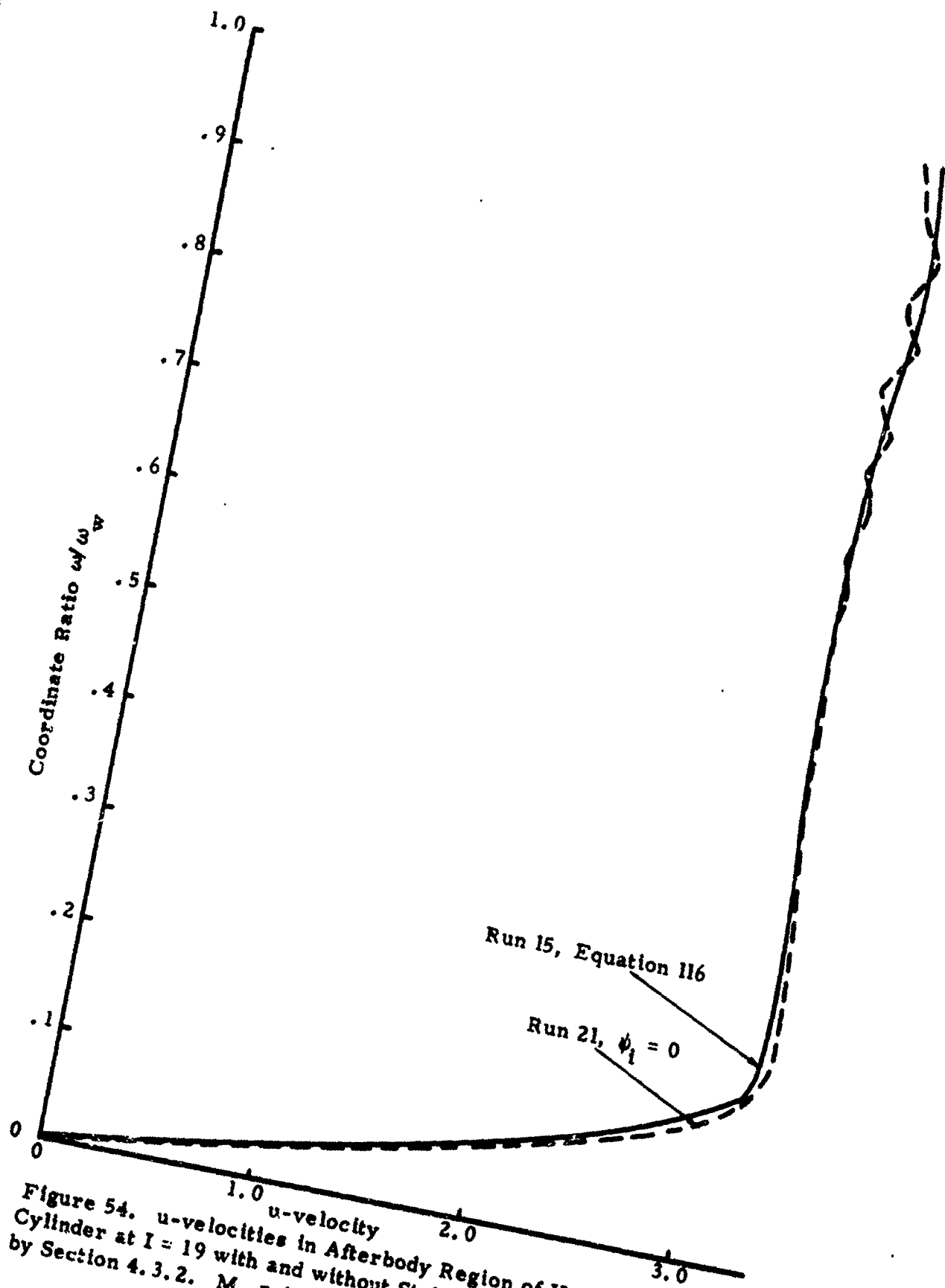


Figure 54. u-velocities in Afterbody Region of Hemisphere-Cylinder at $I = 19$ with and without Stabilizing Terms. Computed by Section 4.3.2. $M_o = 4$ and $Re_o = 4000$.

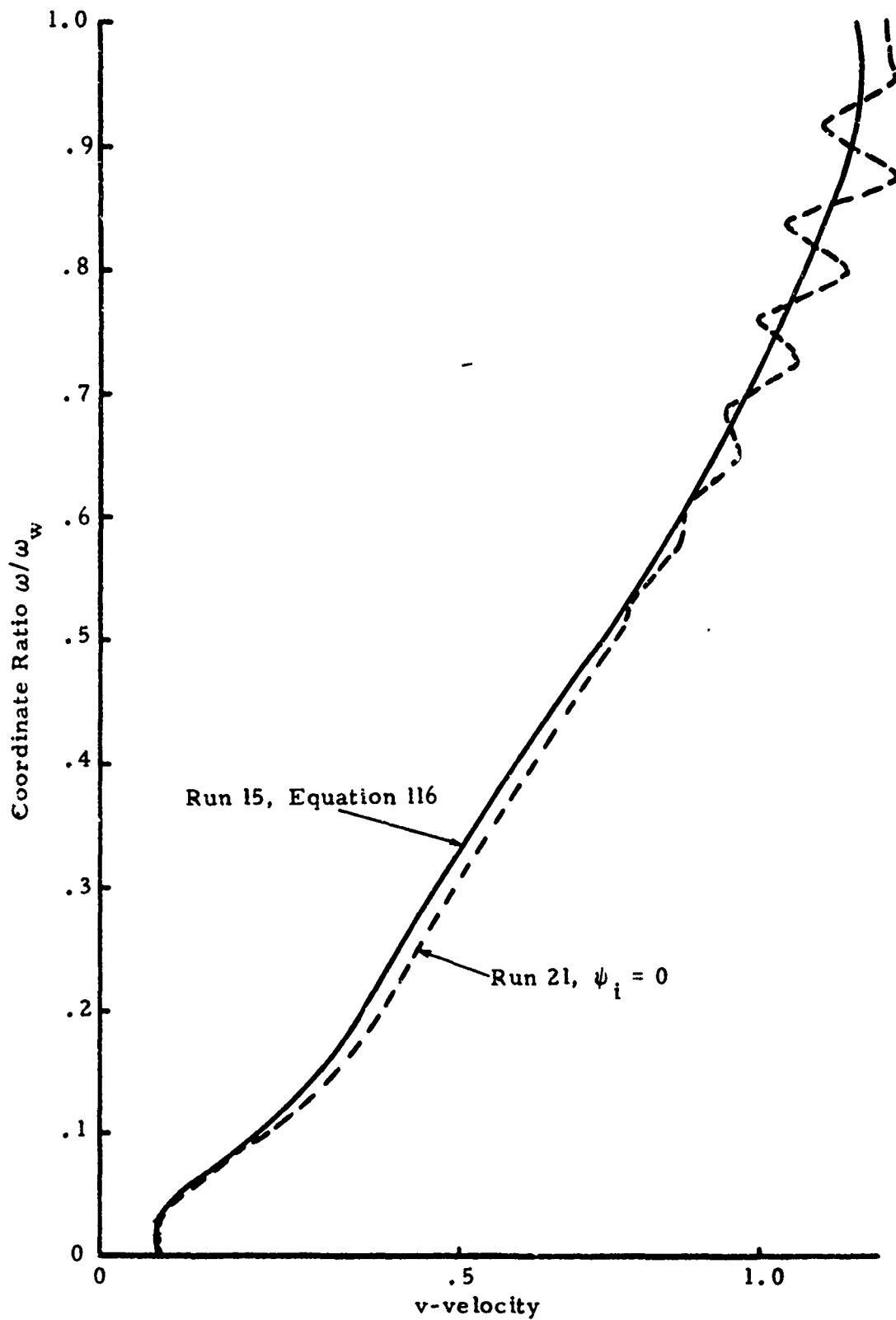


Figure 55. v -velocities in Afterbody Region of Hemisphere-Cylinder $I = 19$ with and without Stabilizing Terms. Computed by Section 4.3.2. $M_o = 4$ and $Re_o = 4000$.

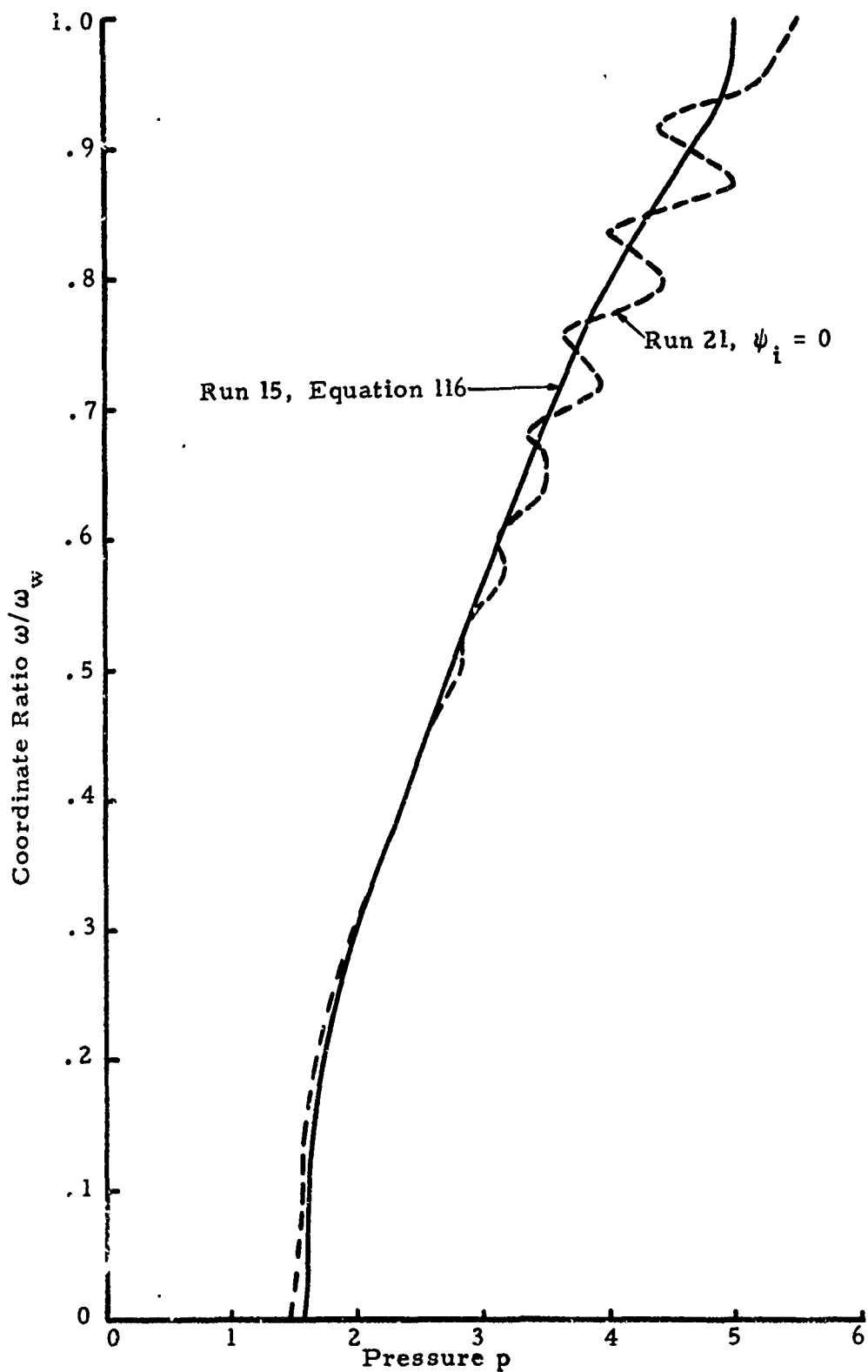


Figure 56. Pressures in Afterbody Region of Hemisphere-Cylinder at $I = 19$ with and without Stabilizing Terms. Computed by Section 4.3.2. $M_o = 4$ and $Re_o = 4000$.

5.6 Summary of Results

Considerable analyses and computations preceded the successful solution of viscous flow around a hemisphere-cylinder to develop techniques. Those analyses and computations seemed to indicate:

1. The body related coordinates of section 3.3.2 are applicable to most blunt bodies.
2. The nonlinear coordinate transformations of section 3.3.3 permit adequate resolution in the boundary layer without an excessive total number of nodes.
3. To obtain steady results, initial values should be as accurate as possible to enhance stability and reduce computer time.
4. Techniques for boundary values at the body surface and downstream boundary have a major effect on stability and accuracy.
5. Precise application of the method of characteristics was the only technique that was satisfactory for wave fitting.
6. The differencing technique of section 4.3.2 with stabilizing terms should be applicable to a wide variety of axisymmetrical inviscid or viscous flows.

The most valuable result of this investigation is the complete set of numerical techniques of section 4 for axisymmetrical, viscous, compressible flows around blunt bodies. Results are presented for viscous, compressible flow around a hemisphere-cylinder at free stream Mach and Reynolds numbers of 4 and 4000 and for flows around

hemispheres at Mach numbers of 2 and 4 and Reynolds numbers of 10^3 , 4×10^3 , 10^4 and 10^5 .

6. CONCLUSIONS

1. A complete set of numerical techniques for axisymmetrical, viscous, compressible flows around blunt bodies was developed.
2. An accurate solution was obtained for viscous compressible flow around a hemisphere-cylinder for freestream Mach and Reynolds numbers of 4 and 4000 respectively.
3. Numerical stability was achieved with stabilizing terms, but their necessity was not established.
4. Approximate results can be obtained for the forebody region of a hemisphere-cylinder with a free stream Mach number of 4 and Reynolds number of 4000 by solving the corresponding system of a hemisphere alone.

REFERENCES

1. Aungier, R. H., "A Computational Method for Exact, Direct, and Unified Solutions for Axisymmetric Flow over Blunt Bodies of Arbitrary Shape (Program Blunt)," AFWL-TR-70-16, Jul 1970.
2. Aungier, R. H., "A Computational Method for Two-Dimensional, Axisymmetric and Three-Dimensional, Blunt Body Flows (Program Attack)," Technical Report No. AFWL-TR-70-124, Feb 1971.
3. Aungier, R. H., "A Time-Dependent Numerical Method for Calculating the Flow About Blunt Bodies," Technical Report No. AFWL-TR-68-52, Aug 1968.
4. Baer, A. L., "Pressure Distributions on a Hemisphere-Cylinder at Supersonic and Hypersonic Mach Numbers," AEDC-TN-61-96, Aug 1961.
5. Belotserkovskii, O. M., "On the Calculation of Flow Past Axisymmetric Bodies with Detached Shock Waves Using an Electronic Computing Machine," Applied Mathematics and Mechanics, Vol 24, Mar 1960, pp 745-755.
6. Belotserkovskii, O. M., and Chushkin, P. I., The Numerical Solution of Problems in Gas Dynamics, Basic Developments in Fluid Dynamics, Vol. I (N. Holt, Editor), Academic Press, New York, 1965, pp 1-126.
7. Bohachevsky, I. O., and Mates, R. E., "A Direct Method for the Calculation of the Flow About an Axisymmetric Blunt Body at Angle of Attack," AIAA Journal, Vol. 4, No. 6, Jun 1966, pp 776-782.
8. Bohachevsky, I. O., and Rubin, E. L., "A Direct Method for Computation of Nonequilibrium Flows with Detached Shock Waves," AIAA Journal, Vol. 4, No. 4, April 1966, pp 600-606.
9. Boison, J. C., and Curtiss, H. A., "An Experimental Investigation of Blunt Body Stagnation Point Velocity Gradients," ARS Journal, Vol. 29, No. 2, Feb 1959.
10. Broer, "Pressure Effects on Relaxation and Bulk Viscosity in Gas Motion," Applied Science Research, 1956, pp 55-64.

11. Brong, E. A., and Leigh, D. C., "Method of Belotserkovskii for Asymmetric Blunt-Body Flows," AIAA Journal, Vol. 2, No. 10, Oct 1964, pp 1852-1853.
12. Burstein, S. Z., "Finite Difference Calculations for Hydrodynamic Flow Containing Discontinuities," NYO-1480-33, Sep 1965.
13. Burstein, S. Z., "Numerical Methods in Multidimensional Shock Flows," AIAA Journal, Vol. 2, No. 12, Dec 1964, pp 2111-2117.
14. Chapman, D. R., and Rubesin, M. W., "Temperature and Velocity Profiles in the Compressible Laminar Boundary Layer with Arbitrary Distribution and Surface Temperature," Journal of the Aeronautical Sciences, Vol. 16, No. 9, Sep 1949, pp 547-565.
15. Christian, J. W., Hankey, W. L., and Petty, J. S., "Similar Solutions of the Attached and Separated Compressible Laminar Boundary Layer with Heat Transfer and Pressure Gradient," ARL 70-0025, Feb 1970.
16. Clark, E. L., "Hemisphere-Cylinder Pressure Distributions at Supersonic and Hypersonic Mach Numbers," AEDC-TR-66-179, Dec 1966.
17. Cleary, J. W., "An Experimental and Theoretical Investigation of the Pressure Distribution and Flow Fields of Blunted Cones at Hypersonic Mach Numbers," NACA TN D-2969, Aug 1965.
18. Cohen, C. B., and Reshotko, E., "The Compressible Laminar Boundary Layer with Heat Transfer and Arbitrary Pressure Gradient," NACA Report 1294, 1956.
19. Cohen, C. B., and Reshotko, E., "Similar Solutions for the Compressible Boundary Layer with Heat Transfer and Pressure Gradient," NACA TN 3325, Feb 1955.
20. Courant, R., Friedrichs, K. O., and Lewy, H., "On the Partial Differential Equations of Mathematical Physics," Math. Ann. 100, 1928, pp 32-74.
21. Crocco, L., "A Suggestion for the Numerical Solution of the Steady Navier-Stokes Equations," AIAA Journal, Vol. 3, No. 11, Oct 1965, pp 1824-1832.

22. Davis, R. T., "The Hypersonic Fully Viscous Shock-Layer Problem," Sandia Laboratories Report SC-RR-68-840, Dec 1968.
23. Davis, R. T., and Flügge-Lotz, I., "Second Order Boundary Layer Effects in Hypersonic Flow Past Axisymmetric Blunt Bodies," Journal of Fluid Mechanics, Vol. 20, May 1964, pp 593-623.
24. DeJarnette, F. R., "Application of Lax's Finite-Difference Method to Nonequilibrium Hypersonic Flow Problems," NASA TR R-234, Mar 1966.
25. Der, J. Jr., "A Study of General Three-Dimensional Boundary Layer Problems by an Exact Numerical Method," AIAA Paper No. 69-138, Jan 1969.
26. Dorodnitsyn, A. A., "On a Method of Numerical Solution of Some Nonlinear Problems of Aero-Hydrodynamics," Proc. 9th International Congress of Applied Mechanics, Vol. 1, p 485, University of Brussels, 1957.
27. Drake, R. M., Jr., "Calculation Method for Three-Dimensional Rotationally Symmetrical Laminar Boundary Layers with Arbitrary Free-Stream Velocity and Arbitrary Wall-Temperature Variation," Journal of the Aeronautical Sciences, Vol. 20, No. 5, May 1953, pp 309-316, 330.
28. Dwyer, H. A., "Solution of a Three-Dimensional Boundary-Layer Flow with Separation," AIAA Journal, Vol. 6, Jul 1968, pp 1336-1342.
29. Eaves, R. H., Jr., "An Empirical Correlation of Pressure on Blunt-Nosed Cylindrical Afterbodies at Hypersonic Mach Numbers," AEDC-TR-68-62, May 1968.
30. Emery, A. F., "An Evaluation of Several Differencing Methods for Inviscid Fluid-Flow Problems," Sandia Corporation SCL-DC-66-78, Mar 1967.
31. Erdos, J., and Zakka, V., "Numerical Solution of Several Steady State Wake Flows of the Mixed Supersonic/Subsonic Type by a Time-Dependent Method and Comparison with Experimental Data," AIAA Paper No. 69-649, Jun 1969.
32. Flügge-Lotz, I., and Johnson, A. F., "Laminar Compressible Boundary Layer Along a Curved Insulated Surface," Journal of the Aeronautical Sciences, Vol. 22, Jul 1955, pp 445-454, 490.

33. Fox, L., Numerical Solution of Ordinary and Partial Differential Equations, Pergamon Press, Addison-Wesley Publishing Company, Inc., 1962.
34. Gary, John, "On Certain Finite Difference Schemes for Hyperbolic Systems," Mathematics of Computation, Vol. 18, No. 85, January 1964, pp 1-17.
35. Godunov, S. K., "Finite Difference Method for Numerical Computation of Discontinuous Solutions of the Equations of Fluid Dynamics," Matematicheskii Sbornik, Vol. 27 (89), No. 3; translated by I. Bohachevsky, 1959.
36. Godunov, S. K., Zabrodin, A. V., and Prokopov, G. P., "The Differences Schemes for Two-Dimensional Unsteady Problems in Gas Dynamics and the Calculation of Flows with a Detached Shock Wave," Journal of Computing Mathematics and Mathematical Physics, Academy of Sciences, USSR, Vol. 1, No. 6, translated by T. Strelkokk; edited by N. Holt, Nov-Dec 1961.
37. Hasting, S. M., Parsh, J., and Redman, E. J., "Experimental Investigation of the Pressure Distribution on Axi-symmetric Flat-Face Cone-Type Bodies at Supersonic and Hypersonic Speeds," NAVORD Report 5659, Oct 1957.
38. Hayes, W. D., and Probstein, R. F., Hypersonic Flow Theory, Volume I, Inviscid Flows, 2nd Edition, Academic Press, 1966.
39. Inouge, M., and Lomax, H., "Comparison of Experimental and Numerical Results for the Flow of a Perfect Gas About Blunt-Nosed Bodies," NASA TN D-1426. Sep 1962.
40. Kendall, J. M., Jr., "Experiments on Supersonic Blunt-Body Flows," Progress Report 20-372, Jet Propulsion Lab., California Institute of Technology, Feb 1959.
41. Kramer, R. F., and Lieberstein, H. M., "Numerical Solutions of the Boundary Layer Equations Without Similarity Assumptions," Journal of the Aero Space Sciences, Vol. 26, Aug 1959, pp 508-514.
42. Kubota, T., "Investigation of Flow Around Simple Bodies in Hypersonic Flow," GALCIT Memo No. 40, Jun 1957.
43. Lapidus, A., "A Detached Shock Calculation by Second Order Finite Differences," Courant Institute of Mathematical Sciences, NYO-1480-69, Feb 1967.

44. Lax, P. D., "Weak Solutions of Nonlinear Hyperbolic Equations and Their Numerical Computation," *Communications on Pure and Applied Mathematics*, Vol. VII, No. 1, Feb 1954, pp 159-193.
45. Lax, P. D., and Wendroff, B., "Systems of Conservative Laws," *Communications on Pure and Applied Mathematics*, Vol. 13, No. 2, May 1960, pp 217-237.
46. Love, E. S., "A Reexamination of the Use of Simple Concepts for Predicting the Shape and Location of Detached Shock Waves," *NACA TN 4170*, Dec 1957.
47. MacCormack, R. W., "The Effect of Viscosity in Hypervelocity Impact Cratering," *AIAA Hypervelocity Impact Conference*, Paper No. 69-354, 1969.
48. Mangler, W., "Zusammenhang Zwischen Ebenen und Rotations-symmetrischen Grenzschichten in Kompressiblen Flussigkeiten," *ZAMM 28*, 1948, pp 97-103.
49. Masson, B. S., Taylor, T. D., and Foster, R. M., "Application of Godunov's Method to Blunt-Body Calculations," *AIAA Journal*, Vol. 7, No. 4 Apr 1969, pp 694-698.
50. Moeckel, W. E., "Approximate Method for Predicting Form and Location of Detached Shock Waves Ahead of Plane or Axially Symmetric Bodies," *NACA TN 1921*, 1949.
51. Moretti, G., "Improved Time-Dependent Techniques for the Blunt-Body Problem," Vol. II, *Sandia Laboratories Report SC-CR-68-3728*, Sep 1968.
52. Moretti, G., and Abbett, M., "A Fast, Direct, and Accurate Technique for the Blunt Body Problem," *Technical Report No. 583*, General Applied Sciences Laboratories, Inc., Jan 1966.
53. Moretti, G., and Bleich, G., "Three-Dimensional Inviscid Flow About Supersonic Blunt Cones at Angle of Attack," Vol. I, *Sandia Laboratories Report SC-CR-68-3728*, Sep 1968.
54. Moretti, G., and Salas, M. D., "The Blunt Body Problem for a Viscous Rarefied Gas Flow," *AIAA Paper No. 69-139*, Jan 1969.
55. Moretti, G., and Salas, M. D., "Numerical Analysis of the Viscous Supersonic Blunt Body Problem - Part I," *PIBAL Report No. 70-48*, Nov 1970.

56. Reichle, H. G., Jr., "Hemisphere-Cylinder Pressure Distributions at Subsonic, Transonic, and Supersonic Mach Numbers," NASA, MTP-AERO-62-30, Mar 62.
57. Richtmyer, R. D., "Progress Report in the Mach Reflection Calculation," NYO-9764, CIMS, New York University, 1961.
58. Richtmyer, R. D., "A Survey of Finite Difference Methods for Non-Steady Fluid Dynamics," National Center for Atmospheric Research, NCAR Tech. Note 63-2, Boulder, CO, Aug 1962.
59. Richtmyer, R. D., and Morton, K. W., Difference Methods for Initial Value Problems, 2nd Edition, Interscience Publishers, New York, 1967.
60. Rosenhead, L., (Editor), Laminar Boundary Layers, Oxford University Press, 1963.
61. Rusanov, V., "Calculation of Interaction of Non-Steady Shock Waves with Obstacles," National Research Council of Canada, Translation No. 1027, 1962.
62. Scala, S. M., and Gordon, P., "Solution of the Time Dependent Navier-Stokes Equations for the Flow Around a Circular Cylinder," AIAA Journal, Vol. 6, No. 5, May 1968, pp 815-822.
63. Schlichting, H., Boundary Layer Theory, Sixth Edition, McGraw-Hill Book Company, 1966.
64. Skoglund, V. J., "Principles of Fluid Mechanics," ME 503 Notes, The University of New Mexico, Albuquerque, New Mexico, 1964.
65. Skoglund, R. J., Cole, J. K., and Staiano, E. F., "Development and Verification of Two-Dimensional Numerical Techniques for Viscous Compressible Flows with Shock Waves," Sandia Laboratories Report SC-CR-67-2679, Aug 1967.
66. Skoglund, V. J., and Gay, B. D., "Improved Numerical Techniques and Solution of a Separated Interaction of an Oblique Shock Wave and a Laminar Boundary Layer," Bureau of Engineering Research Final Report ME-41(69) S-068, University of New Mexico, Jun 1969.
67. Staiano, E. F., "A General Numerical Procedure for Solutions of Viscous Compressible Flows with Shock Waves," PhD Dissertation, University of New Mexico, May 1967.

68. Stewartson, K., "Correlated Incompressible and Compressible Boundary Layers," *Proceeding Royal Society (London) Series A*, Vol. 200, No. A1060, Dec 1949, pp 84-100.
69. Swenson, E. V., "Numerical Computation of Hypersonic Flow Past a Two-Dimensional Blunt Body," *AEC Research and Development Report NYO-1480-1*, Aug 1964.
70. Swigart, R. J., "A Theory of Asymmetric Hypersonic Blunt-Body Flows," *AIAA Journal*, Vol. 1, No. 5, May 1963, pp 1034-1042.
71. Traugott, S. C., "An Approximate Solution of the Direct Supersonic Blunt-Body Problem for Arbitrary Axisymmetric Shapes," *Journal of the Aerospace Sciences*, Vol. 27, May 1960, pp 361-370.
72. Van Dyke, M. D., "The Supersonic Blunt-Body Problem - Review and Extension," *Journal of Aerospace Sciences*, Vol. 25, Aug 1968, pp 485-495.
73. Von Neumann, J., "Proposal and Analysis of a Numerical Method for the Treatment of Hydrodynamical Shock Problems," *National Defense and Research Committee Report AM551*, 1944.
74. Von Neumann, J., and Richtmyer, R. D., "A Method for the Numerical Calculation of Hydrodynamic Shocks," *Journal of Applied Physics*, Vol. 21, No. 3, May 1950, pp 232-237.
75. Wells, C. S., Jr., and Blumer, C. B., "Laminar Compressible Boundary Layer on a Blunt Body," *AIAA Journal*, Vol. 6, No. 1, Jan 1968, pp 159-160.